BETA-LACTAMASE LIGAND RECOGNITION

by

Deniz Menekşedağ

B.S., Chemical Engineering, Yıldız Technical University, 2010

Submitted to the Institute for Graduate Studies in
Science and Engineering in partial fulfillment of
the requirements for the degree of
Master of Science

Graduate Program in Chemical Engineering
Boğaziçi University

2012

ACKNOWLEDGEMENTS

I would like to express my sincere gratitude to my thesis supervisor Assist. Prof. Elif Özkırımlı Ölmez and co-supervisor Assoc. Prof. Berna Sarıyar Akbulut for their guidance, encouragement and motivation during my research.

I would like to thank my thesis committee members, Prof. Canan Atılgan, Prof. Türkan Haliloğlu and Prof. Zeynep İlsen Önsan, for insightful discussions and evaluation of this work.

I am grateful to Assist. Prof. Burak Alakent for his help with the trajectory analysis calculations.

I gratefully thank Pınar Kanlıkılıçer, Aslıgül Doğan and Naze Gül Avcı for their guidance with their previous studies and help throughout my work.

Special thanks to Begüm Alaybeyoğlu, Gizem Özbüyükkaya and Aybike Nurocak for sharing all the good and bad times. I am grateful to my lab partners, Ahmet Özcan, Seval Aladağ, Oya Gürsoy Yılmaz and Kadriye Simay Yalaz for their friendship and encouragement.

Biggest thanks to my family for their everlasting support and encouragement during whole my educational life. Heartfelt thanks to my fiancée, Fatih Erol, for his endless help, patience and motivation during my research.

Graduate student scholarship provided by TUBITAK BIDEB and research funding provided by TUBITAK Research Grants 108M644 and 109M229 and Bogazici University Research Grants 08A502 and 09HA504P are gratefully acknowledged.

ABSTRACT

BETA-LACTAMASE LIGAND RECOGNITION

Beta-lactamases hydrolyze the beta-lactam ring of antibiotics, rendering them ineffective. Understanding the inhibitor recognition mechanism of beta-lactamases will give important information toward the fight against beta-lactamase mediated antibiotic resistance. Most inhibitors of beta-lactamase bind to the active site and thus inhibit beta-lactamase in a competitive manner. In this study, inhibitor recognition mechanism of beta-lactamase was examined using molecular dynamics simulations and *in vitro* kinetic experiments. Simulations were performed on apo and BLIP bound forms of two clinically relevant beta-lactamases, TEM-1 and SHV-1 in order to elucidate the change in dynamics and energetics upon BLIP binding. An allosteric inhibitor binding site, near the H10 helix (residues 218-230), was previously discovered in TEM-1 and SHV-1. Multiple sequence alignment of beta-lactamases shows that Trp229, which resides on the H10 helix, is a highly conserved residue within the beta-lactamase family. Simulations were repeated on the W229A mutant forms of TEM-1 and SHV-1 beta-lactamase in order to investigate the role of Trp229 in ligand recognition mechanism of beta-lactamase. Simulations resulted in higher H10 mobility in TEM-1 and SHV-1 beta-lactamases in the presence of BLIP and higher cross correlations with BLIP. Higher affinity toward BLIP was observed in W229A mutant TEM-1 but not in mutant SHV-1 beta-lactamase. The results indicate the presence of the communication between allosteric site and active site of beta-lactamase. Molecular dynamics simulations were performed on 10 different TEM-1 – peptide complexes, with various mutations done on the peptide. The structural, dynamic and energetic examination of the simulation trajectories revealed that the G48F mutant of the peptide comprising BLIP residues 45 to 53 had strong nonbonded interactions between enzyme and peptide and higher affinity toward TEM-1. *In vitro* experiments were carried out with four different peptides. The peptide comprising BLIP residues 45 to 53 and a peptide that has additional pVEC residues at the N-terminus of its sequence designed based on 45-53 region of BLIP were found to have similar inhibitory effects on TEM-1 beta-lactamase activity.

ÖZET

BETA-LAKTAMAZ LİGAND BAĞLANMASI

Beta-laktamazlar antibiyotiklerin beta-laktam halkalarını hidrolize ederek antibiyotikleri etkisiz hale getirir. Beta-laktamazların inhibitor tanıma mekanizmalarının anlaşılması beta-laktamaz kaynaklı antibiyotik direnci ile savaşılması için önemli bilgiler sağlayacaktır. Pek çok inhibitor, beta-laktamazın aktif bölgesine bağlanarak beta-laktamazı yarışmalı olarak inhibe eder. Bu çalışmada beta-laktamazın inhibitor tanıma mekanizması moleküler dinamik simülasyonları ve *in vitro* deneyler ile incelenmiştir. Simülasyonlar iki klinik açıdan alakalı beta-laktamaz olan TEM-1 ve SHV-1 beta-laktamazlarının serbest ve BLIP bağlı yapıları üzerinde, BLIP bağlanmasının enerji ve dinamikler üzerine etkisinin aydınlatılması amacıyla gerçekleştirilmiştir. TEM-1 ve SHV-1 beta-laktamazlarında H10 sarmalının yakınında, bir allosterik bağlanma bölgesi vardır. Beta-laktamazların çoklu dizi hizalamaları sonucunda H10 sarmalı üzerinde bulunan Trp229, beta-laktamaz ailesi içerisinde oldukça korunmuş bir kalıntı olarak saptanmıştır. Simülasyonlar beta-laktamazın ligand tanıma mekanızmasında Trp229 kalıntısının rolünü saptayabilmek için W229A mutant TEM-1 ve SHV-1 beta-laktamazları ile tekrar edilmiştir. Simülasyonlar sonucunda, BLIP varlığında TEM-1 ve SHV-1 beta-laktamazlarında yüksek H10 hareketliliği ve BLIP ile yüksek çapraz korelasyonlar saptanmıştır. BLIP'e karşı yüksek ilgi mutant TEM-1'de gözlemlenirken, mutant SHV-1'de saptanamamıştır. Elde edilen sonuçlar beta-laktamazın allosterik bölgesi ile aktif bölgesi arasında bir iletişim olduğunu göstermektedir. Moleküler dinamik simülasyonları peptit üzerinde farklı mutasyonlar içeren 10 farklı TEM-1 – peptit kompleksi üzerinde gerçekleştirilmiştir. Simülasyonların yapısal, dinamik ve enerjik analizleri sonucunda BLIP'in 45-53 bölgesini kapsayan peptitin G48F mutant formunun TEM-1'e yüksek ilgi ile bağlandığını göstermiştir. Dört farklı peptit ile *in vitro* deneyler gerçekleştirilmiştir. BLIP'in 45-53 bölgesini kapsayan peptit ile başında hidrofobik pVEC kalıntıları taşıyan ve BLIP'in 45-53 bölgesi temel alınarak oluşturulan peptit, TEM-1 beta-laktamaz aktivitesi üzerinde benzer inhibitor etkileri göstermiştir.

TABLE OF CONTENTS

LIST OF FIGURES

LIST OF TABLES

LIST OF SYMBOLS

C_α	carbon alpha atom
$c(i,j)$	covariance
$C(i,j)$	correlation
m_i	mass
r_i	3N set of atomic coordinates
f_i	forces acting on atoms
α	alpha
Å	angstrom
Ω	omega
ΔG	binding free energy
ΔG_{clash}	measure of steric overlaps between atoms
ΔG_{el}	electrostatic contribution to binding free energy
ΔG_{hbond}	energy of hydrogen bonds
ΔG_{kon}	additional electrostatic contribution to binding free energy
ΔG_{solvH}	hydrophobic solvation contribution to binding free energy
ΔG_{solvP}	polar solvation contribution to binding free energy
ΔG_{vdw}	van der Waals contributions to binding free energy
ΔG_{wb}	contribution of interactions involve more than two hydrogen bonds
Δr_i	displacement vectors
ΔS_{mc}	entropic cost of fixing backbone atoms
ΔS_{sc}	entropic cost of fixing side chain atoms

LIST OF ACRONYMS / ABBREVIATIONS

A	Alanine
Ala	Alanine
Arg	Arginine
Asn	Asparagine
Asp	Aspartic Acid
BLIP	Beta-lactamase Inhibitory Protein
C	Cysteine
Cys	Cysteine
D	Aspartic Acid
E	Glutamic Acid
Elec	Electrostatic
F	Phenylalanine
G	Glycine
Gln	Glutamine
Glu	Glutamic Acid
Gly	Glycine
H	Histidine
His	Histidine
I	Isoleucine
Ile	Isoleucine
L	Leucine
Lys	Lysine

M	Methionine
Met	Methionine
MD	Molecular Dynamics
MSF	Mean Square Fluctuation
N	Asparagine
NMR	Nuclear Magnetic Resonance
P	Proline
PenG	Penicillin G
Phe	Phenylalanine
Pro	Proline
R	Arg
RMSD	Root Mean Square Deviation
S	Serine
Ser	Serine
T	Threonine
T	Temperature
Thr	Threonine
Trp	Tryptophan
Tyr	Tyrosine
V	Valine
Val	Valine
VDW	Van der Waals
Y	Tyrosine
W	Tryptophan

1. INTRODUCTION

1.1. Beta-lactamase Mediated Antibiotic Resistance

The advent of sulfonamides in the 1930's paved the way for the therapeutic applications of several classes of antibiotics in medicine (Essack, 2001). Today, beta-lactam antibiotics, such as penicillin, penicillin derivatives, cephalosporins, cephamycins, carbapenems, monobactams and monocarbams, are the most varied and extensively used antimicrobial agent in the treatment of bacterial infections because of their high efficacy, low cost, ease of delivery and minimal adverse reactions (Wilke *et al.*, 2005). Since the introduction of penicillin in 1940's, bacteria have evolved resistance to beta-lactam antibiotics typically by misuse or underuse of these drugs (Fisher *et al.*, 2005). Antibiotic resistance is a worldwide health problem in the management of infectious diseases. There are three major ways for bacteria to avoid the lethal effects of the beta-lactam antibiotics. Either altered penicillin binding proteins exhibit low affinity for beta-lactam antibiotics or bacteria can protect themselves by losing the outer membrane proteins in order to restrict the entry of the beta-lactams into the periplasmic space and inner membrane. Production of the antibiotic-inactivating enzymes, beta-lactamases, which efficiently catalyze the irreversible hydrolysis of the beta-lactam ring amide bond is one of the most important resistance mechanisms (Babic *et al.*, 2006, Essack, 2001).

Beta-lactamases are classified into four classes, class A, B, C and D, based on their structural information and catalytic mechanism. Class A, C and D enzymes have a serine residue, whereas class B enzymes have divalent metal cations (Zn^{2+}) in their active sites (Ambler, 1980, Majiduddin *et al.*, 2002).

Two strategies have been used to combat the escalating problem of beta-lactamase mediated antibiotic resistance; either a modification is done on the antibiotic structure in order to make it no longer a substrate for the enzyme, or combination therapies that include both beta-lactam antibiotics and beta-lactamase inhibitors are used (Williams, 1999). The use of beta-lactamase inhibitors such as clavulanic acid, sulbactam and tazobactam has proven to be successful in treating infections; however bacteria have developed inhibitor

resistance and hence there is intense research toward the development of novel inhibitors (Buynak, 2006).

1.2. TEM-1 and SHV-1 Beta-lactamases

TEM-1 beta-lactamase, encoded by *bla*$_{\text{TEM-1}}$ gene, is among the most prevalent plasmid-encoded enzyme found in gram negative bacteria (Wiedemann *et al.*, 1989). The crystal structure of *Escherichia coli* TEM-1 beta-lactamase was determined in the 1990's (Jelsch *et al.*, 1993, Strynadka *et al.*, 1992). TEM-1 is a globular protein which consists of 263 amino acids. The structure of TEM-1 beta-lactamase is represented in Figure 1.1a and the Ambler residue numbering of the secondary structural elements is given in Table 1.1. The protein has two main domains; the first domain includes a main beta sheet formed by five antiparallel beta strands onto which H1, H10 and H11 helices are packed. A large hydrophobic core is present which is comprised of the interface between this beta sheet and the mentioned helices. The second domain is made of eight helices comprised of H2 to H9. These two domains are connected by two hinge regions which are held by salt bridges and hydrogen bonds; the interface of the two domains corresponds to the substrate binding site, and includes the conserved catalytic residues, Ser70, Lys73, Ser130, Glu166, Asn170, Lys234 and Arg244 (Arg243 in TEM-1 – BLIP structure) (Strynadka *et al.*, 1996, Zhang and Palzkill, 2004). Ambler residue numbering is used throughout this thesis (Ambler *et al.*, 1991). The first hinge region is formed by the salt bridge between Arg43 and Glu64, the salt bridge between Arg61 and Glu64 and the hydrogen bond between Glu37 and Arg61. The second hinge region (residues 212 to 222) is formed by the salt bridge between Arg222 and Asp233. In addition to the main beta sheet, there are two small two-stranded beta sheets (SB and SC) each made of two residues (Jelsch *et al.*, 1993).

The substrate binding cavity is composed of several regions. Residues of S3 beta sheet, 234-237, and S4 beta sheet, Arg244, is on one side of the substrate binding cavity. Arg244 is a highly conserved residue among beta-lactamases and it has been postulated to play a role in the initial substrate recognition mechanism. The mutations done in the position comprised by Arg244 show that this residue contributes to binding stabilization and a strong hydrogen bond has been proposed to be present between Arg244 and substrate carboxylate (Zafaralla *et al.*, 1992).

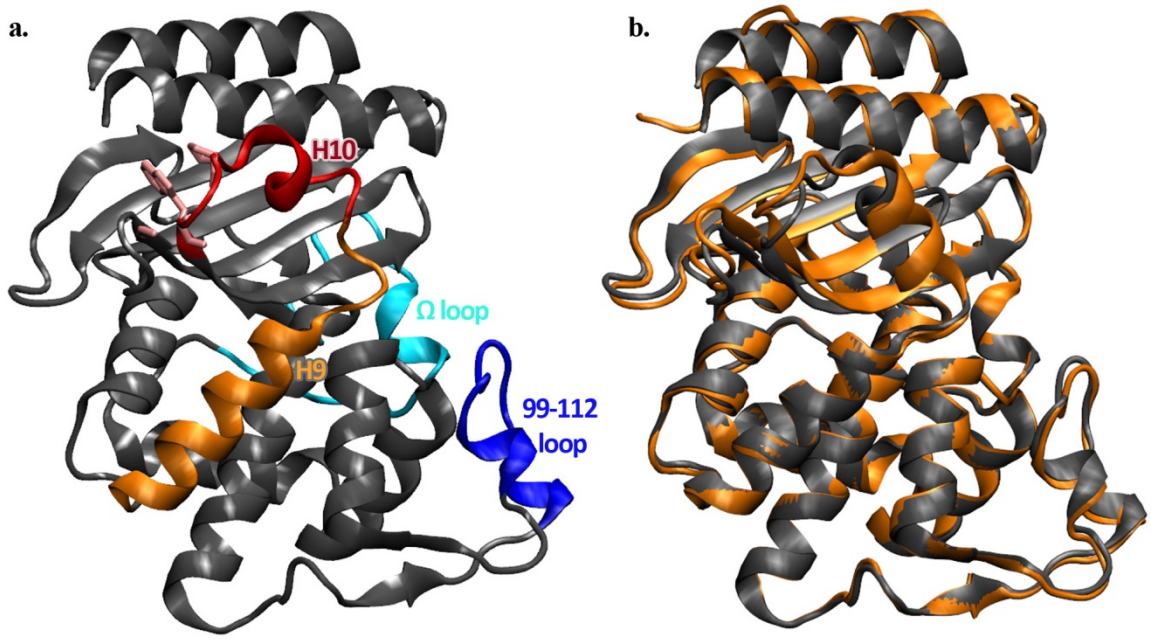

Figure 1.1. (a) TEM-1 structure; H9, H10 helices, Ω and 99-112 loops are highlighted. (b) Superimposed structures of TEM-1 (gray) and SHV-1 (orange) beta-lactamases. The RMSD between TEM-1 (pdb code: 1zg4) and SHV-1 (pdb code: 1shv) structures is 1.4 Å.

Glu104 and Tyr105 are on a solvent exposed loop on the N-terminus side of H3 helix. Ser130, which is on the loop connecting H4 and H5 helices, is on the opposite site of the cavity. The side chain of Val216 is present in the cleft of acylating Ser70. The Ω loop is a conserved structural element which is located at the protein-solvent interface, and it is comprised of the residues 161 to 179, forms the other edge of the substrate binding site and carries the Glu166, which acts as the catalytic base in the acylation and deacylation reaction mechanisms (Jelsch *et al.*, 1993, Minasov *et al.*, 2002). The Ω loop is a more constrained structural element in TEM-1 beta-lactamase among other beta-lactamases because of the existence of the strictly conserved salt bridge between Arg164 and Asp179, and the NMR studies also confirmed the high degree order of this exposed loop on the picosecond to nanosecond timescale (Jelsch *et al.*, 1993, Savard and Gagne, 2006). MD simulations on TEM-1 show that the Ω loop undergoes a flap-like transitional motion in 5 ns timescale (Roccatano *et al.*, 2005) and longer simulations done on TEM-1 show that Ω loop is not solidly anchored to the protein core as stated by the previous studies. The N-terminus of this loop is highly structured because of the packing on H6 helix. The central part (residues 166 to 170) shows limited flexibility and the motions observed in the last

part, comprising residues 171 to 179, are the most important ones; higher flexibility is measured within this region (Fisette *et al.*, 2010).

Adjacent to the active site cavity, there is a protruding loop and helix, comprising residues Gln99 to His112, which have a convex surface with a largely negative electrostatic potential (Strynadka *et al.*, 1996). The 99-112 loop of beta-lactamase carries the Tyr105, which is mainly involved in substrate discrimination and stabilization. Aromatic residues at position 105 were identified to prevent steric hindrance with substrate molecules by the formation of a rigid, stabilizing wall that restricts the cavity size and the substrate movement, hence the position 105 has shown to play an important role in substrate stabilization. The NMR studies done on Y105D mutants show that several active site residues of TEM-1 beta-lactamase display significantly altered motions possibly resulting in a reduced catalytic efficiency, despite the fact that many of them are far away from the mutation site (Doucet *et al.*, 2007).

Table 1.1. The secondary structural elements in TEM-1 beta-lactamase (Jelsch *et al.*, 1993).

Helices		**Antiparallel beta sheets**	
	Residue number		*Residue number*
		Main beta sheet	
H1	26 – 40	**S1**	43 – 50
H2	69 – 85	**S2**	56 – 60
H3	109 – 111	**S3**	230 – 237
H4	119 – 128	**S4**	244 – 251
H5	132 – 142	**S5**	259 – 266
H6	145 – 154	**Sheet B**	
H7	168 – 170	**SB1**	66 – 67
H8	183 – 195	**SB2**	180 – 181
H9	201 – 212	**Sheet C**	
H10	221 – 224	**SC1**	94 – 95
H11	272 - 288	**SC2**	117 – 118

SHV-1 has 68% identical sequence and similar substrate specificity profile with TEM-1 beta-lactamase. The structure of SHV-1 (Figure 1.1b) consist two domains in which one is α-helical and the second one consists of five-stranded antiparallel beta-sheets surrounded by α-helices. The most of the nonconservative sequence differences between these two enzymes are observed at solvent exposed positions comprised of residues 92, 98, 100, 120, 146, 147, 198, 201, 202, 212, 213, 255, 273 and 281. Changes at the positions 266 and 267, from Thr and Gly in TEM-1 to Arg and Asp in SHV-1, result in longer side chains and solvation bridges, which have the potential to stabilize the Ω loop. The catalytic site is composed of six important residues Ser70, Lys73, Ser130, Glu166, Asn170 and Lys234, identical to TEM-1. However large differences are observed between TEM-1 and SHV-1 at the mouth of the binding cavity; distances from backbone atoms of 104-105 loop or 130-132 loop across the 235-238 beta strand are significantly greater in SHV-1. The amino acid differences at position 104 which is located at the 99-112 loop, Asp104 in SHV-1 and Glu104 in TEM-1, makes the mouth larger in SHV-1 and that might be the reason for the differences observed in substrate profiles of these two enzymes (Kuzin *et al.*, 1999).

Sequence differences are observed in the conserved structural element Ω loop at position 167, Pro in TEM-1 and Thr in SHV-1, position 175, Gly in TEM-1 and Asn in SHV-1, position 177, Ala in TEM-1 and Glu in SHV-1. A significant difference in the Ω loop of the TEM/SHV pair is caused by the additional stabilization of one edge of the Ω loop (172-176) in SHV-1, resulting from linkages with hydrogen-bonding residues Arg266 and Asp267 on the beta sheet. As mentioned this stabilization is not present in TEM-1 (Kuzin *et al.*, 1999).

The H10 helix region, which is located above the active site, forms one part of the hinge region of the enzyme (residues 212 to 222) as mentioned before (Jelsch *et al.*, 1993). The hydrophobic region flanked by H10 and H11 (residues 271-289) has been shown to bind the crystallization adjuvant Cymal-6 in (Kuzin *et al.*, 1999) and an allosteric inhibitor (Horn and Shoichet, 2004), suggesting that this region may serve as an additional binding site in drug design efforts. The allosteric inhibitor inserts between the cleft formed by H10 and H11 and interacts with the hydrophobic residues of the beta sheet as well as Arg244 and Ser235. Arg244 assumes a novel orientation in the allosteric inhibitor bound state and

this new orientation as well as disruption of the hydrophobic core were suggested to play a role in allosteric inhibition (Horn and Shoichet, 2004).

1.2.1. Sequence Conservation around the Allosteric Binding Site

Previous studies in our laboratory had shown that H10 dynamics are affected by BLIP binding (Doğan, 2011, Kanlıkılıçer, 2008). This region is an allosteric inhibitor binding site for TEM-1 and SHV-1 (Kuzin *et al.*, 1999, Horn and Shoichet, 2004). In order to investigate the communication between the active site and the allosteric site, detailed sequence and structural analysis of the H9-H10 region (Meneksedag *et al.*, submitted) was performed. 28 class A beta-lactamases (The list is given in Appendix A) were superimposed (Figure 1.2a) and the conserved residues were identified after the structural alignment using multiseq module (Roberts *et al.*, 2006) of VMD. Structural alignment of 28 class A beta-lactamases showed that H10 is a mobile element, while Ω loop is more rigid. H10 is most different from the others in the SHV-2 structure (PDB code: 1n9b). As expected the active site residues are highly conserved. The Trp229 residue on the H10 C-terminus and its interacting partners, Pro226 (H10) and Pro252 (in the loop connecting S4 and S5 beta sheets), highlighted in pink in Figure 1.1a and indicated by the black circle in Figure 1.2b, are also highly conserved.

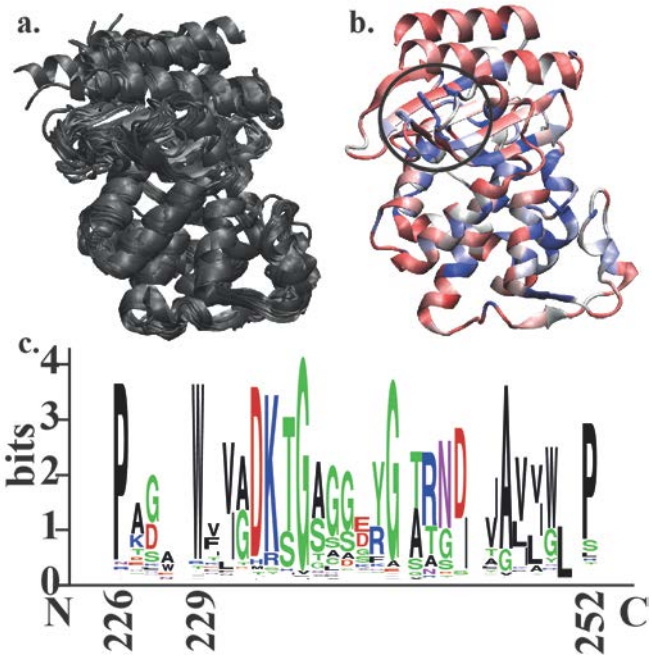

Figure 1.2. (a) Structural alignment of 28 class A beta-lactamases (b) TEM-1 structure is colored with respect to the sequence identity. Highly conserved residues are in blue and least conserved are in red. (c) Logo plot representation of the sequence alignment (Meneksedag *et al.*, submitted).

The conservation of Trp229 was further established by multiple sequence alignment of beta-lactamase sequences using COBALT (Papadopoulos and Agarwala, 2007). Top 78 sequences that align with the beta-lactamase sequence with high identity scores extracted from BLAST (Altschul *et al.*, 1990) were used as input. Representation of the resulting sequence alignment with a logo plot (Crooks *et al.*, 2004) also shows the high conservation of Trp229 across the family.

1.3. Inhibitors of Beta-lactamase

Beta-lactamase inhibitors are structurally related to penicillin; they retain the amide bond of the beta-lactam group with a modified side chain in order to bind irreversibly to beta-lactamases and render them inactive (Williams, 1999). There are two major groups of clinically important beta-lactamase inhibitors; clavulanic acid and penicillanic acid sulphone, sulbactam and tazobactam. Commercial combined therapies which are in clinical use and include both beta-lactam antibiotics and beta-lactamase inhibitors are as follows:

sulbactam combined with ampicillin and cefoperazone, tazobactam combined with piperacillin, clavulanic acid combined with ticarcillin and amoxicillin. However, the small inhibitors in clinical use are not very effective and rapidly degraded; furthermore the number of mutant beta-lactamases which are highly resistant to these commercial inhibitors is increasing rapidly (Essack, 2001, Strynadka *et al.*, 1994, Williams, 1999).

1.3.1. Beta-lactamase Inhibitory Protein

Streptomyces clavuligerus was previously shown to produce beta-lactamase inhibitory protein (BLIP). BLIP (Figure 1.3) has an amino acid sequence of 165 residues, which consists of two tandemly linked 76 amino acid domains each featuring a helix-loop-helix motif packed against a four-stranded beta sheet. The two domains of BLIP which lie next to each other result in an eight-stranded antiparallel beta sheet. In both domains, parallel orientation of helices to the strands of the sheet results in a small hydrophobic core between them (Doran *et al.*, 1990, Strynadka *et al.*, 1994). The concave surface of the eight-stranded sheet consists of predominantly polar, uncharged residues such as Ser, Thr and Tyr; there are also three tryptophan and two phenylalanine residues in this concave surface. The two analogous loops formed by Ala46 to Tyr51 and Asp135 to Gly145 located between beta strands two and three in each domain are the two significantly disordered regions of BLIP. Together with the concave surface and these two beta-hairpin loops are the key regions of interaction in beta-lactamase complexes (Strynadka *et al.*, 1996).

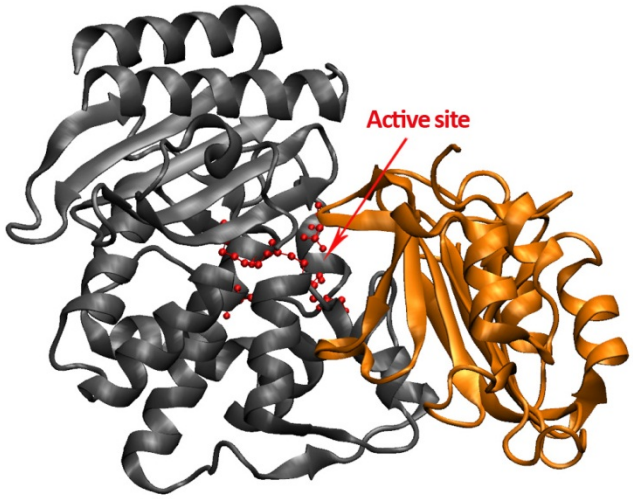

Figure 1.3. Structure of TEM-1 (gray) – BLIP (orange) complex. Active site residues are highlighted in red and indicated by the red arrow.

BLIP binds TEM-1 with 1000 fold higher affinity than it binds to SHV-1 (Petrosino *et al.*, 1999). The difference in position 104 between these two beta-lactamases, which is Glu in TEM-1 and Asp in SHV-1, was investigated (Hanes *et al.*, 2011) in order to explain the reason behind the significant difference in their affinities for BLIP. D104E mutation done in SHV-1 resulted in ~1000 fold increase in the affinity toward BLIP. A salt bridge is present in TEM-1 – BLIP complex between Glu104 of TEM-1 and Lys74 of BLIP, but it is not in SHV-1 – BLIP structure. This salt bridge was proposed to contribute the difference in the inhibitor affinity of TEM-1 and SHV-1 beta-lactamases. D104E mutation was carried out in SHV-1 – BLIP structure and the salt bridge which is determined to be present between Glu104 of TEM-1 and Lys74 of BLIP successfully restored in SHV-1 – BLIP structure. Additionally, this salt bridge was also formed with the mutation of E73M done in BLIP (Hanes *et al.*, 2011).

Beta-lactamase – BLIP interface has been extensively studied by using structural, computational, and biophysical methods. The major interactions in the active site of TEM-1 are with BLIP residues Ala46 to Tyr51 which forms a beta-hairpin. Asp49 is a key residue which forms four strong hydrogen bonds with four important conserved residues which are involved in catalysis and substrate binding; Ser130, Lys234, Ser235 and Arg244. The comparison of the structure with TEM-1 – penicillin G complex indicates the carboxylate of Asp49 mimics the carboxylate of penG (Strynadka *et al.*, 1996). Mutation

of Asp49 to Ala resulted in ~40 fold decrease in the binding affinity to TEM-1 and SHV-1 (Petrosino *et al.*, 1999, Zhang and Palzkill, 2003).

The Ala46-Tyr51 hairpin on BLIP (with the sequence of AAGDYY) is stabilized by the stacking of the phenolic rings of two Tyrosine residues in BLIP, Tyr50 and Tyr51, and a conserved Pro107 in TEM-1. A direct hydrogen bond is present between the hairpin residues and the side chain hydroxyl of Tyr105 of TEM-1. Also several van der Waals contacts with the residues in S3 beta strand, residue 235 to 238, contribute the stabilization of this beta-hairpin (Strynadka *et al.*, 1996). The roles of the fully buried charged residues, Tyr50, Tyr51 and Phe142, in the binding specificity had been studied by Alanine scanning mutagenesis (Zhang and Palzkill, 2003). Removal of Tyr50 side chain increases the binding affinity of BLIP to TEM-1 but not to SME beta-lactamase. The Y51A mutation has almost no effect on the binding affinity to TEM-1, however the mutation affect binding in SME-1 beta-lactamase by altering the position of Tyr50 of BLIP and the conformation of the loop comprised by residues 136 to 144 of BLIP, which inserts into the active site pocket of beta-lactamase (Zhang and Palzkill, 2003). The comparison between TEM-1 complexes with BLIP and PenG shows that the side chain of Phe142 of BLIP mimics the position of the benzyl group in PenG, in binding mechanism to TEM-1 beta-lactamase. The Gly residue of BLIP at position 48 helps to fill the region occupied by Phe142, thus possibly mimicking the interactions made by Phe142 (Strynadka *et al.*, 1996). The side chain of Phe142 in BLIP interacts with several active site residues, Glu104, Tyr105, Asn170, Gly238, Glu240, in TEM-1 and substitution of Ala at the position 142 resulted in significant decrease in binding affinity (Petrosino *et al.*, 1999, Zhang and Palzkill, 2003). The importance of the position 43 in BLIP occupied by a Tyr residue is also confirmed with the Alanine scanning mutagenesis; the substitution of Ala instead of Tyr resulted in ~40 fold decrease in binding affinity of TEM-1 to BLIP (Zhang and Palzkill, 2003).

Alanine-scanning mutagenesis has been used to identify BLIP hot spot residues and these residues have been grouped into six clusters that contribute to binding in an independent manner (Reichmann *et al.*, 2007a, Reichmann *et al.*, 2007b). The cluster residues of TEM-1 beta-lactamase and BLIP are given in Table 1.2. The residues that are different in SHV-1 are indicated in parenthesis.

Table 1.2. Cluster residues located in the beta-lactamase – BLIP interface (Reichmann *et al.*, 2007a).

Clusters	Beta-lactamase residues	BLIP residues
C1	Ser130, Lys234, Ser235 (Thr235), Arg243 (Arg244)	Asp49
C2	Glu104 (Asp104), Tyr105, Asn170	Lys74, Phe142, Tyr143
C3	Gln99, Asn100 (Gln100)	His148, Trp150, Arg160
C4	Val103, Pro167, Glu168	Trp162
C5	Met129, Val216	Phe36, Tyr50
C6	Glu110	Ser71, Ser113

1.3.2. Peptide Inhibitors of Beta-lactamase

The ability of BLIP to inhibit TEM-1 and SHV-1 beta-lactamases has led to the studies to investigate BLIP based peptide inhibitors. As stated before, the crystal structure of TEM-1 – BLIP indicates that residues 46 to 51 of BLIP (Figure 1.4) make critical interactions with the active site of TEM-1 beta-lactamase (Strynadka *et al.*, 1996).

In a previous study (Rudgers *et al.*, 2001) the inhibition potential of the proposed region of BLIP, residues 46 to 51, was investigated. In order to test if the beta turn from BLIP residues 47 to 50 could bind to beta-lactamase, a peptide with the sequence N-biotin-GSGCAAGDYYC-COOH was synthesized. This sequence corresponds to BLIP residues Ala 46 to Tyr 51 flanked on either side by cysteine residues. After synthesis, the peptide was oxidized in order to form a disulfide bond between these cysteine residues for generating a cyclic peptide. This cyclic peptide was shown to bind TEM-1 by ELISA. The peptide without the biotin, with a sequence of N-CAAGDYYC-COOH, bearing the BLIP residues 46 to 51 showed 603 μM inhibition which is approximately 10^6 fold weaker than BLIP. As a control peptide, a protein kinase C substrate which has no homology to BLIP based peptide was used. In order to identify whether the disulfide bond is critical for binding to beta-lactamase or not, a reduced peptide was tested for enzyme inhibition. The reduced peptide, whose sequence is identical to the cyclic one, inhibited TEM-1 at 488 μM; indicating that the disulfide bond is not required for beta-lactamase inhibition. A peptide that has a sequence identical to that of 40-51 region of BLIP was also tested for

binding to TEM-1 and the peptide was shown to inhibit TEM-1 with a K_i of 359 μM (Rudgers *et al.*, 2001).

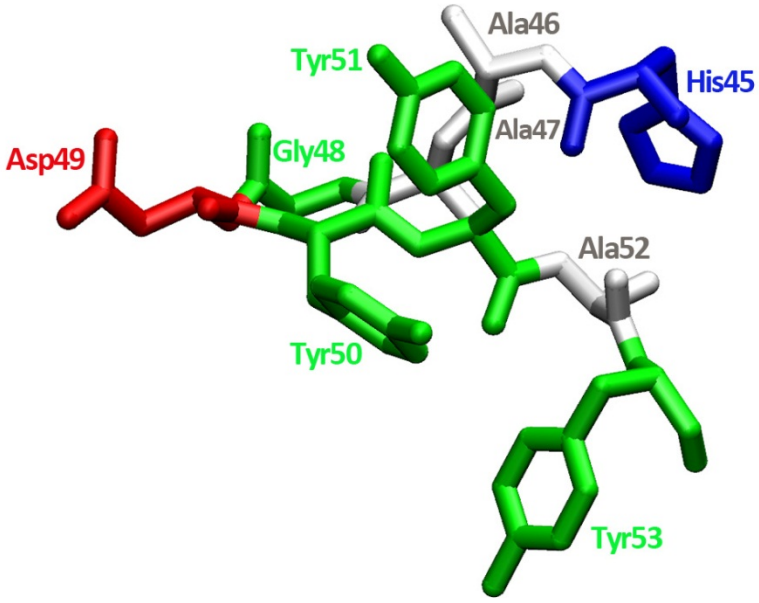

Figure 1.4. 45-53 region of BLIP (with the sequence of HAAGDYYAY). Residues are colored with respect to the amino acid types.

In another study (Huang *et al.*, 2000) phage display was used to determine which residues in the type II beta turn region of BLIP, residues 47 to 50, are critical for binding. Ala47 is at the position i, Gly48 is at i+1, Asp49 is at i+2 and Tyr50 is at i+3; in the BLIP beta turn sequence. The data obtained from phage display libraries show a strong preference for serine at position 47 (i). Glycine was selected at position 48 (i+1); other potential residues for the i+1 position are serine and alanine. For the i+2 position; asparagine, serine and aspartate residues were selected. At position i+3, threonine and glycine were identified to have the highest potential. These results indicate that although wild type BLIP binds and inhibits TEM-1, the sequence of BLIP is not optimal for binding to TEM-1 beta-lactamase (Huang *et al.*, 2000).

Another phage display study (Huang *et al.*, 2003) was carried out in order to identify the peptides that bind to TEM-1. A library of random 7-mers flanked by cysteine residues was sorted in the peptide selection. Peptide arrays were created by using SPOT synthesis.

A peptide, which has the sequence RRGHYY-NH_2, was found to play an important role in beta-lactamase binding. The importance of the specific sequence of the peptide was determined by using protein kinase substrate, kemptide with the sequence LRRASLG-NH_2, as a control. The peptide inhibited TEM-1 beta-lactamase at 136 μM, it was also shown to inhibit class B anthracis Bla1 enzyme and class C P99 beta-lactamase. This peptide shares 50% sequence identity with the 46-51 region (with the sequence of AAGDYY) of BLIP (Huang *et al.*, 2003).

The library of peptide based potential inhibitors of TEM-1 was investigated by using yeast two hybrid system (Sun *et al.*, 2005). A 24 amino acid peptide, whose sequence is FTIHCSVTAAGDYYCVHGANGTSF, named as P1 was found to inhibit the activity of TEM-1 beta-lactamase. The core region of the peptide, AAGDYY, was identified as the critical interaction region with the active site of TEM-1 beta-lactamase. The sequence of this core region is identical with the sequence 46-51 region of BLIP. In another study (Xie *et al.*, 2010), mutations and amino acid replacements were done on the previously reported peptide, P1. P1, SRFTIHCSVTAA GDYYCVHGANGTSF, and P1-A, FRFTIHCSVTAAGDAYCYHGANGTSF, were found to inhibit TEM-1, and P1-A had the strongest inhibition potential among different mutants of P1. In vivo inhibition experiments revealed that both P1 and P1-A inhibit the growth of Klebsiella pneumonia, which is resistant to penicillins and extended-spectrum cephalosporins, and P1-A showed much stronger inhibition than P1. The residue 15 in P1 is equivalent to Tyr50 in BLIP; and this Tyr residue was shown to be important in binding to beta-lactamase (Sun *et al.*, 2005, Xie *et al.*, 2010).

An inhibitory active site specific Ig (Ab1), which is able to induce anti-idiotypic Igs (Ab2) was produced by starting from beta-lactamase (Yribarren *et al.*, 2003). Beta-lactamase like Ig (IgG 9G4H9) was found to be a true anti-idiotypic Ig by generating polyclonal Ab3, which recognizes beta-lactamase. In the investigation of peptide inhibitors which are specific for the activity of beta-lactamase Ig; a peptide, whose sequence is YHFLWGP, named as Pep 90, was tested for the inhibition of 9G4H9 catalytic activity. The half inhibitory concentration (IC_{50}) for 9G4H9 was $9x10^{-5}$ M while that of BLIP was at around 10^{-5} M. Competitive ELISA, in which IgG 9G4H9 was coated on plates and incubation was done with BLIP on phage, was carried out and the results indicate that Pep

90 expel BLIP from 9G4H9 active site; thus BLIP and Pep 90 share the same interaction site. It has to be noted that the structures of Pep90 and the 46-51 region of BLIP are very different from each other. In another study (Phichith *et al.*, 2010), a cyclic form of Pep 90, whose sequence is CYHFLWGPC, was tested for the inhibition of TEM-1 beta-lactamase and penicillin binding proteins. Pep 90 was found to be a competitive inhibitor of TEM-1 with a K_i of 333±13 µM. To identify the important residues that contribute to binding, mutational analysis was performed. The aromatic residues of Pep 90 was mutated to alanine, and glycine was mutated to proline, proline was mutated to glycine. The results revealed that central tryptophan residue was essential for the inhibitory effect of Pep 90 on beta-lactamase activity. It also has to be noted that Pep 90 was identified to have a loop structure similar to that of BLIP. Inhibition properties of Pep 90 were mainly attributed to Trp and Pro residues. On the basis of that fact, two peptidomimetics were synthesized: Pep90-WAza (CYHFLWAzaGPC) and Pep90-PD (CYHFLWGPDC), where WAza is DL-7-azatryptophan and PD is the D enantiomer of proline. Both Pep90-WAza and Pep90-PD inhibited class A beta-lactamase activity with IC_{50} values of 592.2±29.6 and 436.3±21.8 µM, respectively. These values were almost two times higher than that for Pep 90, however the inhibition properties of Trp and Pro residues were reported to be maintained when they were replaced with their peptidomimetic versions (Phichith *et al.*, 2010, Yribarren *et al.*, 2003). A summary of peptides which were designed to inhibit TEM-1 beta-lactamase and their K_i values are given in Table 1.3.

Table 1.3. Peptide inhibitors of TEM-1 beta-lactamase from literature.

Peptide Sequence	**K_i Values**	**Reference**
CAAGDYYC (cyclic)	603 µM	Rudgers *et al.*, 2001
CAAGDYYC	488 µM	
HCRGHAAGDY	359 µM	
HSAYSDTRRGDYG-NH_2	298±36 µM	Huang *et al.*, 2003
RRGHYY-NH_2	136±20 µM	
AAGHYY-NH_2	438±30 µM	
CYHFLWGPC (cyclic)	333±13 µM	Phichith *et al.*, 2010
SRFTIHCSVTAAGDYYCVHGANGTSF	379 nM	Xie *et al.*, 2010
FRFTIHCSVTAAGDAYCYHGANGTSF	108 nM	
FRFTIHCSVTAAGDGYCYHGANGTSF	307 nM	
FRFTIHCSVTAAGDCYCYHGANGTSF	1650 nM	
FRFTIHCSVTAAGDRYCYHGANGTSF	2510 nM	

1.4. Objectives and Plan of the Study

In this work, using MD simulations, the dynamic properties of BLIP binding to TEM-1 and SHV-1 beta-lactamases were investigated in order to obtain information on enzyme specific and class specific properties of the ligand recognition mechanism. To this end, 10 ns MD simulations were carried out on apo TEM-1 and SHV-1 as well as on TEM-1 or SHV-1 bound to BLIP. After examining the simulations and the effect of BLIP binding to the two beta-lactamases, H10 helix was identified to be a structural element that is highly affected by BLIP binding. Furthermore, this region was observed to have a differential response to BLIP binding in TEM-1 and SHV-1. Sequence conservation analysis showed that Trp229 residue of H10 is highly conserved in the beta-lactamase family and that it has a stacking interaction with Pro229 and Pro252. In order to determine the possible contribution of this residue to the dynamics of H10 as well as to inhibitor binding, simulations were repeated with W229A mutant forms of TEM-1 and SHV-1 in the apo and BLIP bound forms.

10 different peptides were designed based on the previously reported peptide inhibitors of TEM-1 beta-lactamase and substitution of different amino acids at different positions has been carried out in order to identify the residues that contribute to binding and to design a peptide with high binding affinity toward beta-lactamase. The dynamics of the beta-lactamase – peptide complexes were investigated by 10 ns MD simulations and energetic analysis was used to determine the binding free energy. *In-vitro* enzyme kinetic experiments were carried out in order to confirm the inhibition potential and investigate the inhibition mechanism of the proposed peptides.

2. COMPUTATIONAL METHODS

2.1. Molecular Dynamics Simulations

MD simulations provide information about the internal motions and dynamical behavior of proteins on an atomic level; hence a more complete understanding of proteins can be achieved by combining theory and experiments with computer simulations. The first MD simulation of a biological macromolecule, bovine pancreatic trypsin inhibitor, was carried out 35 years ago on the ps timescale (McCammon *et al.*, 1977) and since then, with the advances in methodology and technology, the simulations are now able to be carried out with larger and more complex systems and on longer time scales (Karplus and McCammon, 2002).

MD simulations use the classical equations of motion to calculate the atomic motions as a function of time. With the given initial conditions, atomic coordinates and velocities, the forces acting on atoms are calculated by the equations;

$$m_i \ddot{r}_i = f_i \tag{2.1}$$

$$f_i = -\frac{\partial}{\partial r_i} U \tag{2.2}$$

where f_i 's are the forces acting on atoms for i=1, 2, …N. The force terms are derived by using the potential energy of the system, U (r^N), in which $r^N = r_1, r_2, \ldots r_N$ are the 3N set of atomic coordinates (Allen, 2004). The combination of these two equations is integrated for small time steps, Δt, to converge an acceptable solution.

2.1.1. Initial Coordinates

Three sets of MD simulations were carried out. In the first set, simulations on TEM-1 and SHV-1 beta-lactamases in the presence and absence of BLIP were performed. In the second set, simulations were repeated for W229A mutants of TEM-1 and SHV-1. In the

third set, simulations on TEM-1 in the presence of 10 different peptides were performed. The starting crystal structures for apo beta-lactamases and their complexes with BLIP were obtained from Protein Data Bank (PDB) (Berman *et al.*, 2000). PDB code: 1zg4 for apo TEM-1 (Stec *et al.*, 2005), PDB code: 1shv for apo SHV-1 (Kuzin *et al.*, 1999), PDB code: 1jtg for TEM-1 – BLIP complex (Lim *et al.*, 2001), PDB code: 2g2u for SHV-1 – BLIP complex (Reynolds *et al.*, 2006) were used as initial configurations. The initial coordinates of the peptides were based on either 45-52 or 45-53 region of BLIP. The missing coordinates of Asp214 on TEM-1 β-lactamase in TEM-1- BLIP complex structure were completed based on the coordinates in the apo structure. Unbound BLIP coordinates were extracted from the SHV-1 - BLIP complex structure. Building of hydrogen atoms and the computational mutagenesis were carried out by using the psfgen module of VMD (Humphrey *et al.*, 1996).

2.1.2. System Setup

The initial models were solvated in a rectangular box of TIP3 water model with a minimum margin of 10 Å. Neutralization was carried out by adding 97 Na^+ and 89 Cl^- ions in complex systems, 67 Na^+ and 60 Cl^- ions in apo systems, into the system in order to represent a more biological environment. Periodic boundary conditions were used to give the periodic cell its shape and size by defining three periodic cell basis vectors in which the vectors are perpendicular to each other to form a rectangular 3-D box. In order to prevent the escaping of molecules by crossing the periodic boundary, the coordinates of all the molecules are translated to a mirror point on the opposite side of the cell. The long range electrostatic interactions were calculated by using Particle Mesh Ewald (PME) method (Darden *et al.*, 1993). Ewald summation method is used for treating the long range electrostatic interactions in the system when periodic boundary conditions are present. A 3-D grid, namely a particle mesh, is created over a system whose charge is distributed and the forces on atoms are calculated from this system charge (Phillips *et al.*, 2005). SHAKE algorithm (Ryckaert *et al.*, 1977), which consists of a numerical integration method based on 3-N Cartesian coordinates, is used in order to constrain the bonds that involve hydrogen atoms. Energy minimization was carried out in order to remove the unfavorable interactions which may lead to failure of the simulations, with a three step procedure. The system is first minimized for 1000 steps using harmonic constraints on the protein atoms

with a force constant of 50 kcal/mol, then the procedure is repeated with a force constant of 30 kcal/mol for additional 1000 steps, and the final minimization step was carried out for 1000 steps with no constraints on protein atoms. 100 ps heating period is simulated by a gradual increase of temperature to 300 K from an initial temperature of 50 K, with 10 K increase in temperature in every 4000 steps. 10 ns simulations were then performed at a constant temperature of 300 K and a constant pressure of 1 atm. MD simulations were run by using NAMD molecular dynamics package (Phillips *et al.*, 2005), which is designed for high performance simulation of large biomolecular systems. NAMD uses the Newton equations of motions which were described in Equations 2.1 and 2.2 and a common potential energy function which comprises stretching, bending and torsional bonded interactions, and nonbonded interactions corresponding to van der Waals forces and electrostatic interactions. NAMD is compatible with CHARMM (Mackerell *et al.*, 1998) and AMBER (Weiner and Kollman, 1981) force field specifications. In this study CHARMM27 force field parameters with CMAP correction (Mackerell *et al.*, 2004) were used. A time step of 1 fs was used to integrate the Newton's equation of motion and the coordinates were stored every 1 ps.

2.2. Trajectory Analysis

2.2.1. Root Mean Square Deviations

RMSD values of the simulation snapshots with respect to the initial coordinates were calculated as an estimate of structural convergence. The calculation is done after superimposing the C_α atoms and calculating the time average of the simulation snapshots based on the period during which RMSD – time profile has reached equilibrium. The Tcl script which is used to generate the average structure is given in Appendix A. In order to be consistent in all calculations, the production run period is taken to be six ns (4-10 ns) in all simulation systems. The RMSD calculations were done over the same set of C_α atoms, TEM-1 or SHV-1 beta-lactamase, BLIP or peptide, complex; unless otherwise stated. The N- and C-terminus of the proteins are highly flexible as they are exposed to the external environment; hence they have high deviations and fluctuations. The RMSD and MSF calculations were therefore done on the C_α atoms excluding the first and last three residues of beta-lactamase (residues 29 to 287 in apo TEM-1, 29 to 285 in TEM-1 – BLIP, 29 to

289 in apo and BLIP bound SHV-1 simulations), BLIP (residues 4 to 162) and complex (as a combination of beta-lactamase and BLIP residues excluding the mentioned ones). The calculations were carried out by using the RMSD trajectory tool of VMD.

2.2.2. Mean Square Fluctuations

Mean square fluctuations (MSF) of the simulation systems are calculated as a measure of mobility. Previously calculated time averaged coordinates were used. As mentioned in previous section, the calculations were done by excluding the first and last three residues of enzyme, ligand and complex in order not to be affected by the movements of these residues. The MSF calculations were carried out by using Matlab, the script used in MSF calculations is given in Appendix A.

2.2.3. Dynamic Cross Correlations

The correlation of the atomic motions plays an important role in comprehending the biological functions of proteins; cross correlations can provide new insights about the collective motions. In order to generate the cross correlation matrices of simulation systems, equations 2.3 and 2.4 are used;

$$c\,(i,j) = < \Delta r_i . \Delta r_j > \tag{2.3}$$

$$C(i,j) = \frac{c(i,j)}{[c(i,i)c(i,j)]^{1/2}} = \frac{< \Delta r_i . \Delta r_j >}{< \Delta r_i{}^2 >^{1/2} < \Delta r_j{}^2 >^{1/2}} \tag{2.4}$$

in which Δr_i and Δr_j are the displacement vectors for atoms *i* and *j*, respectively and *c(i,j)* is the covariance. The brackets represent the ensemble average. The diagonal elements of the covariance matrix (i=j) are the mean square fluctuations, $<\Delta r_i^2>$. The cross correlations or normalized covariance is calculated with Equation 2.4. For completely correlated motions *C(i,j)* = 1, for completely anticorrelated motions *C(i,j)* = -1 (Ichiye and Karplus, 1991).

2.2.4. Intermolecular Interaction Energy Calculations

Nonbonded interactions, comprising the van der Waals and electrostatic interactions, between enzyme and ligand (BLIP or peptide) were calculated by using the NAMD energy plugin of VMD for the simulation time points. The calculations were done every 250 ps of the simulation trajectories and the retrieved energy values were averaged based on the six ns production period.

2.2.5. Binding Free Energy Calculations

Binding free energy between enzyme and ligand or peptide was calculated by using FoldX algorithm, which provides a quantitative estimate of the importance of the interactions contributing to the stability of proteins and protein complexes (Schymkowitz *et al.*, 2005). The simulation snapshots were generated every 25 ps from the trajectory files by using Wordom (Seeber *et al.*, 2007). The snapshots were then treated by using RepairPDB command of FoldX, which identifies the residues with bad torsion angles, van der Waals' clashes or total energy and repairs them. The repairing procedure is as follows: First all the Asn, Gln and His residues are identified and flipped by 180 degrees in order to prevent the incorrect rotamer assignment caused by symmetry observed in the electron density of these amino acids' carboxamide groups. Then a small optimization step is carried out to eliminate small van der Waals' clashes. The residues that have bad energies are identified and the amino acid side chains are optimized in order to explore different rotamer combinations and find new energy minima (Schymkowitz *et al.*, 2005).

The repaired pdb files were used as input to binding free energy calculations. The analysis was carried out by using the AnalyzeComplex command, which determines the interaction energy between two molecules by unfolding the selected targets and determining the stability of remaining molecules, and then subtracting the sum of the individual energies from the global energy. The FoldX force field uses Equation 2.5 in the free energy calculations,

$$\Delta G = a.\Delta G_{vdw} + b.\Delta G_{solvH} + c.\Delta G_{solvP} + d.\Delta G_{wb} + e.\Delta G_{hbond} + f.\Delta G_{el} + g.\Delta G_{kon} + h.T\Delta S_{mc} + k.T\Delta S_{sc} + l.\Delta G_{clash} \quad (2.5)$$

in which ΔG_{solvH} and ΔG_{solvP} are the hydrophobic and polar solvation terms, ΔG_{vdw} represents the sum of van der Waals contributions. ΔG_{wb} term consists of an explicit calculation of the interactions between protein and water molecules involving more than two hydrogen bonds. ΔG_{hbond} represents the energy of hydrogen bonds and ΔG_{el} is the electrostatic contribution to the free energy which is calculated from the Coulomb's law. ΔG_{kon} is an additional electrostatic contribution which is calculated between atoms of different polypeptide chains. The entropic cost of fixing the backbone and side chains is represented by ΔS_{mc} and ΔS_{sc}, respectively. ΔG_{clash} is a measure of the steric overlaps between atoms. The coefficients a, b, c, d, e, f, g, h, k and l are the relative weights of the different energy terms (Schymkowitz *et al.*, 2005).

2.2.6. Flexible Peptide Docking to Beta-lactamase

Flexible docking of peptides to TEM-1 beta-lactamase was carried out by using Rosetta FlexPepDock webserver which refines the starting structures in 200 independent simulations and ranks them based on their Rosetta generic full atom energy score (London *et al.*, 2011). In Rosetta energy function, atomic interactions are calculated using Lennard-Jones potential, implicit solvation model is used in describing hydrophobic effects and electrostatic desolvation cost related to burial of polar atoms, and hydrogen bonds are defined by the explicit hydrogen bonding potential. The explicit solvent structure, long range electrostatic interactions, residual dynamics and massive entropy change of the molecule are omitted in the all atom Rosetta energy function. The interface energy, which is the total energy of the complex less the energy of its partners when separated, was investigated in all the enzyme – peptide complexes (Das and Baker, 2008).

3. LIGAND BINDING ANALYZED BY MOLECULAR DYNAMICS SIMULATIONS

MD simulations were performed on apo and BLIP bound forms of both wild type and mutant TEM-1 and SHV-1 beta-lactamases and on TEM-1 and BLIP based peptide complexes. The simulation trajectories were analyzed in order to determine the change in dynamics and energetics upon mutation and binding of ligand to beta-lactamase. Three new simulations were performed in this study; the other simulations were obtained from previous studies done in our laboratory (Doğan, 2011, Kanlıkılıçer, 2008). All of the simulations were analyzed and compared in the following sections using new analysis methods and calculations.

3.1. Simulations on Beta-lactamase – BLIP Complexes

MD simulations of both wild type and mutant TEM-1 and SHV-1 beta-lactamases in the apo form or in complex with BLIP were performed for 10 ns. The list of simulation systems is given in Table 3.1.

3.1.1. Stability of Simulation Systems

As a first step, the stability of the simulations was investigated by examining the RMSD – time profiles of enzyme ligand and complex coordinates and by calculating the RMSD between the time averaged coordinates and the initial coordinates (Table 3.1). The RMSD calculations were carried out with the procedure described in Section 2.2.1. The RMSD values were calculated over the same set of atoms, such as beta-lactamase C_α atoms, BLIP C_α atoms or complex C_α atoms. The average C_α coordinates deviated from the initial structures by 0.8-1.3 Å for the beta-lactamase, 0.6-1.4 Å for BLIP and 1.1-1.9 Å for the complex C_α atoms, showing that the simulations reached equilibrium at a relatively similar structure to the initial coordinates. In addition, the RMSD between the time averaged and initial coordinates of the six structural elements, which were identified to be important in terms of ligand interactions, are listed in Table 3.2.

Table 3.1. RMSD values (Å) of beta-lactamase, BLIP and complexes in each simulation system and MSF values ($Å^2$) are in parenthesis. Simulations marked with asterisks were from previous studies (*: Kanlıkılıçer, 2008; **: Doğan, 2011).

Simulation system	Beta-lactamase	BLIP	Complex
Apo TEM-1*	0.76 (0.38)		
Apo TEM-1 W229A**	0.94 (0.34)		
TEM-1 – BLIP*	0.82 (0.27)	1.43 (0.34)	1.87 (0.46)
TEM-1 W229A – BLIP	1.02 (0.36)	0.69 (0.36)	1.16 (0.54)
Apo SHV-1**	0.97 (0.29)		
Apo SHV-1 W229A	1.35 (0.42)		
SHV-1 – BLIP**	0.81 (0.31)	0.82 (0.44)	1.08 (0.53)
SHV-1 W229A – BLIP	1.14 (0.34)	1.00 (0.37)	1.42 (0.62)
BLIP*		0.64 (0.54)	

Table 3.2. RMSD values (Å) of the structurally important regions of beta-lactamase. MSF values ($Å^2$) are in parenthesis

Simulation system	H10 helix	H9-H10 helices	99-112 loop	Ω loop	Ω loop flexible tip	Active site residues
Apo TEM-1	1.64 (0.88)	1.25 (0.66)	0.67 (0.50)	0.59 (0.32)	1.21 (0.82)	0.56 (0.22)
Apo TEM-1 W229A	2.14 (0.72)	1.92 (0.55)	0.90 (0.43)	0.69 (0.38)	1.43 (1.05)	0.56 (0.20)
TEM-1 – BLIP	0.89 (0.64)	1.05 (0.53)	0.86 (0.22)	0.99 (0.28)	1.38 (0.80)	0.71 (0.12)
TEM-1 W229A – BLIP	2.69 (0.96)	2.02 (0.70)	0.38 (0.29)	1.09 (0.35)	2.00 (1.05)	0.64 (0.15)
Apo SHV-1	2.67 (0.37)	2.02 (0.31)	0.65 (0.42)	0.55 (0.27)	0.64 (0.66)	0.59 (0.12)
Apo SHV-1 W229A	3.56 (0.95)	3.16 (0.72)	1.78 (0.92)	0.68 (0.31)	0.78 (0.75)	0.99 (0.25)
SHV-1 – BLIP	1.31 (0.61)	0.99 (0.39)	0.93 (0.35)	1.08 (0.58)	0.86 (1.28)	0.67 (0.23)
SHV-1 W229A – BLIP	2.06 (0.71)	1.82 (0.47)	1.12 (0.32)	1.40 (0.50)	1.73 (1.03)	1.10 (0.19)

Beta-lactamase and BLIP binding interface is divided into six clusters which comprise important interactions between the enzyme and ligand (Reichmann *et al.*, 2007a, b), as previously stated in the Section 1.3.1 and listed in Table 1.2. The RMSD and MSF values of these regions were calculated and compared in order to analyze the change in the interaction between beta-lactamases and BLIP due to the W229A mutation (Table 3.3).

Table 3.3. RMSD values (Å) of the cluster residues of beta-lactamase in complex structures. MSF values ($Å^2$) are in parenthesis.

Simulation system	**C1**	**C2**	**C3**	**C4**	**C5**	**C6**
TEM-1 – BLIP	0.38 (0.10)	0.67 (0.15)	1.60 (0.32)	0.52 (0.16)	1.04 (0.20)	0.65 (0.25)
TEM-1 W229A – BLIP	0.58 (0.13)	0.45 (0.22)	0.68 (0.43)	0.59 (0.19)	1.49 (0.56)	0.27 (0.22)
SHV-1 – BLIP	0.46 (0.13)	1.00 (0.39)	1.59 (0.60)	0.92 (0.29)	0.78 (0.19)	0.65 (0.27)
SHV-1 W229A - BLIP	1.04 (0.15)	1.19 (0.29)	1.75 (0.53)	1.08 (0.23)	1.95 (0.27)	0.87 (0.29)

3.1.1.1. Stability of Apo Beta-lactamases. The time averaged Cα coordinates of TEM-1 beta-lactamase deviated from the initial Cα coordinates by 0.8-1.0 Å (Table 3.1). The RMSD profiles of TEM-1 beta-lactamase suggest that TEM-1 stays close to its initial coordinates with RMSD values of less than 2 Å during 10 ns simulations (Figure 3.1).

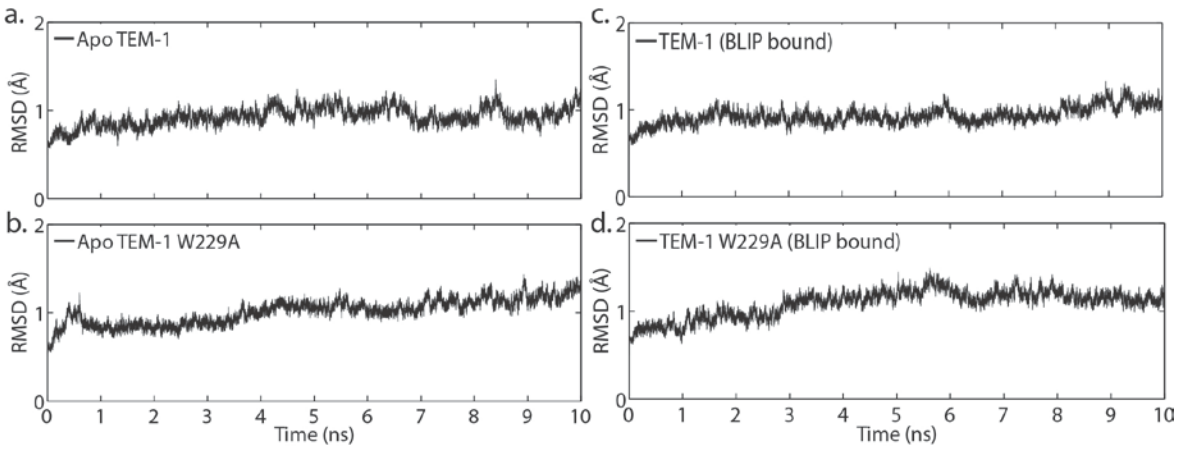

Figure 3.1. RMSD profile of (a) apo TEM-1, (b) apo TEM-1 W229A, (c) BLIP bound TEM-1, (d) BLIP bound TEM-1 W229A beta-lactamase during 10 ns MD simulations.

The time averaged C_α coordinates of SHV-1 beta-lactamase deviated from the initial C_α atoms 0.8-1.3 Å (Table 3.1). The RMSD profiles of SHV-1 beta-lactamase (Figure 3.2) show that SHV-1 stays close to its initial coordinates with a RMSD value of less than 2 Å.

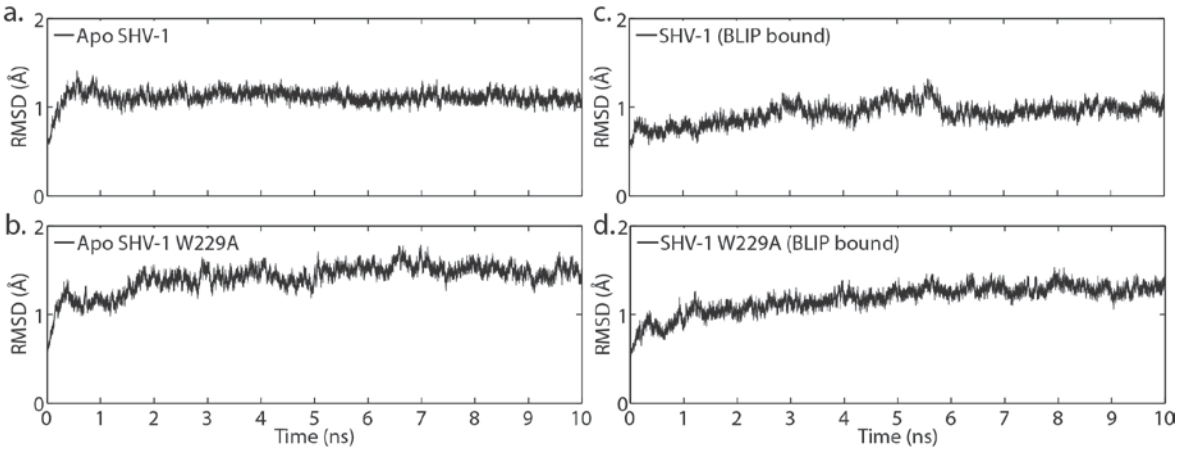

Figure 3.2. The RMSD profile of (a) apo SHV-1, (b) apo SHV-1 W229A, (c) BLIP bound SHV-1, (d) BLIP bound SHV-1 W229A beta-lactamase during 10 ns MD simulations.

When the RMSD values of the structurally important regions were examined, the H10 and H9-H10 helices regions were found to deviate more in SHV-1 compared to TEM-1. The RMSD values of these regions were 1.64 and 1.25 Å in TEM-1 while that of SHV-1 were 2.67 and 2.02 Å, respectively (Table 3.2). The 99-112 and the Ω loops, and the active site residues behaved similar in terms of stability in both beta-lactamases, however a major decrease in the flexible tip of the Ω loop was observed in SHV-1. The RMSD value of the

Ω loop flexible tip was 1.21 Å in TEM-1 while that of SHV-1 was almost half of the value observed in TEM-1, 0.64 Å (Table 3.2).

3.1.1.2. Effect of BLIP Binding on the Stability of Beta-lactamases. Upon BLIP binding, the RMSD value between the average and initial TEM-1 coordinates stays the same at around 0.8 Å. The RMSD profiles of apo and BLIP bound TEM-1 (Figure 3.1a, c) were also similar to each other reaching equilibrium at a value of less than 1 Å. While BLIP binding does not significantly affect the overall deviation of TEM-1, it affects the deviation of the structurally important regions such as 99-112 loop, Ω loop and the active site. Upon BLIP binding, the deviation of these regions from their initial coordinates increased remarkably. The small increase in the overall beta-lactamase deviation was caused by these regions, since the RMSD values of H10 helix and H9-H10 helices region decreased as a result of BLIP binding from their initial values of 1.64 Å and 1.25 Å, to 0.89 Å and 1.05 Å; respectively.

The RMSD value of SHV-1 in apo form (0.97 Å) was higher than in BLIP bound form (0.81 Å) (Table 3.1). When the individual structural components were examined, it is observed that the decrease in the overall RMSD value upon BLIP binding was caused by the H10 helix and H9-H10 helices region. The RMSD of these regions in apo form were 2.67 Å and 2.02 Å, respectively. Upon binding of BLIP to SHV-1, the RMSD of these regions became 1.31 Å and 0.99 Å, respectively (Table 3.2). This suggests that, binding of BLIP makes the H9-H10 helices and so the beta-lactamase itself deviate less than its initial coordinates.

When the stability of the cluster residues was examined, it was observed that the cluster residues behave in a different manner in TEM-1 and SHV-1. The RMSD values of C1, C2 and C4 were higher in SHV-1 compared to TEM-1, while a significant decrease was apparent in SHV-1. The RMSD values of C3 and C6 were almost the same in both beta-lactamases (Table 3.3).

3.1.1.3. Effect of W229A Mutation on the Stability of Apo Beta-lactamases. A significant change in the deviation was observed upon W229A mutation in TEM-1 beta-lactamase. In the apo structure of TEM-1, the overall beta-lactamase deviation increased as a result of

mutation. W229A mutation affected all the structurally important regions which are listed in Table 3.2 and caused an overall increase in the RMSD value from 0.76 Å to 0.94 Å (Table 3.1). The RMSD – time profile of TEM-1 W229A mutant (Figure 3.1b) was similar to that of wild type TEM-1 (Figure 3.1a).

Mutation of W229A caused an overall increase in apo SHV-1 (Table 3.1). The RMSD values of beta-lactamase and all the individual structural components became higher as a result of mutation (Table 3.2). The RMSD – time profile of wild type SHV-1 (Figure 3.2a) was more stable compared to that of mutant SHV-1 (Figure 3.2b).

3.1.1.4. Effect of W229A Mutation on the Stability of BLIP bound Beta-lactamases. In BLIP bound simulations, despite the overall increase in TEM-1 deviation, the structurally important regions had a different response to W229A mutation. H9-H10 helices region and the Ω loop deviated more than their wild type coordinates but the 99-112 loop and active site residues became more stable. A significant change was observed in 99-112 loop, its RMSD decreased from 0.86 Å and became 0.38 Å as a result of mutation (Table 3.2).

When the RMSD values of the cluster residues of BLIP bound simulations of TEM-1 in both wild type and mutant forms were examined, it was observed that C1 and C5 deviated more in the mutant form while C2, C3 and C6 deviated less. The RMSD values of C1 and C5 were 0.38 and 1.04 Å in wild type; 0.58 and 1.49 Å in mutant, respectively. The RMSD values of clusters that deviate less upon mutation, C2, C3 and C6, were 0.67, 1.60 and 0.65 Å in wild type; 0.45, 0.68 and 0.27 Å in mutant, respectively. The C4 had an RMSD value of at around 0.5 Å in both wild type and mutant, indicating that mutation does not have a major effect in the deviations observed between Met129 and Val216 in TEM-1 and Phe36 and Tyr50 in BLIP (Table 3.3).

Mutation of W229A caused an overall increase in BLIP bound SHV-1 (Table 3.1). The RMSD values of beta-lactamase and all the individual structural components became higher as a result of mutation (Table 3.2). A major deviation was observed in cluster residues of BLIP bound SHV-1 structure upon mutation of W229A. All the RMSD values of the cluster residues increased, especially C1 and C5 are the clusters which were affected

most by the mutation. The difference between wild type and mutant RMSD values of C1 and C5 was 0.6 and 1.2 Å, respectively (Table 3.3).

3.1.1.5. Stability of BLIP. The average Cα coordinates of BLIP deviated from its initial coordinates 0.6-1.4 Å in all simulation systems (Table 3.1). BLIP stays closer to its initial coordinates during beta-lactamase bound simulations (Figure 3.3).

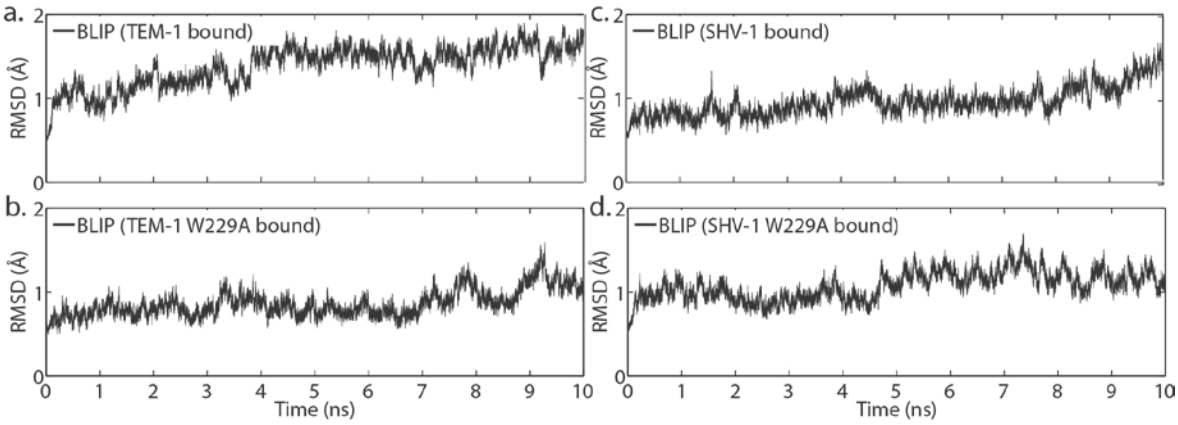

Figure 3.3. The RMSD profile of (a) TEM-1 bound, (b) TEM-1 W229A bound, (c) SHV-1 bound, (d) SHV-1 W229A bound BLIP during 10 ns MD simulations.

Apo BLIP had a RMSD value of 0.64 Å. Upon TEM-1 binding, its RMSD increased to 1.43 Å; however, when TEM-1 W229A bound, it stays close around 0.6 Å. Binding of SHV-1 to BLIP increased its RMSD to a value of 0.82 Å. However a sudden increase in the RMSD profile of SHV-1 bound BLIP was detected in the last ns of the simulation timescale (Figure 3.3c). Unlike the behavior observed in binding of TEM-1 W229A to BLIP, upon binding of mutant SHV-1, the RMSD of BLIP increased to 1.00 Å; and the RMSD profile of SHV-1 bound BLIP, which tend to increase by the end of simulation, was stabilized (Figure 3.3d).

3.1.1.6. Stability of Beta-lactamase – BLIP Complexes. The RMSD values of the complex systems were lower than 2 Å (Table 3.1), suggesting that average coordinates of the beta-lactamase – BLIP complexes stay close to their starting coordinates. The RMSD – time profiles of the simulation systems are given in Figure 3.4.

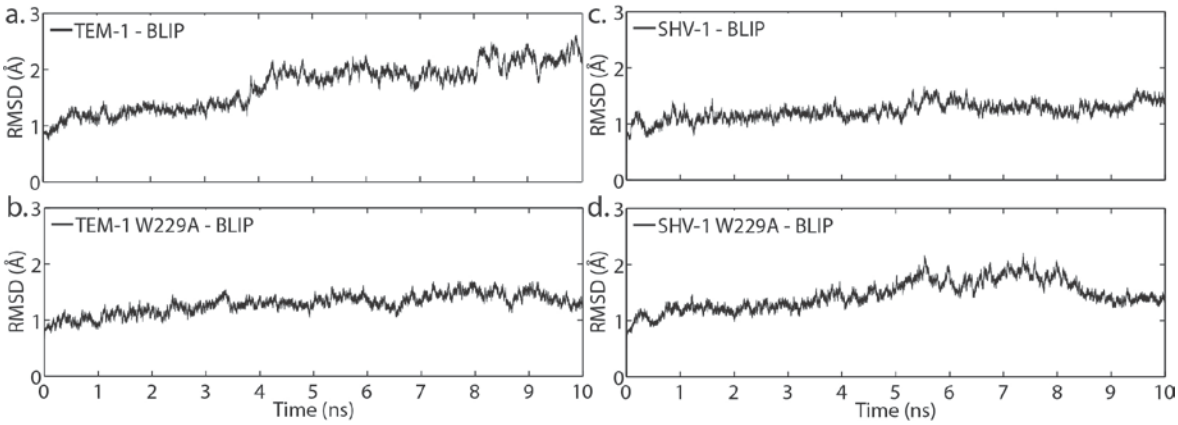

Figure 3.4. The RMSD profile of (a) TEM-1 – BLIP, (b) TEM-1 W229A – BLIP, (c) SHV-1 – BLIP, (d) SHV-1 W229A – BLIP during 10 ns MD simulations.

TEM-1 – BLIP complex has the highest RMSD value among the complex simulation systems with a value of 1.87 Å. The deviations could be observed in the RMSD – time profile (Figure 3.4a). The RMSD value of TEM-1 W229A – BLIP complex was lower at 1.16 Å. This is caused by the lower RMSD value of BLIP in the mutant TEM-1 bound form (0.69 Å) compared to that in the wild type TEM-1 bound form (1.43 Å). In contrast to the response observed upon mutation in TEM-1 complexes, W229A mutation increased RMSD value of SHV-1 – BLIP complex from 1.08 Å to 1.42 Å.

3.1.2. Structural Changes in Simulation Systems due to Mutation

The structural changes between the starting coordinates (1zg4 and 1shv for apo TEM-1 and apo SHV-1; 1jtg and 2g2u for TEM-1 and SHV-1 – BLIP complexes; respectively) and the simulation trajectories were further analyzed by displaying the overlaid structures of initial and time averaged coordinates. Apo TEM-1 and apo SHV-1 average structures are almost the same as their initial structures (Figure 3.5a, c). W229A mutation distorts the H10 helix in apo TEM-1 (Figure 3.5b). In apo SHV-1, mutation causes a part of the 99-112 region to bend, hence Tyr105 gets closer to the region which is occupied by BLIP in the bound form (Figure 3.5d).

In BLIP bound forms, TEM-1 and SHV-1 stay close to their starting coordinates (Figure 3.6a, c). Mutation of W229A causes Val216 to move upwards in TEM-1 by affecting the H10 helix (Figure 3.6b). As observed in TEM-1, Arg215 and Val216 move

from their initial coordinates by shifting to left and upwards, respectively as a result of the H9-H10 helices deviation, in SHV-1 (Figure 3.6d). The stacking arrangement between Pro226, Trp229 and Pro252 (Pro251 in TEM-1 – BLIP complex) is conserved in all wild type simulations.

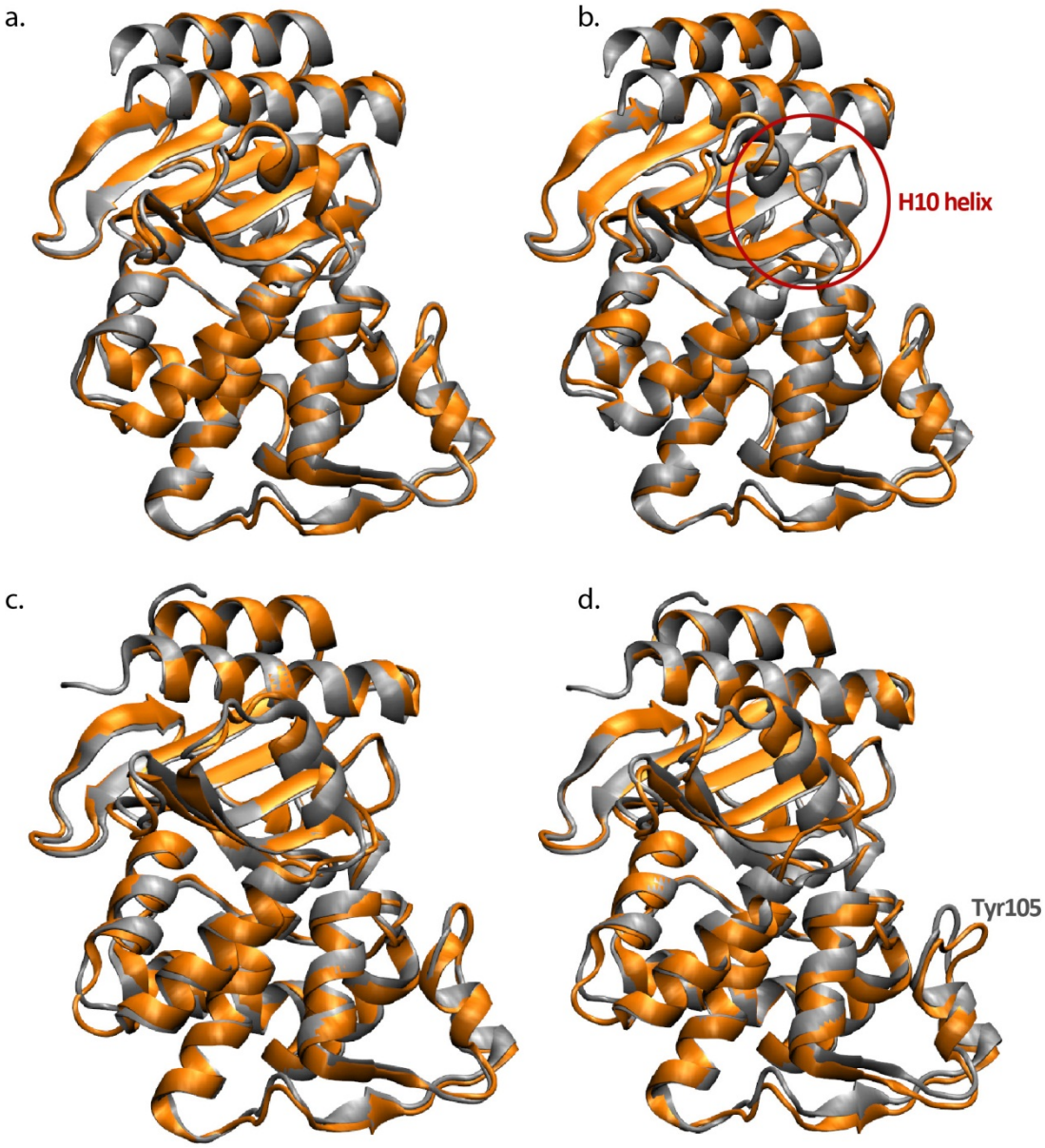

Figure 3.5. Cartoon representation of simulation systems. Initial coordinates are in silver, average simulation structures are in orange. (a) 1zg4 and apo TEM-1. (b) 1zg4 and apo TEM-1 W229A. (c) 1shv and apo SHV-1. (d) 1shv and apo SHV-1 W229A.

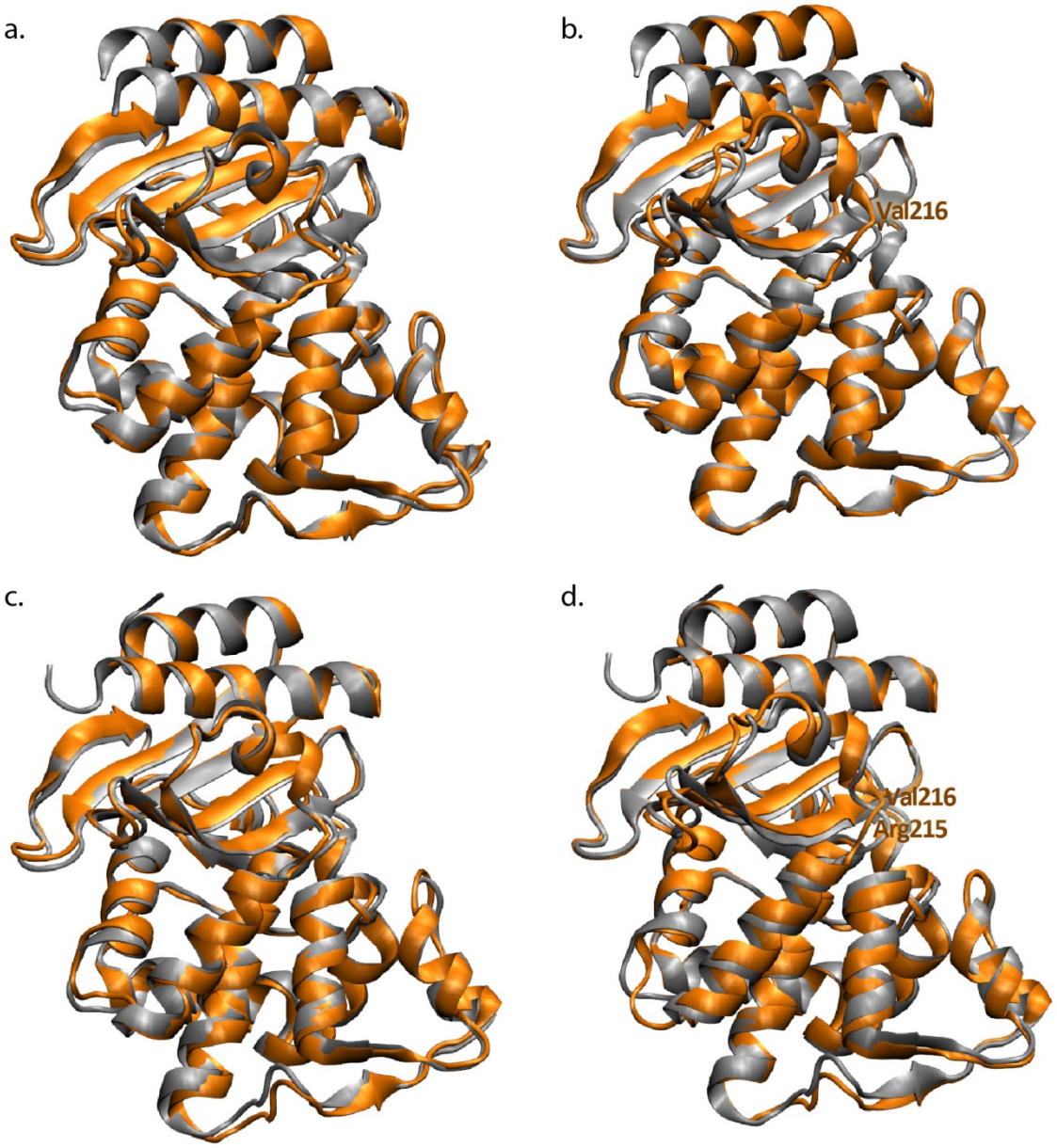

Figure 3.6. Cartoon representation of simulation systems. Initial coordinates are in silver, average simulation structures are in orange. (a) 1jtg and TEM-1 – BLIP. (b) 1jtg and TEM-1 W229A – BLIP. (c) 2g2u and SHV-1 – BLIP. (d) 2g2u and SHV-1 W229A – BLIP.

3.1.3. Dynamics of the Simulation Systems

The regions that contribute to the difference in structure and fluctuations in the simulations were identified by calculating and comparing the residue based MSF values for the different simulation systems. The MSF values of the C_α atoms of the beta-lactamases were calculated after aligning all C_α atoms of the beta-lactamases, except for the 3 N-terminus residues and the three C-terminus residues (calculations were done with the

residues 29 to 287 in apo TEM-1, 29 to 285 in TEM-1 – BLIP, 29 to 289 in apo and BLIP bound SHV-1 simulations). The same procedure was followed for the calculation of the MSF values of BLIP and beta-lactamase – BLIP complexes. The MSF values of the C_α atoms of BLIP in all simulation systems were calculated after aligning all C_α atoms of BLIP, except for the 3 N-terminus and 3 C-terminus residues of BLIP, calculations were done on residues 4 to 162 of BLIP. The complex MSF values were calculated with the combination of these 2 procedures, the first and last 3 residues of beta-lactamase and the first and last 3 residues of BLIP were excluded.

3.1.3.1. Change in Dynamics upon BLIP Binding. The average and residue based MSF values were calculated in order to analyze the change in dynamics upon BLIP binding to TEM-1 and SHV-1.

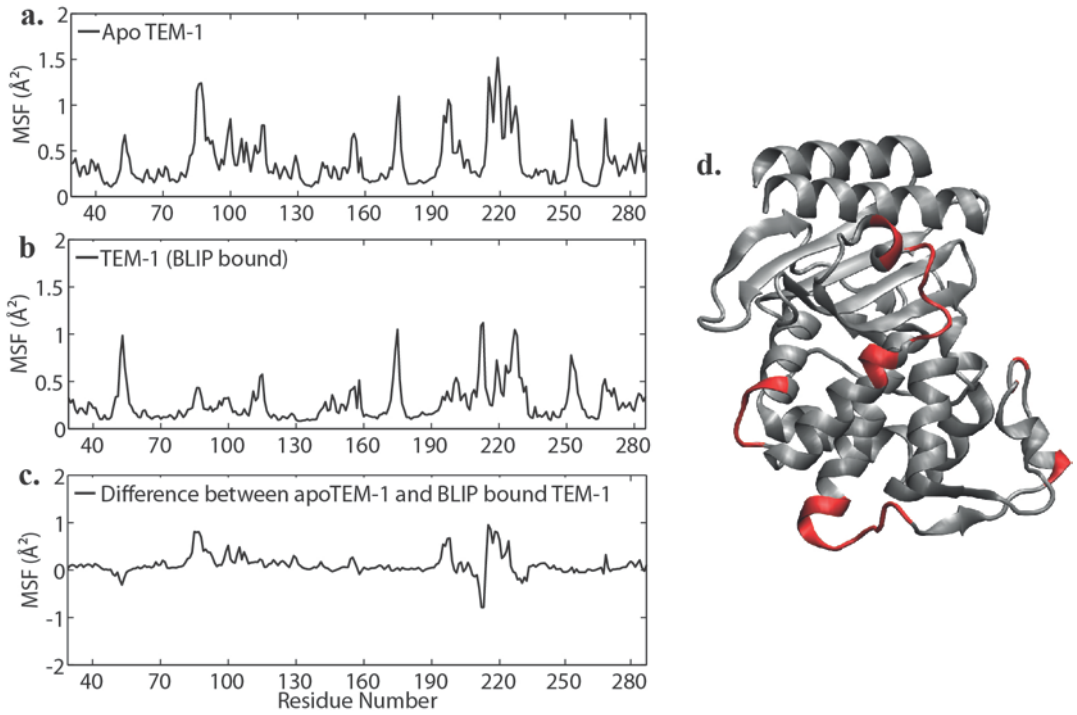

Figure 3.7. The MSF values for the C_α atoms of (a) apo TEM-1, (b) BLIP bound TEM-1 simulations. (c) The difference in MSF values between apo and BLIP bound TEM-1. (d) TEM-1 structure in cartoon representation is shown with the red color indicating regions of MSF difference higher than 0.35 $Å^2$.

TEM-1 loses mobility upon BLIP binding; the MSF value for apo TEM-1 was 0.38 $Å^2$ while it was 0.27 $Å^2$ in the BLIP bound form (Table 3.1). The decrease in overall beta-

lactamase mobility could be observed in all the structurally important regions (Table 3.2). When the residue based MSF values were examined, in apo TEM-1 simulation, the regions which show fluctuations higher than a threshold of 0.7 $Å^2$ were localized to the loop connecting H2 and H3 helices, the N-terminus and C-terminus of the 99-112 loop, the flexible tip of the Ω loop, the loop connecting H8 and H9 helices, H10 helix, the loop connecting S4 and S5 beta sheets (especially residue 254) and the C-terminus of the S5 beta sheet (Figure 3.7a).

The residues which show higher fluctuations than the threshold of 0.7 $Å^2$ in BLIP bound TEM-1 simulation were localized to the regions comprised by the loop connecting S1 and S2 beta sheets, the flexible tip of the Ω loop, H9-H10 helices and the loop connecting S4 and S5 beta sheets (especially residue 254) (Figure 3.7b).

When the difference in MSF (ΔMSF) between the apo and bound simulations was examined, the residues which show higher fluctuations than the threshold of 0.35 $Å^2$ were localized to the regions comprised by the C-terminus of the H2 helix, the loop connecting H2 helix and SC1 beta sheet, 99-112 loop, the loop connecting the H8 and H9 helices and the H9-H10 helices region. All the mentioned regions had higher fluctuations in apo form except the 3 C-terminus residues of H9 helix, which are Met211, Glu212 and Ala213 (Figure 3.7c, d).

SHV-1 mobility nearly stays the same at around 0.30 $Å^2$ upon binding of BLIP. However a significant increase was observed in some structurally important regions such as H10 helix, Ω loop and active site. The mobility of these regions increased almost two-fold compared to the MSF values in the apo state (Table 3.2).

When the residue based MSF values were examined, the loop connecting H2 and H3 helices, C-terminus of the H3 helix, the flexible tip of the Ω loop, the loop connecting H8 and H9 helices, C-terminus of the H10 helix and the loop connecting S4 and S5 beta sheets showed higher fluctuations than the threshold of 0.7 $Å^2$ (Figure 3.8a). Compared to apo TEM-1, it can be said that similar regions show high fluctuations.

In the BLIP bound form of SHV-1, the residues with high fluctuations are found in the loop connecting S1 and S2 beta sheets, the loop connecting H2 and H3 helices, the Ω loop and the H10 helix (Figure 3.8b). These regions are also flexible in the apo simulation. On the other hand, ΔMSF values between apo and BLIP bound simulations showed that the 3 loops connecting H2 and H3 helices, H8 and H9 helices and S4 and S5 beta sheets were more mobile in apo SHV-1. Upon binding of BLIP, the regions comprised by the Ω loop and the N-terminus of the H10 helix had increased mobility (Figure 3.8c, d).

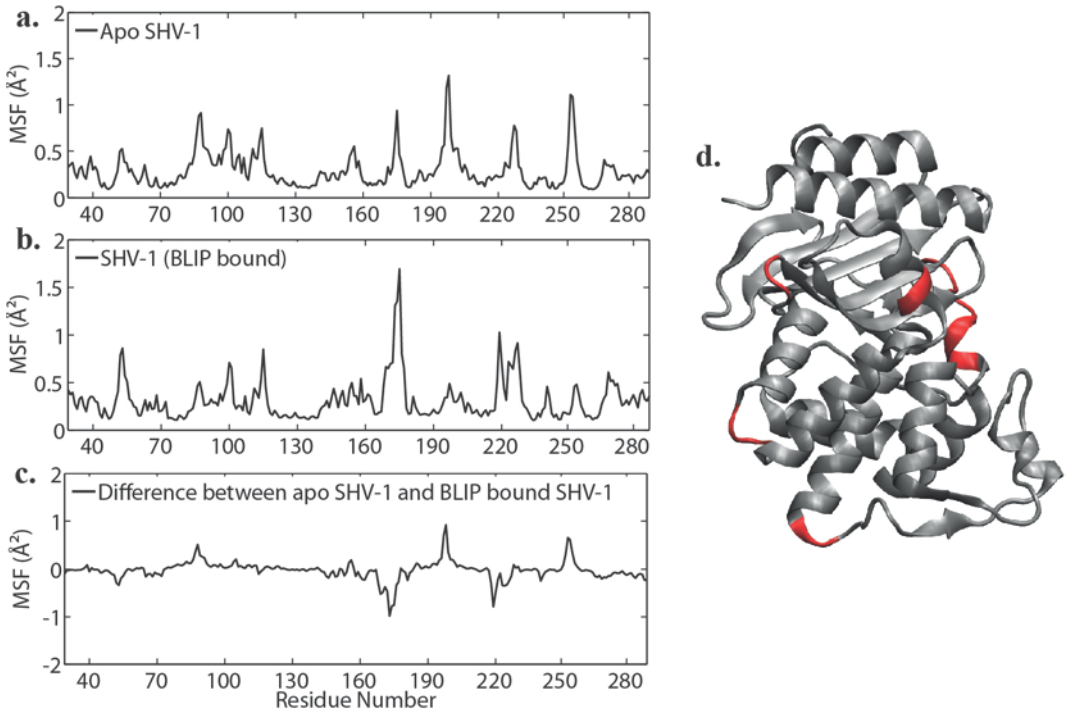

Figure 3.8. The MSF values for the C_α atoms of (a) apo SHV-1, (b) BLIP bound SHV-1 simulations. (c) The difference in MSF values between apo and BLIP bound SHV-1. (d) SHV-1 structure in cartoon representation is shown with the red color indicating regions of MSF difference higher than 0.35 $Å^2$.

The MSF values of the clusters of BLIP bound TEM-1 and SHV-1 were compared and a more mobile behavior was observed in BLIP bound SHV-1. All the MSF values of the cluster residues of SHV-1 were higher than those of TEM-1 (Table 3.3). A major difference in mobility is seen in C2, C3 and C4. Their MSF values were 0.15, 0.32 and 0.16 $Å^2$ in BLIP bound TEM-1, and they increased to 0.39, 0.60 and 0.29 $Å^2$ in BLIP bound SHV-1, respectively.

3.1.3.2. Change in Dynamics upon W229A Mutation. The average and residue based MSF values were calculated and compared in order to analyze the change in dynamics upon the mutation of a highly conserved beta-lactamase residue, Trp229, to Alanine. The effect of mutation on mobility of beta-lactamase was examined in both apo and BLIP bound simulations.

Apo TEM-1 loses mobility upon W229A mutation, the MSF values for wild type and mutant were 0.38 $Å^2$ and 0.34 $Å^2$, respectively. Although the change in overall MSF was not significant, the examination of the MSF values of the structurally important regions showed that the regions except the Ω loop lost mobility upon mutation (Table 3.2).

Similar regions, such as the loop connecting H2 and H3 helices, Ω loop, the loop connecting H8 and H9 helices, H9-H10 helices, the loop connecting S4 and S5 beta sheets, exhibited fluctuations in wild type and mutant apo TEM-1 simulations (Figure 3.9a, b).

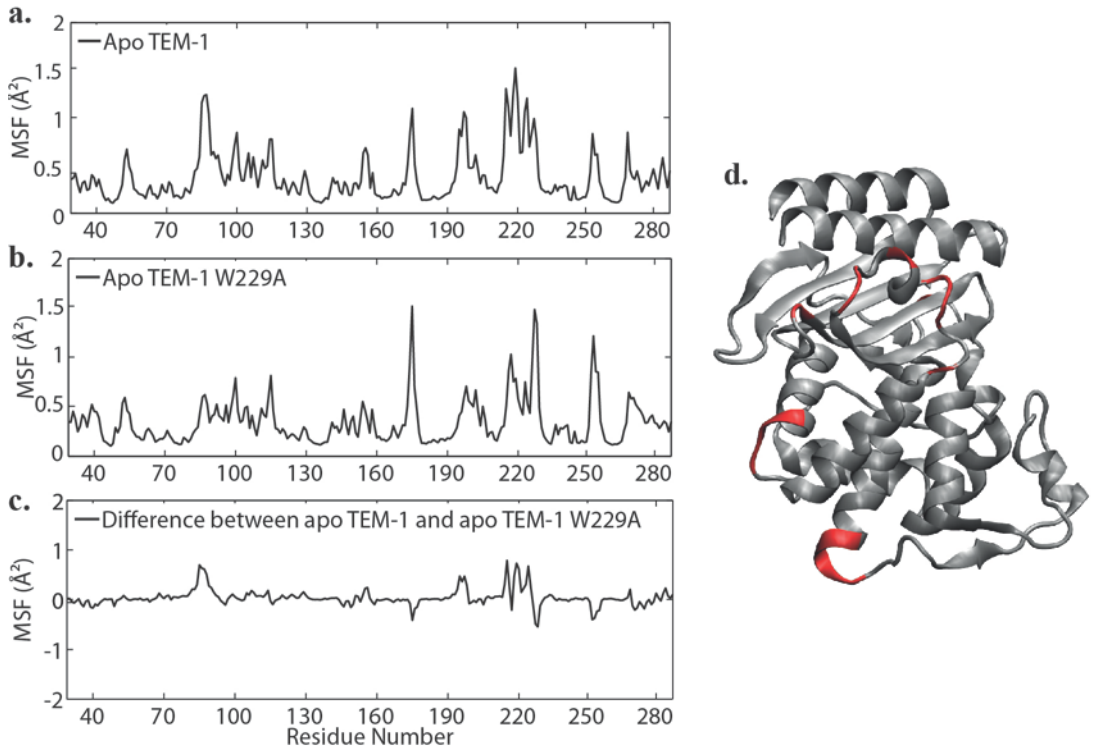

Figure 3.9. The MSF values for the C_α atoms of (a) apo TEM-1, (b) apo TEM-1 W229A. (c) The difference in MSF values between wild type and mutant forms of apo TEM-1. (d) TEM-1 structure in cartoon representation is shown with the red color indicating regions of MSF difference higher than 0.35 $Å^2$.

When the ΔMSF values between wild type and mutant apo TEM-1 were examined, it was observed that almost all the high fluctuating regions were located in wild type. Only the Ω loop, C-terminus of the H10 helix and the N-terminus of the loop connecting S4 and S5 beta sheets (residues 252 and 254) became more mobile upon mutation (Figure 3.9c, d).

In contrast to the response to W229A mutation in terms of mobility detected in apo TEM-1 simulations, mutation favors mobility in BLIP bound forms. The overall MSF value of beta-lactamase in wild type was 0.27 $Å^2$, while it was 0.36 $Å^2$ in mutant (Table 3.2). The mobility of the individual structural elements has increased as a result of mutation. The most significant increase was observed in H10 helix and H9-H10 helices region and also in the flexible tip of the Ω loop (Table 3.2).

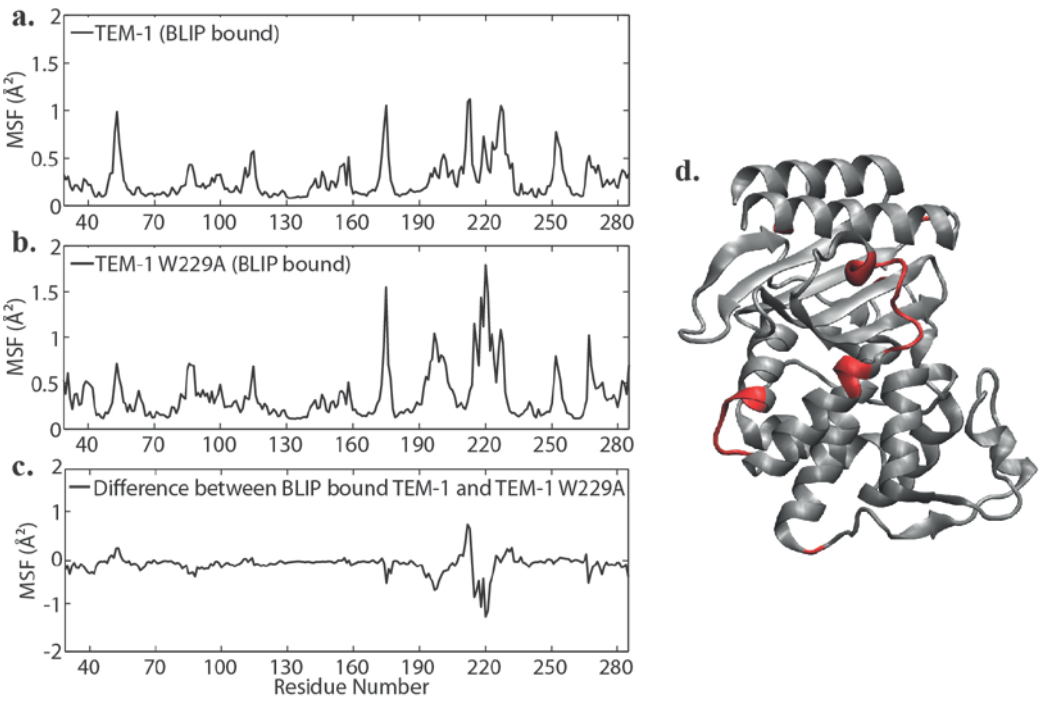

Figure 3.10. The MSF values for the C_α atoms of BLIP bound (a) TEM-1, (b) TEM-1 W229A. (c) The difference in MSF values between wild type and mutant forms. (d) TEM-1 structure in cartoon representation is shown with the red color indicating regions of MSF difference higher than 0.35 $Å^2$.

As mentioned before in BLIP bound TEM-1, regions which show higher fluctuations than the threshold of 0.7 $Å^2$ were the loop connecting S1 and S2 beta sheets, the flexible tip of the Ω loop, H9 and H10 helices and Asp252 which is located in the loop connecting

S4 and S5 beta sheets (Figure 3.10a). Mutation of W229A made these regions fluctuate more and also additional regions became more mobile such as the loop connecting H8 and H9 helices and the Gln267 which is located at the C-terminus of the S5 beta sheet (Figure 3.10b). When the difference between wild type and mutant simulations was examined, Gln88 which is located at the loop connecting H2 and H3 helices, the flexible tip of the Ω loop, the C-terminus of H8 and the loop connecting H8 and H9, C-terminus of H9 and N-terminus of H10, Gln267 gain mobility as a result of mutation. Only the region comprised by Met211, Glu212 and Ala213 residues which are located in the loop connecting H9 and H10 helices were more mobile in wild type bound enzyme (Figure 3.10c, d).

The MSF values of the cluster residues of BLIP bound TEM-1 increased as a result of mutation except C6 (0.25 $Å^2$ in wild type and 0.22 $Å^2$ in mutant). A slight increase was observed in the mobility; however a major difference was detected in C5. The MSF value of C5 has increased from 0.20 to 0.56 $Å^2$ as a result of mutation (Table 3.3). It indicates that Met129 and Val216 of TEM-1 became more mobile and the interaction between these residues and Phe36 and Tyr50 of BLIP may be strengthened.

The mobility of apo SHV-1 increased from 0.29 $Å^2$ to 0.42 $Å^2$ as a result of mutation (Table 3.1). Mobility of all the important regions has increased upon mutation, the significant changes were observed in H10 helix, H9-H10 helices region and in the 99-112 loop (Table 3.2).

Wild type and mutant simulations of apo SHV-1 showed fluctuations in similar regions. However the fluctuations increased remarkably after the mutation of W229A. The regions which show fluctuations higher than the threshold were the loop connecting H2 and H3 helices, C-terminus of the H3 helix and the loop connecting H3 and H4 helices, the flexible tip of the Ω loop, the loop connecting H8 and H9 helices, H9 and H10 helices, and the loop connecting S4 and S5 beta sheets (Figure 3.11b). When the difference between wild type and mutant simulations was examined, it could be seen that almost all the mentioned regions were more mobile in mutant apo enzyme. The regions which show higher fluctuations than the threshold were localized to the 99-112 loop, the loop connecting H8 and H9, C-terminus of the H9, and H10 helix (Figure 3.11c, d).

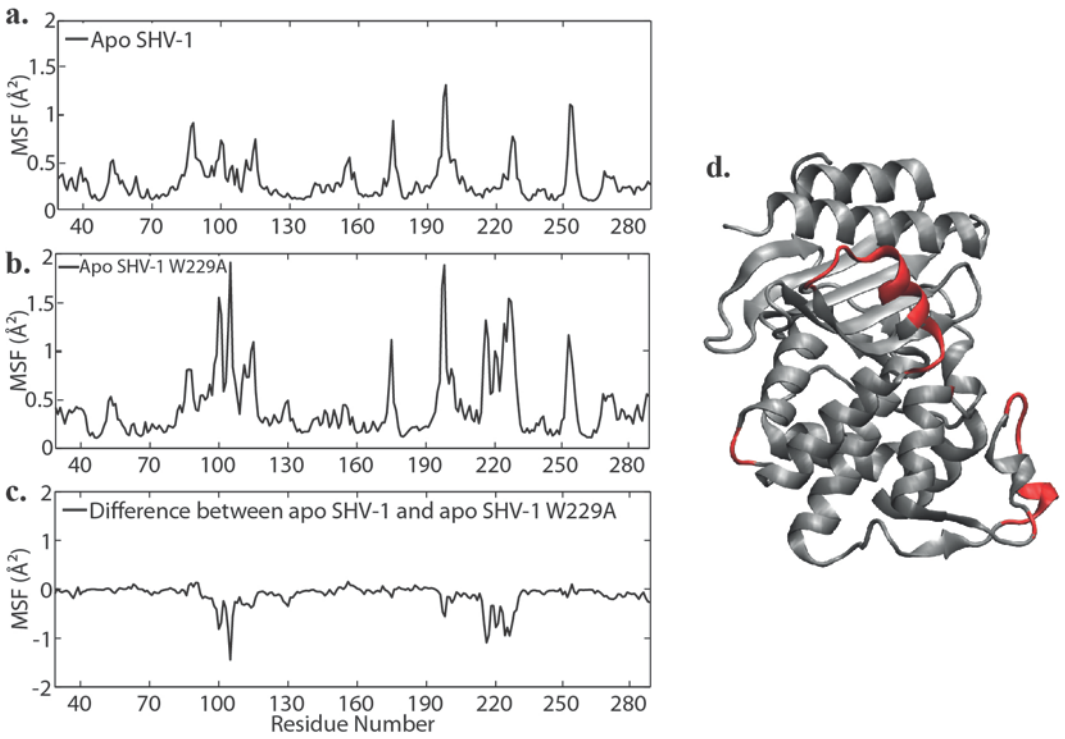

Figure 3.11. The MSF values for the C_α atoms of (a) apo SHV-1, (b) apo SHV-1 W229A. (c) The difference in MSF values between wild type and mutant forms of apo SHV-1. (d) SHV-1 structure in cartoon representation is shown with the red color indicating regions of MSF difference higher than 0.35 $Å^2$.

Unlike the effect of mutation in apo SHV-1 simulations, in BLIP bound SHV-1, mutation does not affect the overall mobility of the enzyme; both the wild type and mutant BLIP bound SHV-1 has a MSF value at around 0.3 $Å^2$ (Table 3.1). The average MSF values of H10 and H9-H10 helices region increased to 0.71 and 0.47 $Å^2$ from 0.61 and 0.39 $Å^2$, respectively. The other structurally important regions lost mobility after the mutation (Table 3.2).

BLIP bound SHV-1 had fluctuating residues which were in the two loops connecting S1 and S2 beta sheets, in the loop connecting S1 and S2 beta sheets and the H2 and H3 helices, the Ω loop and the H10 helix (Figure 3.12a). The mutation caused the Ω loop, the loop connecting H8 and H9 helices, H10 helix and the loop between S4 and S5 beta sheets fluctuate more than the threshold (Figure 3.12b). When the ΔMSF values between wild type and mutant bound enzyme were examined, the loop between the H8 and H9 and the H10 helix were found to fluctuate more in mutant form. The regions which were more

mobile in wild type were comprised by only the residues Ser53 and Leu173, Pro174 which were located in the loop between S1 and S2 beta sheets and in the Ω loop, respectively (Figure 3.12c, d).

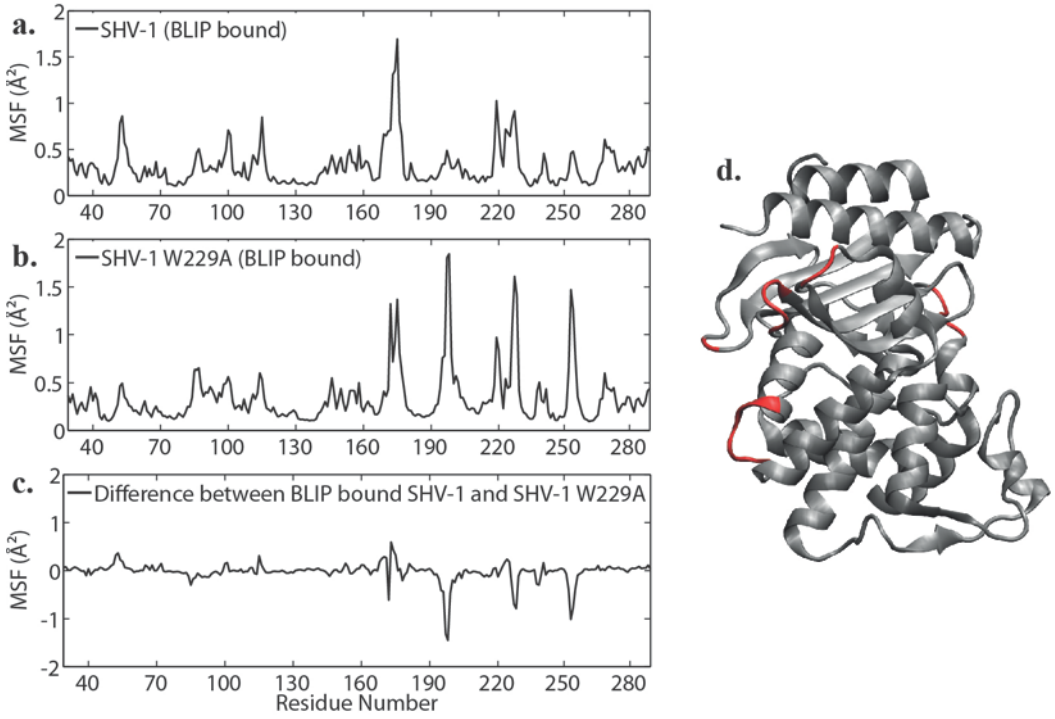

Figure 3.12. The MSF values for the C_α atoms of BLIP bound (a) SHV-1, (b) SHV-1 W229A. (c) The difference in MSF values between wild type and mutant forms. (d) SHV-1 structure in cartoon representation is shown with the red color indicating regions of MSF difference higher than 0.35 $Å^2$.

When the MSF values for the cluster residues of BLIP bound SHV-1 simulation were examined, it was observed that the mobility of C1, C5 and C6 has increased while C2, C3 and C4's mobility has decreased slightly (Table 3.3). The change in MSF values was not as remarkable as seen in BLIP bound TEM-1 simulation, indicating that mutation does not have a major contribution to the dynamics of the cluster residues of SHV-1.

3.1.4. Energy Calculations of the Simulation Systems

3.1.4.1. Intermolecular Interaction Energy Calculations. The intermolecular interaction energy between enzyme and ligand was calculated and compared in order to analyze the binding energetics. The nonbonded interaction energy terms between beta-lactamase and BLIP were examined and average values were calculated with respect to the production run period (4-10 ns), in both wild type and mutant forms of complexes.

Table 3.4. The intermolecular interaction energy terms (kcal/mol) of the simulation systems. Standard deviations are in parenthesis.

Simulation system	Electrostatic Energy	van der Waals Energy	Nonbonded Energy
TEM-1 – BLIP	-429.81 (26.6)	-84.03 (6.4)	-513.84 (25.68)
TEM-1 W229A – BLIP	-509.74 (53)	-104.27 (8.19)	-614.01 (48.41)
SHV-1 – BLIP	-498.51 (33.79)	-93.92 (7.16)	-592.43 (32.74)
SHV-1 W229A – BLIP	-513.32 (41.77)	-97.27 (7.4)	-610.58 (39.12)

The overall interaction between beta-lactamase and ligand is represented with the nonbonded interaction energy terms. Mutation of W229A favors the nonbonded energy between enzyme and ligand in both TEM-1 and SHV-1. The energy values for TEM-1 and SHV-1 were -513.84 and -592.43 in the wild types; -614.01 and -610.58 in the mutants, respectively (Table 3.4, Figure 3.13). The major contribution to the nonbonded energy was due to the electrostatic energy terms in all simulations.

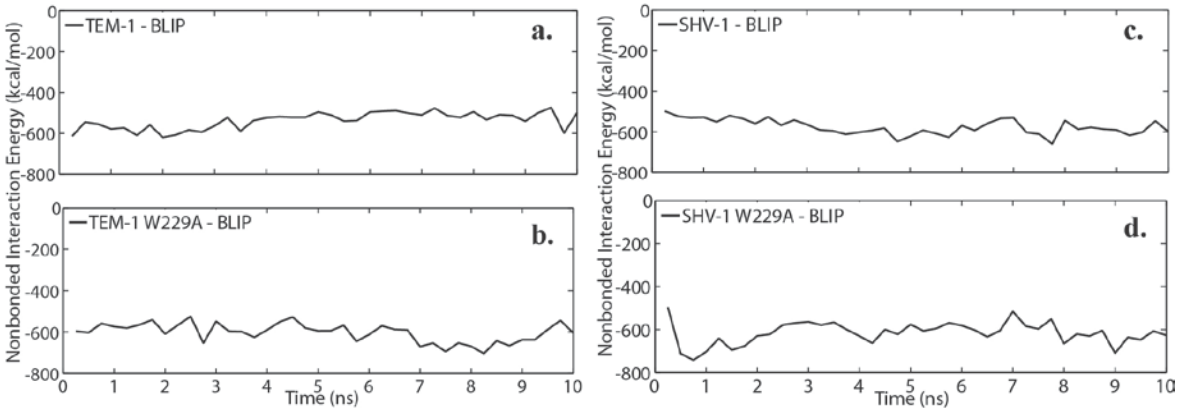

Figure 3.13. The nonbonded energy as a function of time (a) TEM-1 – BLIP, (b) TEM-1 W229A – BLIP, (c) SHV-1 – BLIP, (d) SHV-1 W229A – BLIP simulations.

When the electrostatic energy terms of wild type TEM-1 and SHV-1 complexes were compared, it was seen that SHV-1 – BLIP complex had more favorable electrostatic interaction between enzyme and ligand than TEM-1 – BLIP (-429.81 kcal/mol), with a value of -513.32 kcal/mol (Table 3.4).

Mutation of W229A favors the electrostatic interactions between beta-lactamase and ligand in the simulations with TEM-1. A similar but a weaker response to mutation is observed in SHV-1 simulations. Upon mutation, the electrostatic energy of TEM-1 and SHV-1 – BLIP complexes became -509.74 and -513.32 kcal/mol.

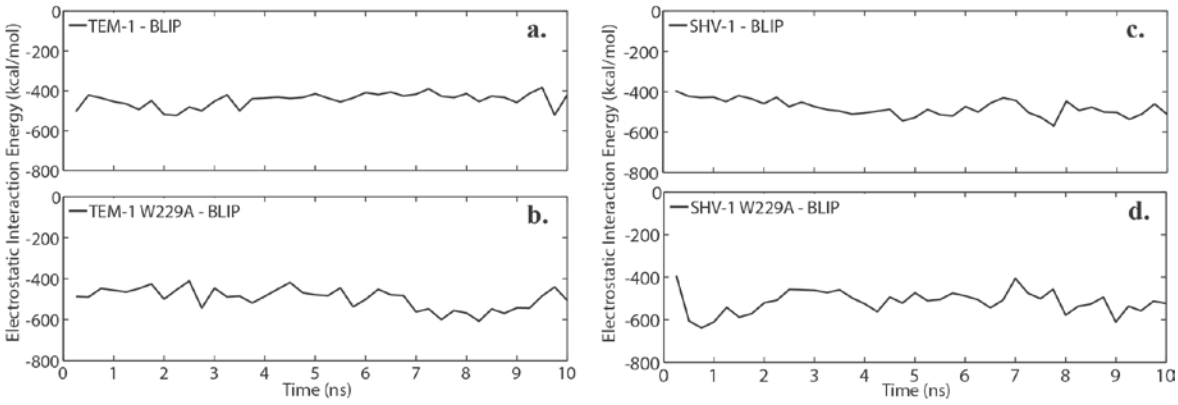

Figure 3.14. The electrostatic energy as a function of time (a) TEM-1 – BLIP, (b) TEM-1 W229A – BLIP, (c) SHV-1 – BLIP, (d) SHV-1 W229A – BLIP simulations.

The electrostatic energy profile of the simulation systems suggests that TEM-1 – BLIP (Figure 3.14a) and SHV-1 – BLIP (Figure 3.14c) complexes had continuous interactions between beta-lactamase and ligand indicated by the small fluctuations during the simulation timescale. However mutation causes higher fluctuations suggesting that the beta-lactamase and BLIP were moving closer together or further away from each other, during the simulations (Figure 3.14b, d).

Among the simulation systems, the most favorable van der Waals interaction was observed in mutant TEM-1 complex with the value of 104.27 kcal/mol. When the wild type simulations were compared, SHV-1 – BLIP had a more favorable van der Waals interaction than TEM-1 – BLIP (-84.03 kcal/mol) with a value around -93.92 kcal/mol.

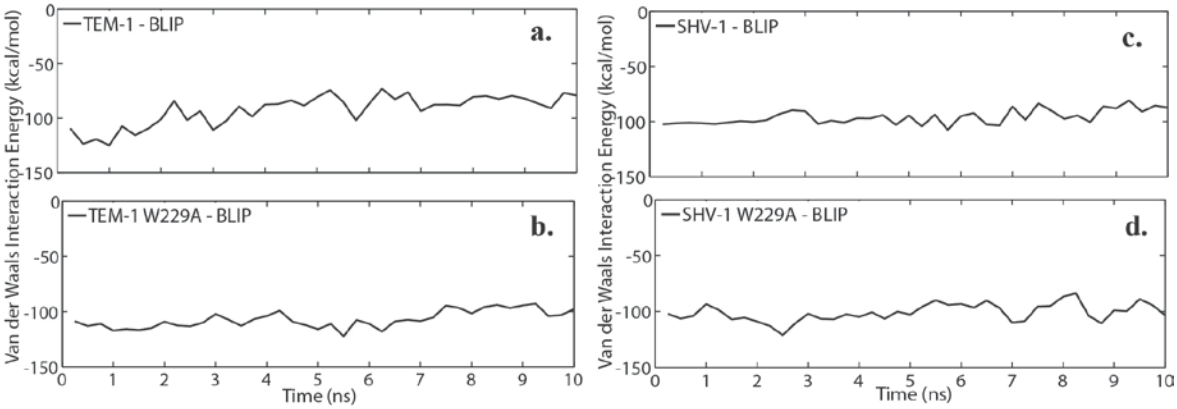

Figure 3.15. The van der Waals energy as a function of time (a) TEM-1 – BLIP, (b) TEM-1 W229A – BLIP, (c) SHV-1 – BLIP, (d) SHV-1 W229A – BLIP simulations.

Mutation favors the van der Waals interactions between enzyme and ligand in both TEM-1 and SHV-1 simulations. In wild type enzymes, the van der Waals energy of TEM-1 and SHV-1 complexes was -84.03 and -93.92 kcal/mol, respectively. Upon mutation van der Waals energy of TEM-1 complex became -104.27 kcal/mol while that of SHV-1 became -97.27 kcal/mol. The favorable van der Waals interactions observed as a result of mutation were significant in TEM-1 but not a major difference was detected in SHV-1 (Table 3.4).

The van der Waals energy profile of TEM-1 simulations showed that, the interaction between TEM-1 and BLIP had a more fluctuating behavior in wild type than the mutant (Figure 3.15a, b). SHV-1 simulations had similar profiles in both wild type and mutant (Figure 3.15c, d).

The interaction between the cluster residues of beta-lactamases and BLIP is a key factor to understand the binding energetics between enzyme and ligand. For this purpose, the electrostatic, van der Waals and nonbonded intermolecular interaction energy terms for the clusters of beta-lactamase – BLIP complexes were calculated and compared in order to analyze the effect of mutation.

Total intermolecular interaction energy between beta-lactamases and BLIP is stated by the nonbonded energy terms. The major contribution to the intermolecular interaction energy is done by the electrostatic interactions in all simulation systems. In TEM-1

simulations, mutation favored the intermolecular interaction between the cluster residues with major changes in the energy terms of C1 and C6. That indicates the W229A mutation effected the interaction between the catalytically important Asp49 of BLIP and Ser130, Lys234, Ser235 and Arg243 of TEM-1. Asp49 of BLIP has a major effect in the inhibition mechanism of TEM-1 and SHV-1 by occupying the catalytic site of beta-lactamases. The favorable intermolecular interaction observed in C1 may be the reason behind the enhanced binding affinity of mutant TEM-1 towards BLIP. It also has to be mentioned that an additional major difference was observed in C6, the interaction between Glu110 of TEM-1 and two Serine residues of BLIP, Ser73 and Ser113 has strengthened (Table 3.5). In contrast to TEM-1 simulations, the mutation disfavors the binding energetics except C2 in SHV-1 simulations. As mentioned before, a favorable electrostatic interaction was detected in C2 of SHV-1 as a result of mutation. This favorable effect observed in C2 was due to the electrostatic effects but overall, the W229A mutation disfavors the intermolecular interaction between SHV-1 and BLIP. If the total intermolecular interaction energy between beta-lactamases and BLIP (Table 3.4) was analyzed, it could be seen that W229A mutation has a remarkable favorable effect in TEM-1 simulations. The overall minor favorable effect upon mutation observed in SHV-1 simulations possibly caused by the loss of the electrostatic interactions between Asp49 and the C1 residues of SHV-1.

Table 3.5. The nonbonded energy terms (kcal/mol) for the cluster residues of beta-lactamases in complex simulation systems. Standard deviations are in parenthesis.

Simulation system	**C1**	**C2**	**C3**	**C4**	**C5**	**C6**
TEM-1 – BLIP	-188.77 (5.1)	-103.77 (4.88)	-27.31 (4.48)	-7.57 (1.43)	-4.72 (0.77)	-10.78 (5.75)
TEM-1 W229A – BLIP	-199.96 (7.71)	-110.90 (4.62)	-32.68 (5.49)	-10.11 (2.92)	-6.58 (1.16)	-31.28 (9.15)
SHV-1 – BLIP	-155.94 (15.20)	-87.03 (4.84)	-20.51 (4.62)	-7.42 (2.46)	-5.50 (1.02)	-31.40 (3.37)
SHV-1 W229A – BLIP	-97.9 (25.36)	-102.83 (6.94)	-13.74 (6.96)	-5.52 (1.30)	-5.54 (1.12)	-23.12 (9.16)

W229A mutation favors the electrostatic interaction in all the clusters of TEM-1 – BLIP complex. The electrostatic interaction between the cluster residues of TEM-1 and BLIP has strengthened as a result of mutation. However, an unfavorable electrostatic interaction was observed due to the mutation in SHV-1. The electrostatic interaction between the cluster residues of SHV-1 and BLIP has weakened upon mutation except C2. As a result of mutation, the electrostatic interaction between Asp104, Tyr105 and Asn170 of SHV-1, and Lys74, Phe142 and Tyr143 of BLIP has strengthened; the energy value for wild type was -80.49 while for the mutant it was -95.18 kcal/mol (Table 3.6).

Table 3.6. The electrostatic energy terms (kcal/mol) for the cluster residues of beta-lactamases in complex simulation systems. Standard deviations are in parenthesis.

Simulation system	**C1**	**C2**	**C3**	**C4**	**C5**	**C6**
TEM-1 – BLIP	-192.01 (6.05)	-94.88 (6.07)	-18.95 (4.60)	-5.64 (1.16)	0.03 (0.52)	-10.30 (5.82)
TEM-1 W229A – BLIP	-206.22 (9.52)	-103.26 (5.50)	-24.30 (5.47)	-7.71 (2.66)	-0.41 (0.92)	-32.00 (9.49)
SHV-1 – BLIP	-158.17 (16.56)	-80.49 (5.57)	-12.12 (5.11)	-5.88 (2.18)	-0.14 (0.56)	-31.81 (3.94)
SHV-1 W229A - BLIP	-96.68 (25.71)	-95.18 (7.66)	-8.80 (6.72)	-4.39 (0.99)	0.36 (0.82)	-23.13 (9.79)

When the van der Waals interaction between the cluster residues of beta-lactamase and BLIP was investigated; different responses to mutation was observed in TEM-1 and SHV-1 (Table 3.7). Mutation had minor favorable effects in C4 and C5 of TEM-1 while the van der Waals interaction between the other cluster residues has weakened upon mutation. In SHV-1, the mutation has favored van der Waals interaction in clusters except C3 and C4, with minor changes in the energy terms.

Table 3.7. The van der Waals energy terms (kcal/mol) for the cluster residues of beta-lactamases in complex simulation systems. Standard deviations are in parenthesis.

Simulation system	C1	C2	C3	C4	C5	C6
TEM-1 – BLIP	4.14 (2.01)	-8.89 (2.34)	-8.36 (1.23)	-1.93 (0.45)	-4.76 (0.48)	-0.49 (0.29)
TEM-1 W229A – BLIP	6.26 (3.00)	-7.64 (2.27)	-8.37 (1.59)	-2.40 (0.98)	-6.17 (0.74)	0.72 (2.05)
SHV-1 – BLIP	2.23 (3.12)	-6.53 (2.16)	-8.39 (1.63)	-1.55 (0.67)	-5.36 (0.66)	0.42 (1.14)
SHV-1 W229A - BLIP	-1.22 (1.45)	-7.65 (1.69)	-4.94 (2.54)	-1.14 (0.61)	-5.90 (0.77)	0.01 (1.19)

3.1.4.2. Binding Free Energy Calculations. Binding free energy between enzyme and ligand, and also the total energy of the apo enzymes were calculated by FoldX algorithm. The total and binding free energy values of simulation systems are given in Table 3.8. Total energy represents the predicted overall stability of the protein. When the total energy values of apo enzymes were compared, TEM-1 is the most stable and ordered protein among the others with a value of -15.37 kcal/mol. Mutation decreased the stability of the protein and the total energy rises to -3.51 kcal/mol (Table 3.8).

Table 3.8. Total and binding free energy (kcal/mol) of simulation systems. Standard deviations are in parenthesis.

Simulation system	Total energy	Binding free energy
Apo TEM-1	-15.37 (8.92)	
Apo TEM-1 W229A	-3.51 (8.41)	
TEM-1 – BLIP		-16.43 (2.44)
TEM-1 W229A – BLIP		-23.03 (2.63)
Apo SHV-1	-6.89 (8.31)	
Apo SHV-1 W229A	7.08 (8.34)	
SHV-1 – BLIP		-17.06 (2.62)
SHV-1 W229A – BLIP		-17.62 (2.77)

Table 3.9. Contributing energy terms (kcal/mol) for the apo simulations, calculated by FoldX. Standard deviations are in parenthesis.

Simulation system	Van der Waals	Electrostatics	Solvation polar	Solvation hydrophobic	Entropy sidechain	Entropy mainchain
TEM-1	-292.74 (2.25)	-21.03 (1.91)	385.59 (3.95)	-385.94 (3.53)	164.36 (2.24)	378.8 (3.83)
TEM-1 W229A	-287.49 (2.93)	-20.17 (1.84)	378.04 (4.68)	-379.56 (4.06)	160.12 (2.53)	378.95 (3.84)
SHV-1	-296.10 (2.68)	-21.82 (2.02)	394.94 (4.26)	-386.98 (3.72)	163.13 (2.30)	390.23 (3.69)
SHV-1 W229A	-289.33 (2.66)	-23.90 (1.91)	389.77 (4.29)	-376.97 (3.73)	161.71 (2.32)	386.90 (3.77)

The energy profiles of apo TEM-1 in both wild type and mutant forms were examined and a similar fluctuating behavior was observed (Figure 3.16a, b). In order to further analyze the reason behind the change in total energy, the contributing energy terms were calculated (Table 3.9). While the van der Waals, electrostatic and hydrophobic solvation terms contributions were more favorable in wild type apo TEM-1, polar solvation and entropic contributions were more favorable in the mutant.

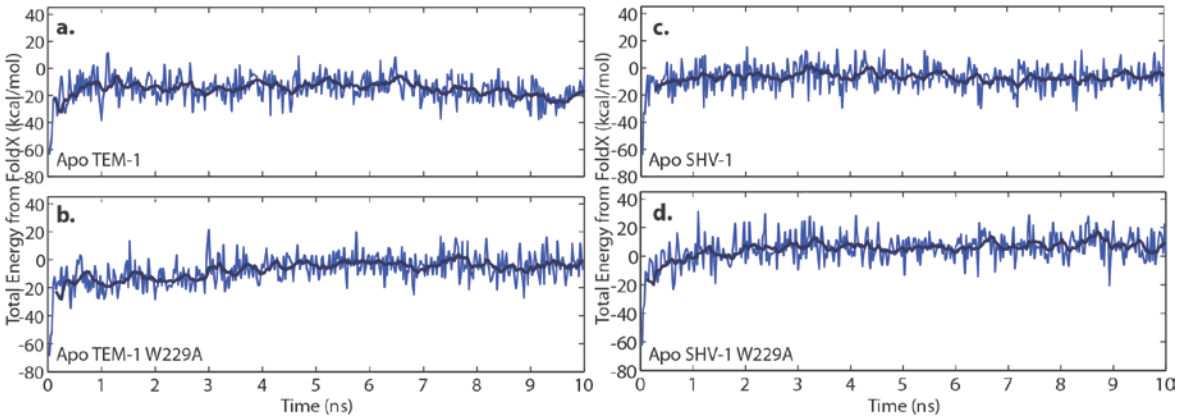

Figure 3.16. Total energy profiles of apo enzymes, (a) apo TEM-1, (b) apo TEM-1 W229A, (c) apo SHV-1, (d) apo SHV-1 W229A, from FoldX.

Mutation disfavors the total energy of the enzyme also in SHV-1. Total energy of wild type apo SHV-1 was -6.89 kcal/mol, while that of mutant was 7.08 kcal/mol (Table 3.8). When the contributing energy terms were examined, van der Waals and hydrophobic

solvation terms contributions were found to be more favorable in wild type enzyme; while electrostatics, polar solvation and entropic contributions were more favorable in the mutant (Table 3.9). An increase in the energy of the mutant simulations was detected at around 2 ns, fluctuations were similar in both wild type and mutant enzymes (Figure 3.16c, d).

However a different response was observed in complex simulations. Mutation favors the binding free energy in TEM-1 – BLIP complex, and does not affect the binding free energy in SHV-1 – BLIP complex. In wild type complexes binding free energy terms were -16.43 and -17.06 kcal/mol for BLIP bound TEM-1 and SHV-1, respectively. Upon mutation a major difference was observed in TEM-1, the energy values became -23.03 and -17.62 kcal/mol for TEM-1 and SHV-1 complexes, respectively (Table 3.8).

Table 3.10. Contributing energy terms (kcal/mol) for the complex simulations, calculated by FoldX. Standard deviations are in parenthesis.

Simulation system	**Van der Waals**	**Electrostatics**	**Solvation polar**	**Solvation hydrophobic**	**Entropy sidechain**	**Entropy mainchain**
TEM-1 – BLIP	-17.66 (1.02)	-5.06 (0.54)	25.33 (1.87)	-22.26 (1.26)	10.31 (1.15)	5.83 (1.14)
TEM-1 W229A – BLIP	-22.11 (1.65)	-5.12 (0.68)	31.20 (2.22)	-27.61 (2.10)	12.37 (1.32)	6.48 (1.24)
SHV-1 – BLIP	-19.92 (1.15)	-4.33 (0.74)	28.67 (1.68)	-24.43 (1.47)	11.85 (1.56)	7.58 (1.04)
SHV-1 W229A – BLIP	-21.09 (1.29)	-4.90 (0.86)	31.18 (2.29)	-25.53 (1.42)	11.66 (1.81)	6.98 (1.30)

When the contributing energy terms were examined, polar solvation and entropic contributions were found to be more favorable in wild type TEM-1 – BLIP complex. However mutation favors the van der Waals, electrostatics, hydrophobic solvation contributions. In SHV-1 – BLIP complex, all the contributing energy terms became more favorable upon mutation except the polar solvation contribution (Table 3.10). The binding free energy profiles of complex simulation systems were examined and different responses due to mutation were observed. Mutation stabilizes the fluctuations observed in wild type TEM-1 complex (Figure 3.17a, b), the mutant TEM-1 complex reaches the equilibrium period at around 3 ns. On the other hand, mutation causes more fluctuations in SHV-1

complex (Figure 3.17c, d) and the mutant system fluctuates continuously during the simulation length.

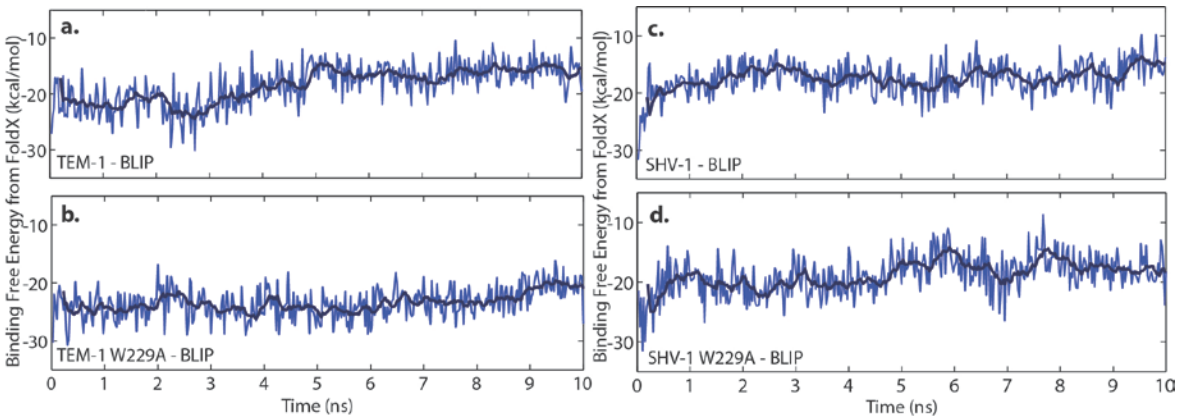

Figure 3.17. Binding free energy profiles of complex systems, (a) TEM-1 – BLIP, (b) TEM-1 W229A – BLIP, (c) SHV-1 – BLIP, (d) SHV-1 W229A – BLIP, from FoldX.

Mutation has different effects on simulation systems. As a result of the mutation of a highly conserved H10 residue, W229, to Alanine; the binding affinity of BLIP to TEM-1 and SHV-1 has increased but the stability of apo enzymes has decreased. The tighter binding observed in mutant TEM-1 complex may result with higher inhibition by BLIP.

3.1.5. Communication between Beta-lactamase and BLIP and within Beta-lactamase

The different response of the structural elements to BLIP binding and W229A mutation suggests that a communication exists between BLIP and beta-lactamase allosteric binding site. In order to investigate this communication, the intermolecular correlations were calculated for different simulation systems. Correlation values higher than a threshold of 0.4 were mapped onto the complex structures. In TEM-1 – BLIP complex, only a few correlation values higher than the threshold were observed and they were localized to the regions comprised of H9-H10 helices (Figure 3.18a, b). With the mutation of W229A, the intermolecular correlations between TEM-1 and BLIP were spread throughout the TEM-1 structure to the regions comprised by S1 and S2 beta sheets, 99-112 region, H5, H8, H9-H10 helices and the C-terminus of the S4 beta sheet (Figure 3.18c, d).

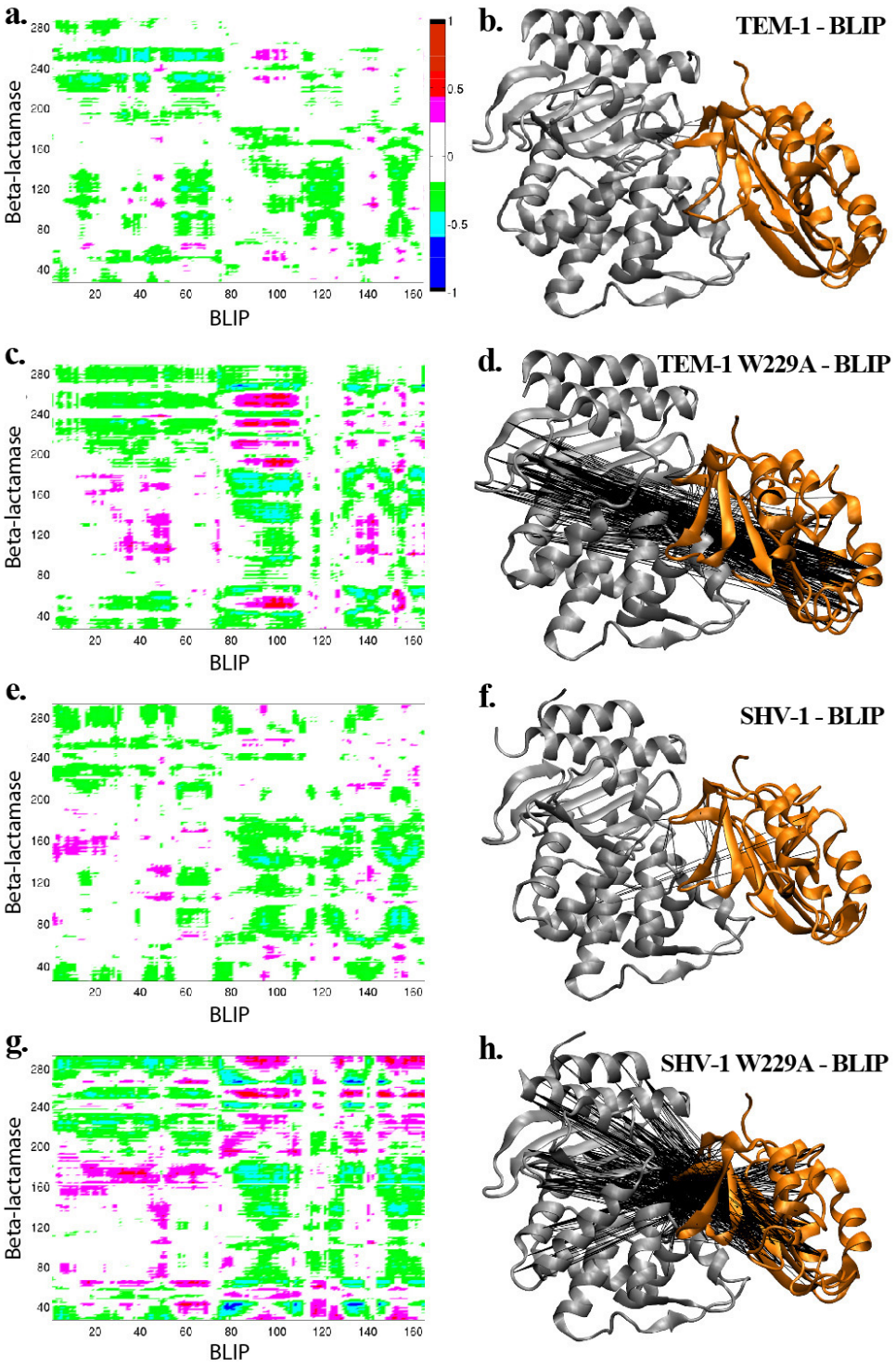

Figure 3.18. Cross correlation maps for C_α atoms of BLIP bound (a) TEM-1, (c) TEM-1 W229A, (e) SHV-1, (g) SHV-1 W229A complexes. The correlation values higher than the threshold of 0.4 are mapped onto the structures; (b), (d), (f), (h) by black lines.

In SHV-1 – BLIP complex, correlations higher than the threshold were observed in Asp104 and Tyr105, the loop connecting H4 and H5 helices, a part of the Ω loop (around Asn170) and Val216 (Figure 3.18e, f). Upon mutation, correlations spread through the structure as observed in TEM-1 W229A – BLIP complex, within the regions H1, H2, H4, H5, H8, H9, H10, H11, S4 and S5 beta sheets, Ω loop, and the middle part of the 99-112 region comprised by the residues Asp104 and Tyr105 (Figure 3.18g, h).

In order to analyze the effect of W229A mutation to the communication pathway between H10 helix and the beta-lactamase itself, the correlations within the beta-lactamase structure were investigated. The residue-residue average correlation coefficients which were calculated between H10 helix and beta-lactamase were plotted in all simulation systems. In apo TEM-1, the beta-lactamase residues which have average H10 correlation coefficients higher than 0.4 were localized to the H10 helix itself within the residues Arg222 to Trp229. A fluctuating behavior was observed through the beta-lactamase structure (Figure 3.19a). Upon mutation of W229A, fluctuations were stabilized and the coefficients higher than the threshold were observed in the same region as in wild type, in H10 helix itself, within the residues Arg222 to Leu225 (Figure 3.19b).

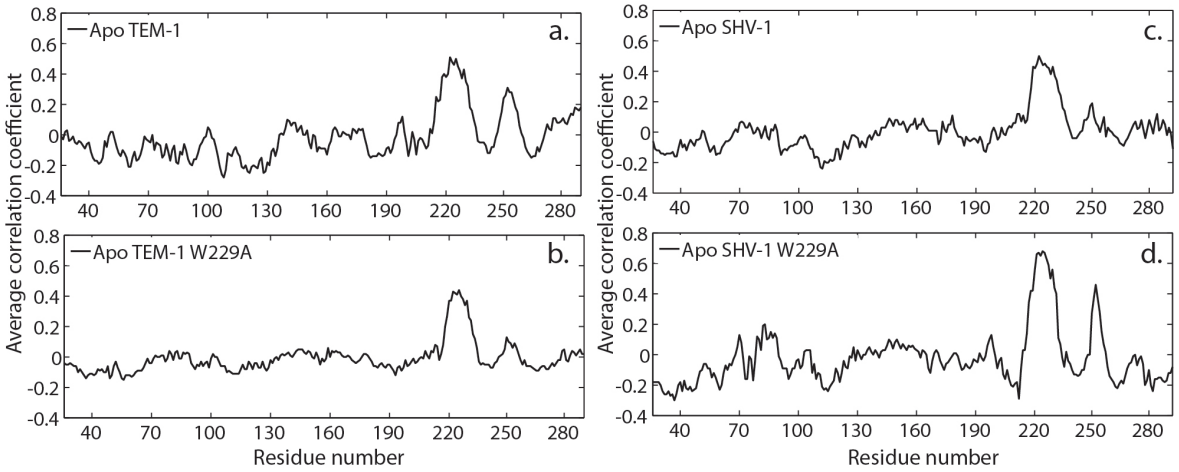

Figure 3.19. Residue-residue correlations between H10 helix and beta-lactamase structures of (a) TEM-1, (b) TEM-1 W229A, (c) SHV-1, (d) SHV-1 W229A.

In apo SHV-1, the residues Pro219 to Trp229 had higher correlation coefficients than the threshold (Figure 3.19c). Mutation caused an increase in the correlation coefficients of these regions (Figure 3.19d). As stated before, Trp229 is in a stacking interaction with Pro226 and Pro252. In wild type apo TEM-1, Pro252 has a high positive correlation coefficient, which is 0.31, but it is not mentioned as it is not higher than the threshold value. Mutation decreased the correlation coefficient of Pro252 to 0.09. In apo wild type SHV-1, Pro252 has a correlation at about 0.06. Upon mutation of Trp229, the correlation coefficient of Pro252 became higher than the threshold. As it is stated, mutation has different effects on the communication between Pro226, Trp 229 and Pro252, in TEM-1 and SHV-1. In wild type TEM-1 a communication pathway exists between H10 helix and Pro252, however due to mutation this communication disrupts. Unlike the response observed in TEM-1, mutation of W229A causes a communication pathway between H10 helix and Pro252 in SHV-1. In both outcomes, the correlation between these three residues proves that the stacking arrangement of Pro226, Trp229 and Pro252 is important in terms of interaction and communication. In both wild type and apo simulations, H10 is highly correlated with itself; each residue in H10 had high positive correlation coefficients calculated based on the movements of other residues in H10 helix.

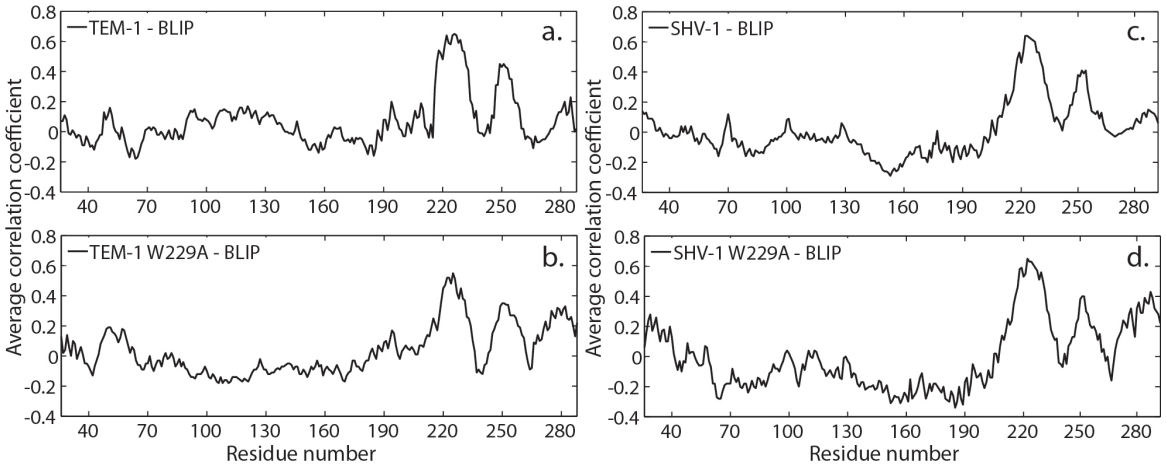

Figure 3.20. Residue-residue correlations between H10 helix and the BLIP bound beta-lactamase structures of (a) TEM-1, (b) TEM-1 W229A, (c) SHV-1, (d) SHV-1 W229A.

In TEM-1 – BLIP complex, the correlations between H10 and beta-lactamase higher than the threshold were localized to the regions comprised by residues Ala217 to Asp233, which are located in H10 helix, and a part of the S4 beta sheet and the loop connecting S4

and S5 beta sheets, especially residues Leu249 to Gly253 (Figure 3.20a). Upon mutation, the H10 helix, especially residues Leu220 to Phe230, had high correlation coefficients (Figure 3.20b). The stacking arrangement of the highly conserved residues is located in Pro226, Trp229 and Pro251 (Pro252 in other simulations) in TEM-1 – BLIP complex. In wild type TEM-1 – BLIP complex, Pro251 has a correlation coefficient of 0.45; mutation decreased this value to 0.35. Despite the decrease, the communication between these residues is observed with the correlation values, and it has to be mentioned that H10 is highly correlated within itself as it is in apo simulations.

In SHV-1 – BLIP complex, as in TEM-1 – BLIP, H10 is highly correlated within itself, especially residues Ala217 to Ile231. Pro252 and Asn254 which are located in the loop connecting S4 and S5 beta sheets also had higher correlation coefficients than the threshold (Figure 3.20c). Mutation increased the correlation coefficients of the H10 helix region; Pro252 had the same correlation as in wild type with a value at around 0.4. An additional residue, Ile287, which is located at the C-terminus of H11 helix is found to have a higher coefficient than the threshold (Figure 3.20d). In both wild type and mutant enzyme – ligand complexes, H10 is highly correlated within itself and a communication between the stacking arrangement residues is also observed as in apo enzymes.

3.2. Simulations on Beta-lactamase – Peptide Complexes

MD simulations were performed on 10 TEM-1 – peptide complexes. The list of peptides used in the simulations is given in Table 3.11. The peptides were designed as to comprise the catalytically important 46-51 loop and the residue numbering of the peptides is based on BLIP numbering. Computational mutagenesis on specific positions is done to analyze the effect of different amino acid substitutions on binding affinity and dynamics of beta-lactamase – peptide complexes. Three new simulations were performed in this study and all the simulations were analyzed and compared in the following sections.

Table 3.11. The list of simulations with the peptides designed based on BLIP sequence. Simulations marked with asterisks were from previous studies (*: Kanlıkılıçer, 2008; **: Doğan, 2011).

Simulation system	**Peptide based on BLIP region**	**Peptide sequence**	**Mutation**
TEM-1 – P1*	Residues 45 to 52	CH_3CO-NH-HAAGDYYA-$CONH_2$	-
TEM-1 – P2	Residues 45 to 52	CAAGDYYC (cyclic)	-
TEM-1 – P3**	Residues 45 to 52	CH_3CO-NH-HWAGDYYA-$CONH_2$	A46W
TEM-1 – P4*	Residues 45 to 52	CH_3CO-NH-HAAGAYYA-$CONH_2$	D49A
TEM-1 – P5**	Residues 45 to 52	CH_3CO-NH-HAAGDAYA-CONH2	Y50A
TEM-1 – P6**	Residues 45 to 52	CH_3CO-NH-HAAGDYAA-$CONH_2$	Y51A
TEM-1 – P7	Residues 46 to 51	CH_3CO-NH-RRGHYY-$CONH_2$	A46R, A47R, D49H
TEM-1 – P8**	Residues 45 to 53	CH_3CO-NH-HAAGDYYAY-$CONH_2$	-
TEM-1 – P9**	Residues 45 to 53	CH_3CO-NH-HAAFDYYAY-$CONH_2$	G48F
TEM-1 – P10	Residues 45 to 53	CH_3CO-NH-LLIIL-HAAGDYYAY-$CONH_2$	-

The peptides were designed as to comprise the important residues of BLIP that make critical interactions with beta-lactamase, either 45-52 (P1) or 45-53 regions (P8) of BLIP was used as initial coordinates. The previously identified cyclic peptide structure (Rudgers *et al.*, 2001) was simulated, with the name of P2, in order to see the effect of the presence of a disulfide bond in the peptide. A46W mutation was carried out, with the name of P3, in order to see the results of the substitution of a bulkier side chain at position 46 in the interactions between peptide and beta-lactamase. Asp49 is a catalytically important residue whose carboxylate mimics the carboxylate of Pen-G (Strynadka *et al.*, 1996); and the substitution of this important residue with Ala resulted in ~40 fold decrease in the binding affinity of BLIP towards TEM-1 and SHV-1 beta-lactamases (Petrosino *et al.*, 1999, Zhang and Palzkill, 2003). A 10 ns simulation was carried out with a peptide carrying this mutation, P4, in order to elucidate the mechanism whereby D49A mutation lowers affinity. The role of Tyr50 in the binding of BLIP to beta-lactamases was studied previously, and removal of the Tyr50 side chain was determined to increase the binding affinity of BLIP to TEM-1 (Zhang and Palzkill, 2003). Simulation on the Y50A mutant peptide, P5, was carried out to obtain information about the effects of the removal of the phenolic ring of Tyr50 to dynamics and energetics. Y51A mutation was previously identified to have no effect in the binding affinity to TEM-1 (Zhang and Palzkill, 2003), hence a simulation was

carried out, with the name of P6, in order to analyze if the peptide with Y51A mutation affects the binding energetics or has no effect as previously stated. The peptide with the sequence of RRGHYY-NH_2 was found to inhibit TEM-1 with a K_i of 136 μM (Huang *et al.*, 2003), a simulation was done with the peptide that has this specific sequence, P7, to analyze the dynamics and energetics in the presence of this peptide. The initial coordinates of P7 were taken from the BLIP 46-51 region, and the A46R, A47R and D49H mutations were carried out using psfgen module of VMD. The simulations were repeated with the region corresponding to residues 45-53 of BLIP, to analyze the effect of the presence of an additional charged residue at the C-terminus of the peptide. Gly48 was previously identified to fill the region occupied by Phe142 of BLIP, whose side chain mimics the position of benzyl group in PenG (Strynadka *et al.*, 1996). Substitution of a Phe residue at position 48 may help to fill this proposed region as well; hence a simulation was carried out, P9, in order to confirm this hypothesis. The last peptide, P10 was designed as to comprise the hydrophobic residues of a cell penetrating peptide, pVEC. Substitution of these hydrophobic residues with Ala resulted in a significant drop in the cellular uptake of the peptide (Elmquist *et al.*, 2006); hence the hydrophobic residues with the sequence of LLIIL were proposed to play an important role in the cellular uptake mechanism of peptides. A simulation was carried out in the presence of these residues at the N-terminus of the BLIP based peptide in order to see the change in affinity toward beta-lactamase.

3.2.1. Stability of Simulation Systems

All the RMSD and MSF values are calculated based on the six ns production run period in which the RMSD time profile has reached equilibrium. The RMSD and MSF values of TEM-1 beta-lactamase, peptides and complexes in different simulation systems are given in Table 3.12. RMSD calculation was carried out with the procedure described in Section 2.2.1 except the third column of Table 3.12. The simulation snapshots were superimposed based on C_α coordinates of TEM-1 and the RMSD was calculated between the initial and time averaged peptide C_α coordinates. These RMSD values provide information on the deviation of the peptides away from their initial positions with respect to TEM-1 beta-lactamase.

Table 3.12. RMSD values (Å) of TEM-1, peptide and complexes in each simulation system and MSF values (Å^2) are in parenthesis.

Simulation system	**Peptide based on BLIP region**	**Mutation**	**TEM-1**	**Peptide**	**Peptide with respect to TEM-1**	**Complex**
TEM-1 – P1	45 to 52	-	0.70 (0.39)	2.03 (1.64)	3.45	0.92 (0.57)
TEM-1 – P2	45 to 52	-	0.77 (0.28)	1.90 (0.52)	3.31	0.95 (0.42)
TEM-1 – P3	45 to 52	A46W	0.69 (0.31)	0.54 (0.11)	2.75	0.83 (0.35)
TEM-1 – P4	45 to 52	D49A	1.08 (0.34)	3.01 (2.71)	7.82	1.71 (0.78)
TEM-1 – P5	45 to 52	Y50A	0.77 (0.38)	1.41 (1.59)	2.62	0.88 (0.55)
TEM-1 – P6	45 to 52	Y51A	0.82 (0.35)	2.70 (1.23)	3.35	0.99 (0.51)
TEM-1 – P7	46 to 51	A46R, A47R, D49H	1.03 (0.30)	1.66 (0.34)	3.22	1.12 (0.35)
TEM-1 – P8	45 to 53	-	0.69 (0.34)	1.33 (1.22)	1.79	0.75 (0.47)
TEM-1 – P9	45 to 53	G48F	0.97 (0.29)	1.96 (0.47)	4.21	1.22 (0.32)
TEM-1 – P10	45 to 53	-	0.85 (0.32)	1.70 (0.78)	2.99	1.06 (0.72)

The stability and dynamics of the structurally important regions of TEM-1 beta-lactamase are investigated in order to analyze the effect of peptide binding to the specific regions of beta-lactamase structure; the RMSD and MSF values are given Table 3.13.

Table 3.13. RMSD values (Å) of the structurally important regions of TEM-1. MSF values (Å^2) are in parenthesis.

Simulation system	H10 helix	H9-H10 helices	99-112 loop	Ω loop	Ω loop flexible tip	Active site residues
TEM-1 – P1	1.21 (1.33)	1.13 (0.89)	0.67 (0.50)	0.74 (0.30)	1.21 (0.80)	0.59 (0.19)
TEM-1 – P2	1.42 (0.55)	1.05 (0.38)	0.82 (0.32)	0.82 (0.34)	1.55 (1.12)	0.49 (0.14)
TEM-1 – P3	1.24 (0.45)	1.02 (0.37)	0.89 (0.46)	0.53 (0.29)	0.85 (0.82)	0.57 (0.17)
TEM-1 – P4	1.63 (0.67)	1.75 (0.50)	1.53 (0.57)	0.70 (0.31)	0.82 (0.82)	0.94 (0.19)
TEM-1 – P5	2.02 (0.77)	1.62 (0.70)	0.95 (0.68)	0.60 (0.34)	1.04 (0.97)	0.60 (0.20)
TEM-1 – P6	1.38 (0.54)	1.52 (0.40)	0.78 (0.48)	0.69 (0.39)	1.15 (1.11)	0.54 (0.19)
TEM-1 – P7	2.07 (0.45)	1.60 (0.36)	0.90 (0.47)	0.88 (0.34)	1.33 (0.87)	0.62 (0.18)
TEM-1 – P8	1.22 (0.62)	1.01 (0.50)	0.96 (0.46)	0.74 (0.48)	1.05 (1.26)	0.60 (0.15)
TEM-1 – P9	1.24 (0.40)	1.59 (0.34)	1.23 (0.32)	1.19 (0.46)	2.31 (1.29)	0.69 (0.15)
TEM-1 – P10	1.30 (0.49)	1.03 (0.37)	1.21 (0.49)	0.69 (0.40)	1.23 (1.15)	0.58 (0.16)

3.2.1.1. Stability of TEM-1 Beta-lactamase. When the RMSD values between the initial and time averaged coordinates of TEM-1 in different simulations were analyzed, the highest RMSD values were observed in P4 (1.08 Å), P7 (1.03 Å) and P9 (0.97 Å) bound systems (Table 3.12). In other simulations, the RMSD values of TEM-1 beta-lactamase were closer to each other at a value of around 0.75 Å.

As stated before, P1 is designed based on the region of BLIP comprised by the residues His45 to Ala52; and P8 is designed based on the BLIP region comprised by the residues His45 to Tyr53. All the other peptides are the mutants of these wild type ones; the

comparison of the simulation systems in terms of stability and dynamics is going to be done based on the two wild type peptides.

P1 bound TEM-1 (Figure 3.21a) has a RMSD value of 0.70 Å; when the cyclic peptide, P2, is bound to TEM-1 (Figure 3.21b) the RMSD value of the beta-lactamase increased to 0.77 Å (Table 3.12). When the structurally important regions were examined; the RMSD values of H10 helix, 99-112 loop, Ω loop and the flexible tip of the Ω loop increased as a result of cyclic structure to 1.42, 0.82, 0.82 and 1.55 Å from the values of they had in wild type 1.21, 0.67, 0.74 and 1.21 Å; respectively. The only parts whose RMSD values were lower than those of the wild type were the H9-H10 helices region and the active site residues. Their RMSD values in the wild type peptide, P1, bound form were 1.13 and 0.59 Å but as a result of P2 binding they became 1.05 and 0.49 Å; respectively (Table 3.13).

The RMSD value of P3 bound TEM-1 is 0.69 Å and it is almost the same as in P1 bound simulation (Table 3.12). The RMSD profile of P3 bound simulation shows a sudden increase at around 2 ns, but the simulation reaches a plateau after 4 ns (Figure 3.21c). P3 binding doesn't affect the stability of H10 helix and the active site region. However it causes a major decrease in the RMSD values of the Ω loop. The RMSD values for Ω loop and its flexible tip became 0.53 and 0.85 Å as a result of A46W mutation. The only part which deviates more than the wild type was the 99-112 region. Its RMSD became 0.89 Å from 0.67 Å (Table 3.13).

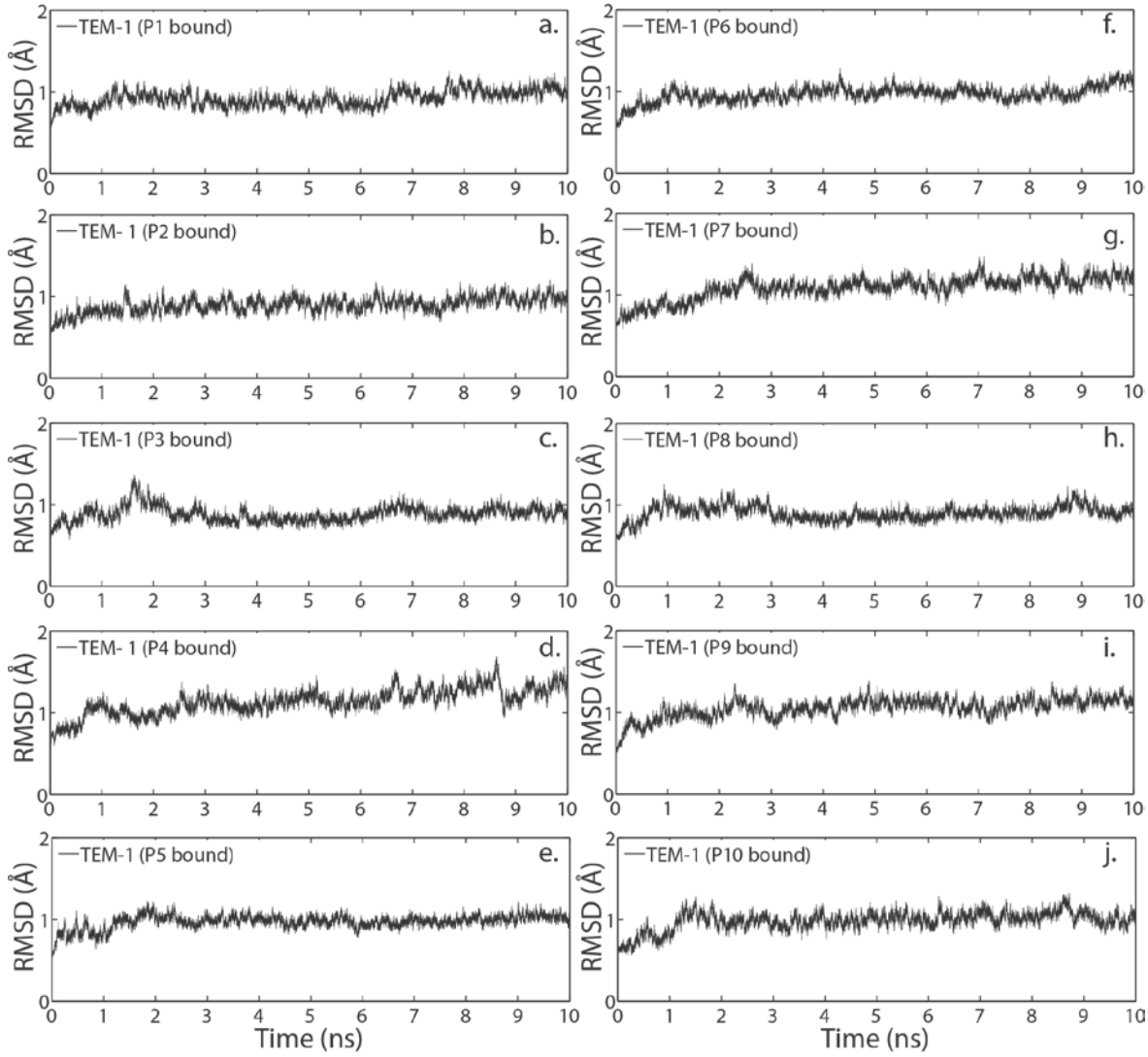

Figure 3.21. The RMSD profiles of (a) P1, (b) P2, (c) P3, (d) P4, (e) P5, (f) P6, (g) P7, (h) P8, (i) P9, (j) P10 bound TEM-1 beta-lactamase during 10 ns MD simulations.

P4 binding increased the RMSD value of TEM-1 in the wild type peptide bound form from 0.71 Å to 1.08 Å (Table 3.12). D49A mutation causes more deviations in the overall structure, when the individual structural components were analyzed it was observed that H10 and H9-H10 helices, 99-112 loop and the active site region show deviations more than the wild type peptide bound TEM-1. Only the Ω loop and its flexible tip became more stable upon D49A mutation (Table 3.13). The RMSD – time profile of TEM-1 – P4 shows a more fluctuating behavior with respect to the TEM-1 – P1 complex. Sudden increase and decreases were detected in the production run period, between 8 and 9 ns (Figure 3.21d). Overall it can be said that D49A mutation makes beta-lactamase more unstable by effecting the deviations of both TEM-1 structure and its important individual components.

Beta-lactamase deviation is not significantly affected by P5 binding. A minor increase in the RMSD value of TEM-1 was observed, the RMSD value of TEM-1 in the P1 bound form was 0.70 Å while in the P5 bound form it became 0.77 Å (Table 3.12). This increase was caused by the deviations observed in H10 helix, H9-H10 helices and the 99-112 region. The RMSD values of these regions increased remarkably as a result of Y50A mutation with respect to the wild type peptide bound form. However deviations observed in the Ω loop has decreased and the active site residues were almost not affected (Table 3.13). The fluctuations observed in the RMSD – time profile of P5 bound TEM-1 are almost the same as in the wild type bound TEM-1 (Figure 3.21e).

P6 binding to TEM-1 increased the beta-lactamase deviation from 0.70 Å to 0.82 Å (Table 3.12). The overall increase in the RMSD value of beta-lactamase is caused by the higher RMSD values of H10 helix, H9-H10 helices and the 99-112 loop in the Y51A mutant peptide bound form. The RMSD values of these regions increased as a result of mutant peptide binding, on the other hand as stated in the other peptides except P2, Ω loop deviation decreased in the mutant peptide bound simulation. Active site residues are almost not affected, a minor decrease in the RMSD value of the active site region was calculated (Table 3.13). Similar fluctuations to the ones in wild type peptide bound form are detected in the RMSD – time profile of P6 bound TEM-1 beta-lactamase (Figure 3.21f).

P7 is the peptide designed based on the BLIP region comprised by residues Ala46 to Tyr51. However this peptide is going to be compared with the wild type peptide designed based on the BLIP region comprised by the residues His45 to Ala52, P1, in terms of stability and dynamics. P7 binding to TEM-1 increased the RMSD value of beta-lactamase from 0.70 Å to 1.03 Å (Table 3.12). All the structurally important regions of beta-lactamase deviated more than the wild type peptide bound simulation; especially a significant increase in the RMSD value of H10 helix is observed; the RMSD value of H10 helix in the P1 bound TEM-1 is 1.21 Å while it became 2.07 Å as a result of mutations A46R, A47R and D49H (Table 3.13). Hence a more fluctuating RMSD – time profile is obtained (Figure 3.21g).

P8 is a wild type peptide which is one residue longer than the P1. The RMSD value of beta-lactamase stays the same with respect to the P1 bound TEM-1, the RMSD values of

TEM-1 were 0.70 and 0.69 Å, in the P1 and P8 bound forms of beta-lactamase; respectively (Table 3.12). The deviations of the structurally important regions of TEM-1 were almost the same as in P1 bound simulation except the 99-112 region. The RMSD value of 99-112 region became 0.96 Å from 0.67 Å as a result of binding of the peptide with an additional Tyr residue at the C-terminus (Table 3.13). A more fluctuating profile compared to the P1 bound simulation was observed before the production run period, after 4 ns a more stable profile is obtained (Figure 3.21h).

P9 is the peptide with a mutation at the position Gly48 in P8. The G48F mutation increased the RMSD value of beta-lactamase from 0.69 Å to 0.97 Å (Table 3.12). H9-H10 helices, 99-112 region, Ω loop and its flexible tip deviated more than wild type peptide bound form. Only the deviation of the H10 helix does not affect from the mutation; its RMSD was 1.22 Å in the wild type peptide bound form and became 1.24 Å upon mutation of G48F (Table 3.13). The fluctuations obtained in the RMSD – time profile of P9 bound TEM-1 are similar to the ones in the wild type peptide, P8, bound simulation (Figure 3.21i).

P10 is the peptide with additional five residues at the N-terminus of the P8. These five residues, LLIIL, are the hydrophobic residues of a cell penetrating peptide, pVEC, which is thought to be playing an important role in the cellular uptake of the BLIP based peptides. The addition of these hydrophobic residues to the N-terminus of the P8 increased the RMSD value of beta-lactamase from 0.69 Å to 0.85 Å (Table 3.12). The RMSD values of the structurally important regions of TEM-1 have affected in a different manner; H10 helix, 99-112 region and the flexible tip of the Ω loop deviated more than the wild type peptide bound simulation, however the deviation of the H9-H10 helices region, Ω loop and the active site residues were not significantly affected (Table 3.13). The RMSD – time profile of the simulation shows that the fluctuations are similar to the P8 bound simulation (Figure 3.21j).

3.2.1.2.Stability of Peptides. Most of the peptides have high deviations from their initial models because of their small size. When the RMSD values of the peptides between the initial and time averaged coordinates, which were calculated after superimposing the C_α atoms of peptides in all simulation systems, were analyzed, a wide range of RMSD values

observed. The lowest RMSD value belongs to the P3, the peptide with the mutation of A46W, and the highest RMSD value is observed in the P4, the peptide with the mutation of D49A (Table 3.12).

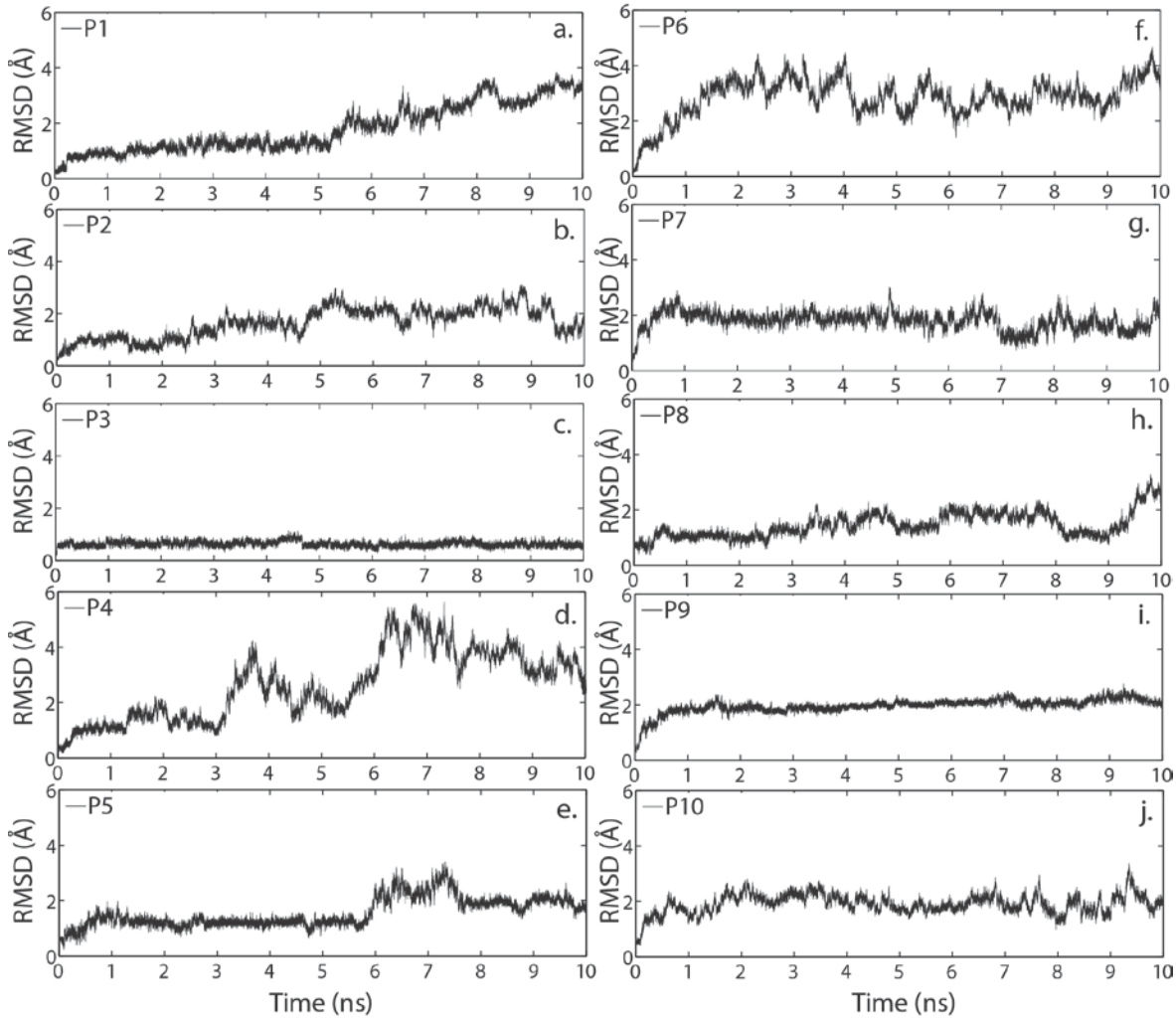

Figure 3.22. The RMSD profiles of (a) P1, (b) P2, (c) P3, (d) P4, (e) P5, (f) P6, (g) P7, (h) P8, (i) P9, (j) P10 peptides during 10 ns MD simulations.

P1 has a RMSD value of 2.03 Å (Table 3.12). The RMSD – time profile of P1 shows high fluctuations in the production run period (Figure 3.22a). The production run period from four ns to the end of simulations is taken after the RMSD profile of TEM-1 beta-lactamase (Figure 3.21) reached equilibrium. However the RMSD – time profile of some of the peptides doesn't reach a plateau value. P2 has a RMSD value of 1.90 Å and the fluctuations observed in the deviation profile (Figure 3.22b) were stabilized compared to P1. Cyclic peptide structure makes the peptide deviate less than the wild type peptide, P1.

P3 has a RMSD value of 0.54 Å and compared to P1, the deviations observed in peptide during the simulation has stabilized (Figure 3.22c) and the RMSD value has decreased significantly, hence due to the A46W mutation the peptide stay close to its initial coordinates.

P4 is the peptide with the mutation of D49A. As stated previously, Asp49 is a catalytically important residue; the carboxylate of this acidic amino acid mimics the carboxylate of penicillin G in the TEM-1 – penicillin complex (Strynadka *et al.*, 1996). Hence a higher deviation and an unstable profile are expected with the substitution of this Aspartic acid residue with Alanine. The RMSD value of the wild type peptide increased to 3.01 Å as a result of the mutation. The RMSD – time profile shows that the peptide has not reached equilibrium and became unstable; the fluctuations were continuous during the simulation timescale (Figure 3.22d).

P5 has a RMSD value of 1.41 Å and it is much lower than that of P1. The deviation profile shows a more stable behavior compared to P1, the fluctuations were dampened upon Y50A mutation (Figure 3.22e).

Y51A mutation causes a more fluctuating profile (Figure 3.22f) with respect to the wild type peptide. The RMSD value of P6 was 2.70 Å while that of the wild type was 2.03 Å. Similar to P6, P7 has a lower RMSD value, 1.66 Å, compared to P1 and the fluctuations were dampened (Figure 3.22g) with the substitution of basic amino acids to the N-terminus of the peptide.

The addition of the Tyr residue to the C-terminus of P1 has lowered the RMSD value of the peptide. P8 has a RMSD value of 1.33 Å while that of P1 was 2.03 Å. The deviation profile of P8 (Figure 3.22h) has showed lower fluctuations in the production run period compared to P1.

P9 has a higher deviation compared to P8, the RMSD values for P8 and P9 were 1.33 Å and 1.96 Å, respectively. Despite the increase in the deviation, the G48F mutation stabilized the fluctuations observed in P8 and the peptide reaches equilibrium after 4 ns

(Figure 3.22i). P10 also has a higher RMSD value, 1.70 Å, with respect to P8. Similar fluctuations to the ones in P8 were observed in P10 (Figure 3.22j).

The RMSD values of the peptides with respect to TEM-1 beta-lactamase (Table 3.11) were calculated between the initial and time averaged coordinates of peptides, after superimposing the simulation snapshots based on C_α coordinates of TEM-1, in order to obtain information about the deviation of peptides while initial and simulation structures of beta-lactamase are aligned. Wild type peptide, P1, and its cyclic form, P2, deviated from their initial coordinates at closer RMSD values with respect to TEM-1; the RMSD values for these peptides were 3.45 and 3.31 Å, respectively. A46W mutation caused a slight decrease in the peptide deviation, the RMSD value with respect to beta-lactamase became 2.75 Å as a result of mutation. The D49A mutation caused a major increase in the peptide deviation with respect to TEM-1, the RMSD value became 7.82 Å as a result of this critical substitution at position 49. The peptides carrying Y50A and Y51A mutations have RMSD values of 2.62 and 3.35 Å, respectively. The substitution of the Arg residues to the N-terminus of the peptide resulted in 3.22 Å peptide deviation with respect to TEM-1 beta-lactamase. Addition of a Tyr residue to the C-terminus of the wild type peptide, P1, stabilized the peptide with respect to TEM-1 with a RMSD value of 1.79 Å. However, G48F mutation done on P8 resulted in a significant increase in the peptide RMSD with respect to beta-lactamase, the RMSD value became 4.21 Å. Addition of the hydrophobic pVEC residues to the N-terminus of the peptide increased the RMSD value with respect to beta-lactamase from 1.79 Å to 2.99 Å. The peptides have similar deviations with respect to TEM-1, the only peptides which have higher deviations were the ones carrying mutant residues at positions 48 and 49 of BLIP.

3.2.1.3. Stability of TEM-1 – Peptide Complexes. The deviations of the complexes with respect to their initial coordinates were examined in all simulation systems; the complexes have RMSD values in the range of 0.8 Å to 1.8 Å (Table 3.12).

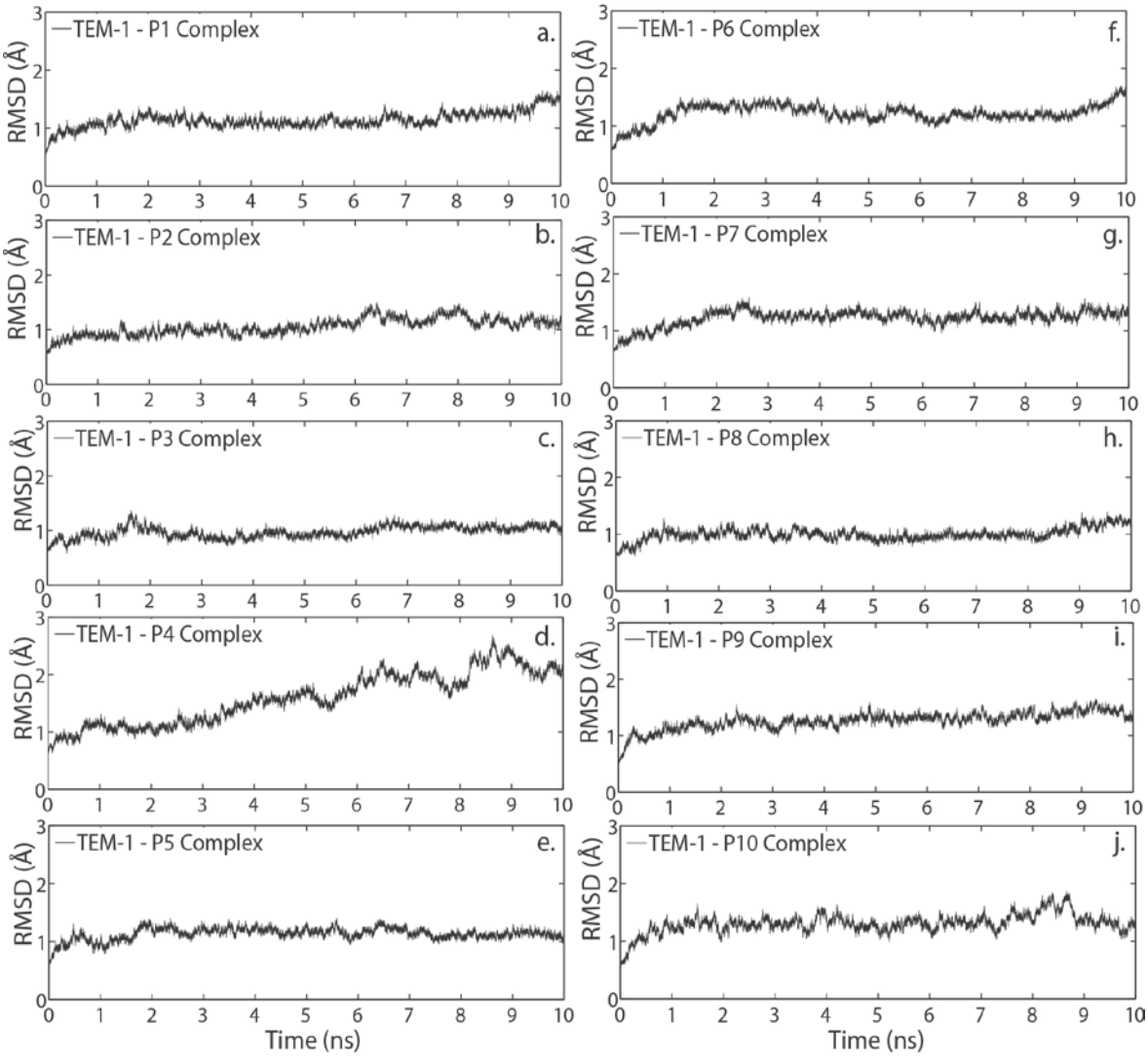

Figure 3.23. The RMSD profiles of TEM-1 bound (a) P1, (b) P2, (c) P3, (d) P4, (e) P5, (f) P6, (g) P7, (h) P8, (i) P9, (j) P10 complexes during 10 ns MD simulations.

TEM-1 – P1 complex has a RMSD value of 0.92 Å. The P2 binding to TEM-1 doesn't affect the deviation compared to wild type complex; the RMSD value for the TEM-1 – P2 complex was 0.95 Å. The RMSD – time profiles of these 2 simulation systems (Figure 3.23a, b) were similar to each other suggesting that cyclic peptide structure has almost no effect on the complex deviation.

The RMSD value for the TEM-1 – P3 complex is 0.83 Å, and it is lower than that of wild type peptide – beta-lactamase complex. The decrease in the RMSD is caused by the lower deviation of the mutant peptide; as mentioned before P3 is the most stable peptide

among the others. The RMSD – time profile of the TEM-1 – P3 complex (Figure 3.23c) also confirms the stabilization upon A46W mutation.

As stated in previous sections, D49A mutation causes both beta-lactamase and the peptide deviate more than expected. Because of the high RMSD values of TEM-1 and the peptide, the TEM-1 – P4 has a RMSD value of 1.71 Å. The deviation profile (Figure 3.23d) shows that TEM-1 – P4 complex doesn't reach equilibrium, high fluctuations are observed during the simulation.

The RMSD values for TEM-1 bound P5, P6 and P7 complexes are 0.88, 0.99 and 1.12 Å; respectively (Table 3.12). Y50A and Y51 mutations don't affect the complex deviations with respect to the wild type peptide – TEM-1 complex; however the mutations at the positions 46, 47 and 49 cause higher deviations in TEM-1 and the overall RMSD value of TEM-1 – P7 complex increased as a result of the high beta-lactamase deviation. The fluctuations observed in the RMSD – time profiles of these complexes (Figure 3.23e, f, g) are similar to the ones in the TEM-1 – P1 complex.

Addition of the Tyr residue to the C-terminus of the wild type peptide, P1, has decreased the RMSD value from 0.92 to 0.75 Å. This decrease is due to the lower deviation of the P8. The RMSD values of P9 and P10 bound complexes are 1.22 and 1.06 Å, respectively. Both the G48F mutation and the addition of the hydrophobic pVEC residues to the N-terminus of the P1 increased the overall complex deviation. The RMSD – time profiles of the P8 and P9 (Figure 3.23h, i) are similar to each other; despite the lower RMSD value of P10 bound complex with respect to that of P9 bound simulation, higher fluctuations were observed in the P10 bound complex simulation (Figure 3.23j).

3.2.2. Dynamics of the Simulation Systems

The dynamics of the simulation systems was investigated by calculating and comparing the MSF values of beta-lactamase, peptide and complexes in all simulation systems in order to change in mobility of upon binding of different peptides to TEM-1 beta-lactamase. The change in the mobility of the regions in beta-lactamase can indicate the importance of these structural components in the ligand recognition mechanism of

beta-lactamase. The MSF values of the beta-lactamase were calculated with the procedure mentioned in Section 2.2.2; by excluding the first and last 3 residues of beta-lactamase. MSF calculation for the peptides was done with all the C_α atoms of the peptide, because of the short peptide sequences. The complex MSF values are calculated by aligning all the C_α atoms of TEM-1, except for the first and last 3 residues, and the peptide. Changes in dynamics upon mutation at the specific regions of the BLIP based peptides were analyzed and gain or lose in mobility upon mutations were compared.

3.2.2.1. Change in Dynamics upon Binding of Peptides Designed Based on the 45-52 Region of BLIP. As previously stated, the simulations were done with 10 different peptides which were designed based on either 45-52 or 45-53 region of BLIP. The wild type peptide which is designed based on the 45-52 region is named as P1 and the comparison of the peptides designed based on this region of BLIP in terms of mobility is going to be done with this wild type peptide, P1.

In the P1 bound TEM-1 simulation, the MSF value of beta-lactamase was 0.39 $Å^2$ while that of peptide and complex were 1.64 and 0.57 $Å^2$, respectively. P2 binding decreased all the RMSD values of enzyme, peptide and the complex to 0.28, 0.52 and 0.42 $Å^2$, respectively (Table 3.12). When the MSF values for the structurally important regions of TEM-1 were examined, it was observed that H10 helix, H9-H10 helices, 99-112 loop and the active site residues lose mobility upon binding of P2 compared to P1 bound simulation while a significant increase in the mobility of the flexible tip of the Ω loop has obtained (Table 3.13).

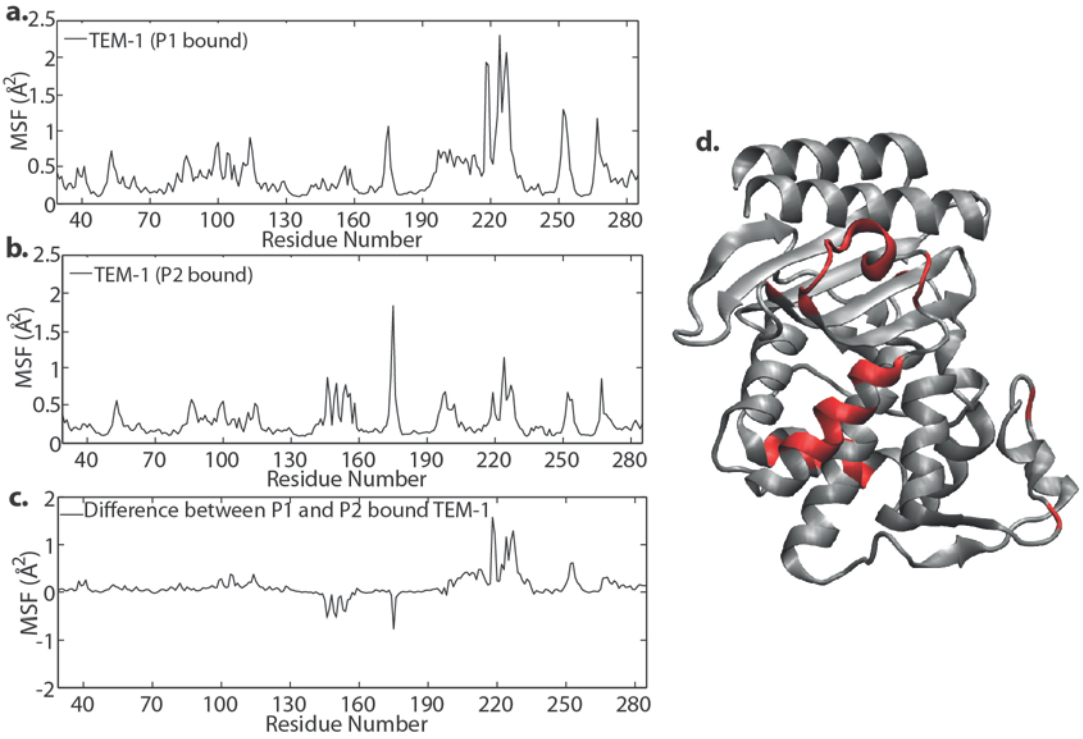

Figure 3.24. The MSF values for the Cα atoms of (a) P1 bound, (b) P2 bound TEM-1. (c) The difference in MSF values between P1 and P2 bound TEM-1 complexes. (d) TEM-1 structure in cartoon representation is shown with the red color indicating regions of MSF difference higher than 0.35 $Å^2$.

The regions which show higher fluctuations than the threshold of 0.7 $Å^2$ in P1 bound TEM-1 simulation were localized to the loop connecting S1 and S2 beta sheets (especially Ser53), N and C-terminus of the 99-112 loop, the flexible tip of the Ω loop (residues Pro174 and Asn175), the loop connecting H8 and H9 helices, H10 helix, the loop connecting S4 and S5 beta sheets and the C-terminus of the S5 beta sheet. Among the mentioned structural regions, H10 helix residues had high MSF peaks (Figure 3.24a). When the cyclic peptide is bound to TEM-1, most of the fluctuations observed in P1 bound simulation are dampened. The regions with the higher fluctuations than the threshold were observed in the regions comprised by H6 helix, the flexible tip of the Ω loop, the C-terminus of H10 and S5 beta sheet (Figure 3.24b). The difference between the MSF values (ΔMSF) of the P1 and P2 bound simulations was examined and it was seen that most of the mobile regions were located in wild type peptide bound TEM-1. The only regions which gain mobility in the cyclic peptide bound simulation were the H6 helix and Asn175 which is located at the Ω loop. The structural regions which have higher MSF values in the wild

type peptide bound form were localized to Glu104 and Thr114, H9-H10 helices and the C-terminus of the S4 beta sheet (Figure 3.24c, d).

Upon P3 binding to TEM-1, beta-lactamase, peptide and the complex lose mobility. The MSF values for these regions were 0.31, 0.11 and 0.35 $Å^2$, respectively (Table 3.12). The A46W mutation mostly affects the fluctuations of the H10 and H9-H10 helices regions, the MSF values for these regions decreased to 0.45 and 0.37 $Å^2$, as a result of the mutant peptide binding compared to wild type peptide bound form. The mobility of the other structurally important regions were not affected by the mutant peptide binding, their MSF values stay close to those of in P1 bound TEM-1 simulation (Table 3.13).

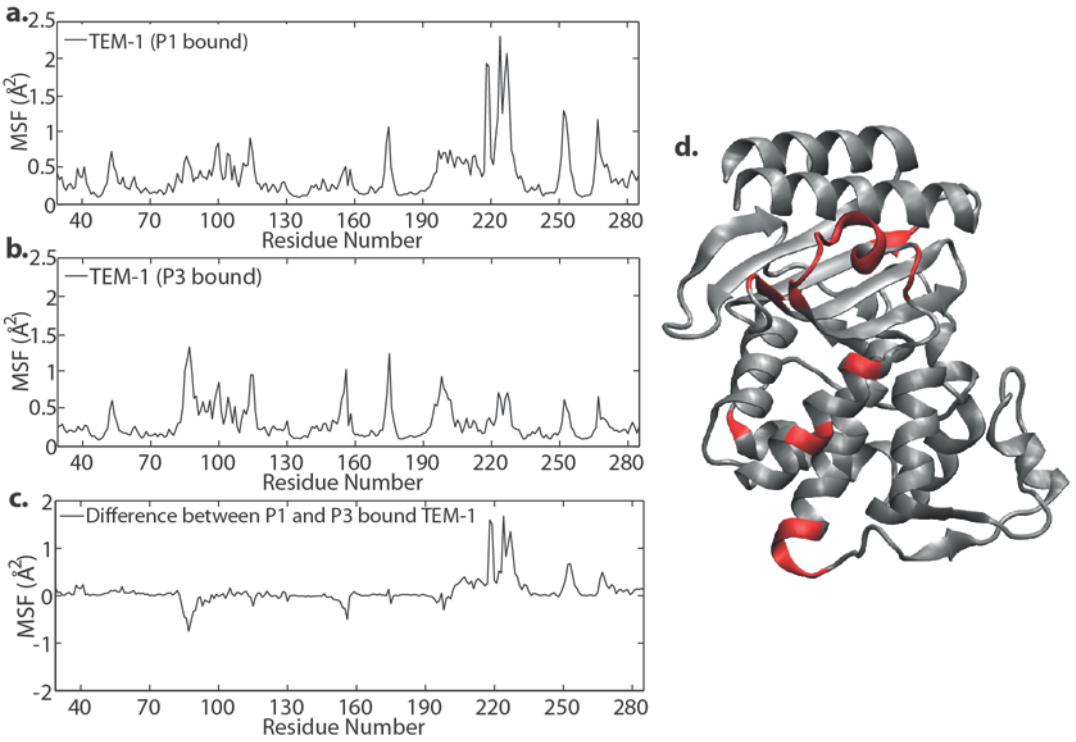

Figure 3.25. The MSF values for the Cα atoms of (a) P1 bound, (b) P3 bound TEM-1. (c) The difference in MSF values between P1 and P3 bound TEM-1 complexes. (d) TEM-1 structure in cartoon representation is shown with the red color indicating regions of MSF difference higher than 0.35 $Å^2$.

The residue based MSF calculations show that most of the mobile regions are located in wild type peptide bound simulation (Figure 3.25a). The regions which gain mobility upon binding of P3 to TEM-1 were localized to the loop connecting H2 helix to SC1 beta

sheet, N and C-terminus of the 99-112 region, C-terminus of the H6 helix (spanning residues Met155 and Gly156), Ω loop, the loop between H8 and H9 helices and the C-terminus of the H10 helix (Figure 3.25b). The ΔMSF values calculated between P1 and P3 bound TEM-1 show that, only the loop spanning residues Asp85 to Gln88 and the Gly156 which is located at the C-terminus of H6 helix gain mobility upon A46W mutation. H9-H10 helices, the loop connecting S4 and S5 beta sheets (spanning residues Pro251 to Lys254), Ser266 and Gln267 which are located at the C-terminus of the S5 beta sheet were more mobile in wild type peptide bound simulation (Figure 3.25c, d).

P4 binding to TEM-1 results in high mobility of the peptide and complex because of the high deviations observed in the structure. It has to be noted that the RMSD value of peptide was way much higher than the other peptides. The MSF values for TEM-1, peptide and complex were 0.34, 2.71 and 0.78 $Å^2$, respectively (Table 3.12). H10 helix and H9-H10 helices lose mobility upon mutation while little increase in the MSF value was observed in other structural components (Table 3.13).

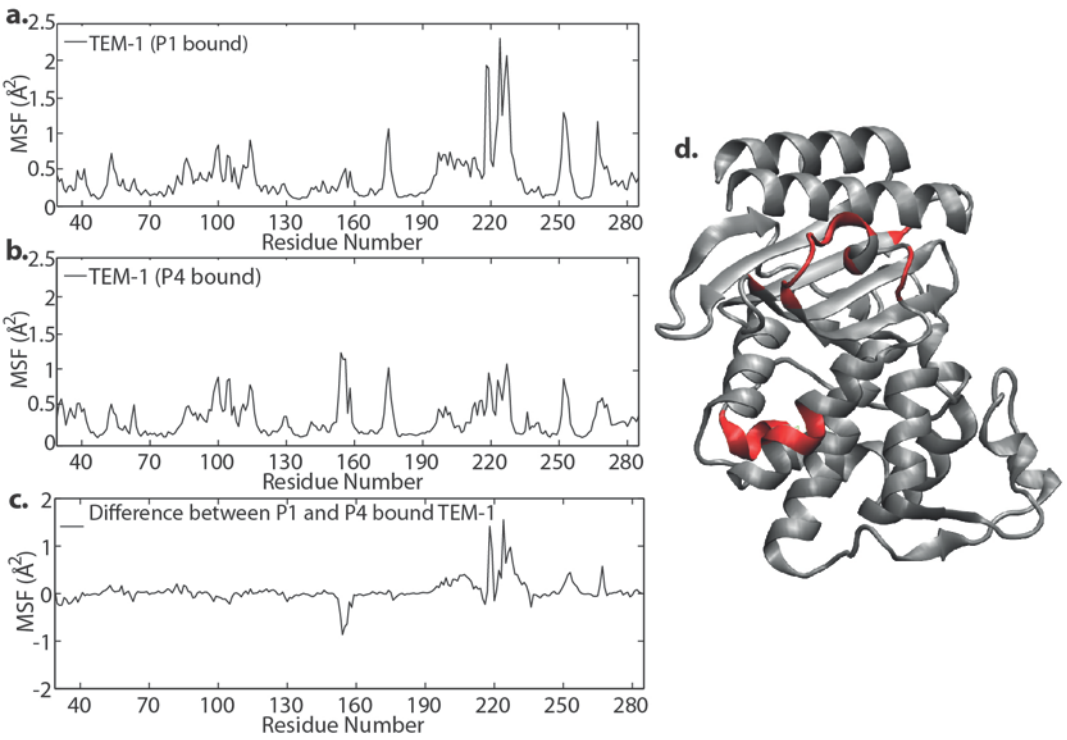

Figure 3.26. The MSF values for the C_α atoms of (a) P1 bound, (b) P4 bound TEM-1. (c) The difference in MSF values between P1 and P4 bound TEM-1 complexes. (d) TEM-1 is colored based on the MSF difference, with a threshold of absolute 0.35 $Å^2$.

The mobile regions of P4 bound TEM-1 were localized to the 99-112 loop, C-terminus of the H6 helix, flexible tip of the Ω loop, H10 helix and the C-terminus of the S4 beta-sheet (Figure 3.26b). The ΔMSF examination shows that most of the regions were more mobile in the wild type peptide bound form. The only region which shows a more mobile behavior is the C-terminus of the H6 helix (spanning residues His153 to Gln156); the others have higher MSF value in the wild type peptide bound TEM-1 (Figure 3.26c).

Mobility of TEM-1, peptide and complex structures are not significantly affected by Y50A mutation. Their MSF values were 0.38, 1.59 and 0.55 $Å^2$ in the P5 bound TEM-1, respectively (Table 3.12). Although the overall MSF values are almost the same as that of P1 bound form, significant changes were observed in H10 helix. The MSF value for H10 helix in P1 bound TEM-1 was 1.33 $Å^2$ while it decreased to 0.77 $Å^2$ upon P5 binding. H9-H10 helices region lost mobility as well. Ω loop and the 99-112 region gained mobility as opposed to H10 and H9-H10 helices. The active site mobility stays the same (Table 3.13).

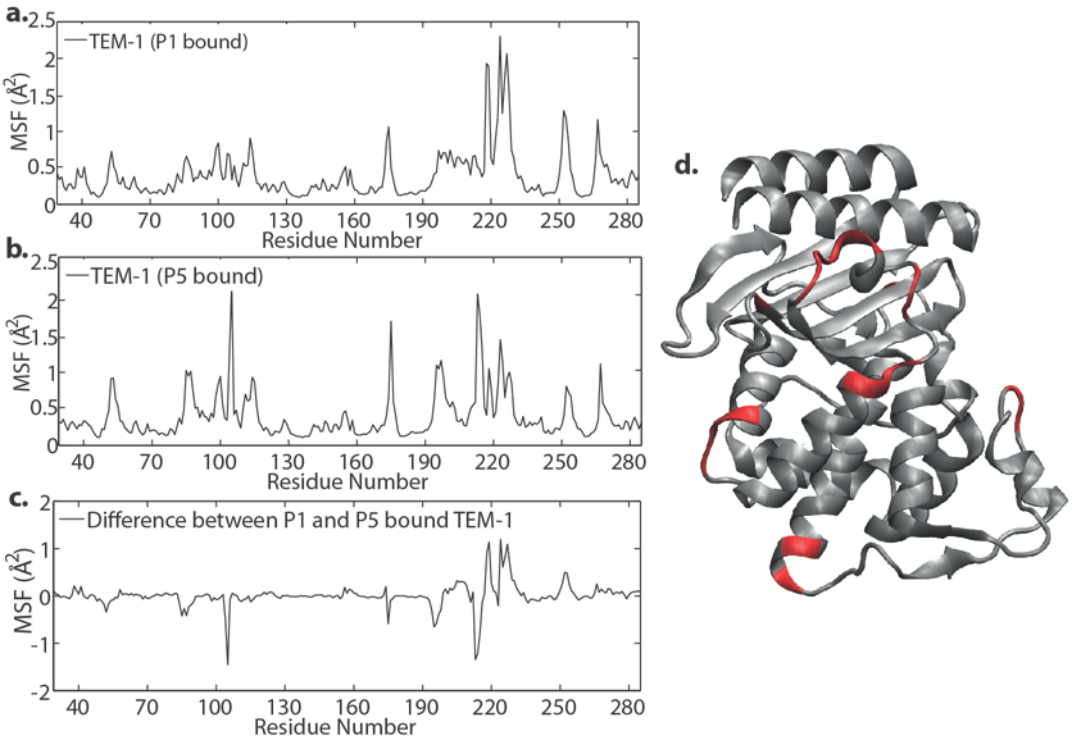

Figure 3.27. The MSF values for the C_α atoms of (a) P1 bound, (b) P5 bound TEM-1. (c) The difference in MSF values between P1 and P5 bound TEM-1 complexes. (d) TEM-1 structure in cartoon representation is shown with the red color indicating regions of MSF difference higher than 0.35 $Å^2$.

The regions that have higher MSF values than the threshold of 0.7 $Å^2$ in P5 bound TEM-1 were the loop connecting S1 and S2 beta sheets, the loop connecting H2 helix and SC1 beta sheet, 99-112 loop, Asn175 which is located at the flexible tip of the Ω loop, the loop connecting H8 and H9 helices, H10 helix, C-terminus of the S4 beta sheet and Gln267 which is located at the C-terminus of the S5 beta sheet (Figure 3.27b). The ΔMSF values show that the regions which have higher motions in mutant were localized to the C-terminus of the H2 helix, the middle part of the 99-112 loop (spanning residues Glu104 and Tyr105), C-terminus of H8 and the C-terminus of H9, while H10 helix and C-terminus of S4 beta sheet (spanning residues Asp252 and Gly253) have higher motions in wild type peptide bound TEM-1 (Figure 3.27c, d).

P6 binding reduced the motions observed in TEM-1, peptide and complex; their MSF values became 0.35, 1.23 and 0.51 $Å^2$ (Table 3.12). Significant changes in mobility were apparent in the H10 and H9-H10 helices region. Their MSF values are reduced remarkably as a result of Y51A mutation. The Ω loop motions are increased while the active site residues are seemed to be not affected (Table 3.13). The structural parts which have higher fluctuations than the threshold of 0.7 $Å^2$ were the C-terminus of the H2 helix, the 99-112 loop, H6 helix, the flexible tip of the Ω loop, the loop connecting H8 and H9 helices, Leu220 and Ala227 which are located at the H10 helix and Gln267 (Figure 3.28b). The ΔMSF values calculated based on the difference between the P1 and P6 bound TEM-1 motions show that Asp115, H6 helix, the flexible tip of the Ω loop spanning residues Pro174 and Asn175, and Thr195 which is located at the C-terminus of the H8 helix gain mobility as a result of Y51A mutation compared to wild type peptide binding. The H9-H10 helices and the C-terminus of the S4 beta sheet spanning residues Asp252, Gly253 and Lys254 are the structural regions which have higher motions in wild type peptide bound enzyme (Figure 3.28c, d).

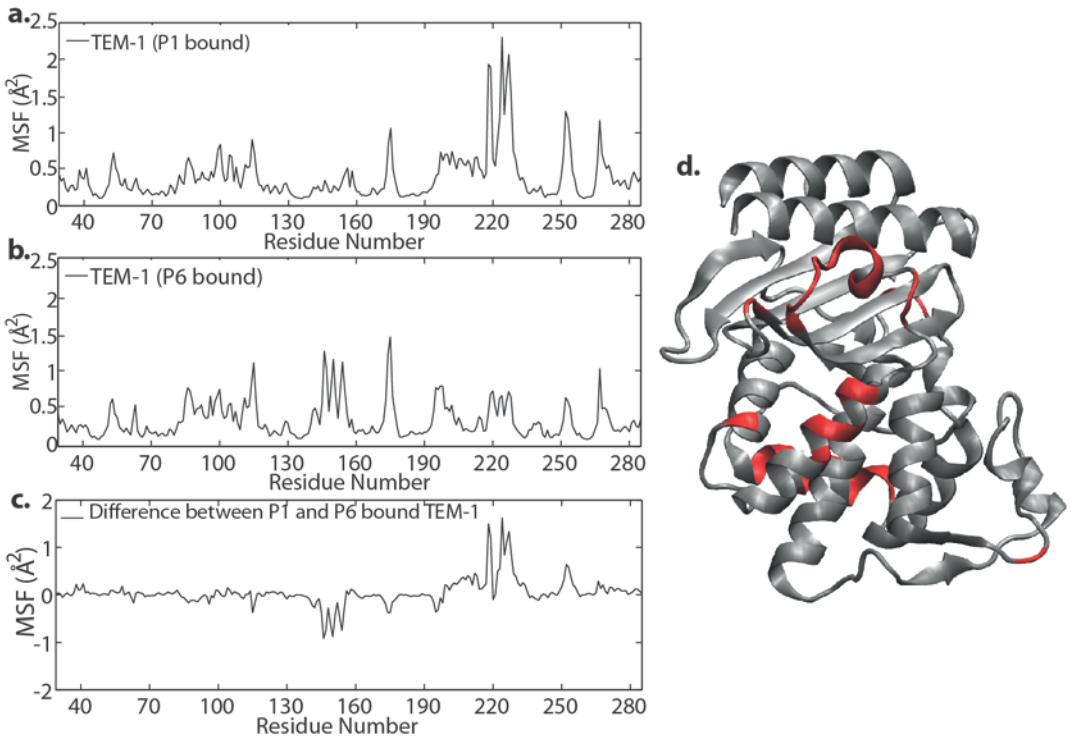

Figure 3.28. The MSF values for the C_α atoms of (a) P1 bound, (b) P6 bound TEM-1. (c) The difference in MSF values between P1 and P6 bound TEM-1 complexes. (d) TEM-1 structure in cartoon representation is shown with the red color indicating regions of MSF difference higher than 0.35 $Å^2$.

P7 binding to TEM-1 reduced its MSF value from 0.39 $Å^2$ to 0.30 $Å^2$. The MSF values for peptide and complex in the P7 bound simulation are 0.34 and 0.35 $Å^2$, respectively (Table 3.12). Significant changes in mobility are apparent in the H10 helix and the H9-H10 helices region compared to wild type. The MSF values of these mentioned regions are decreased remarkably as a result of Arginine substitution to the N-terminus and D49H mutation. The motions of other individual structural components are almost the same as that of wild type peptide bound simulation (Table 3.13). The residue based MSF profile also confirms the low motions, the regions which have higher fluctuations than the threshold of 0.7 $Å^2$ were localized to Ala86 and Gly87 that are located at the C-terminus of the H2 helix, Asn100 which is at the N-terminus of the 99-112 loop, the flexible tip of the Ω loop spanning residues Pro174 and Asn175, the C-terminus of the H8 helix, Ala227 which is at the C-terminus of the H10 helix and Gln267 located at the C-terminus of the S5 beta sheet. The difference in term of motions between the wild type peptide and P7 bound simulations show that only the C-terminus of H8 helix show more fluctuations than the

wild type; the motions of H9-H10 helices and the loop connecting S4 and S5 beta sheets are more apparent in P1 bound enzyme (Figure 3.29c, d).

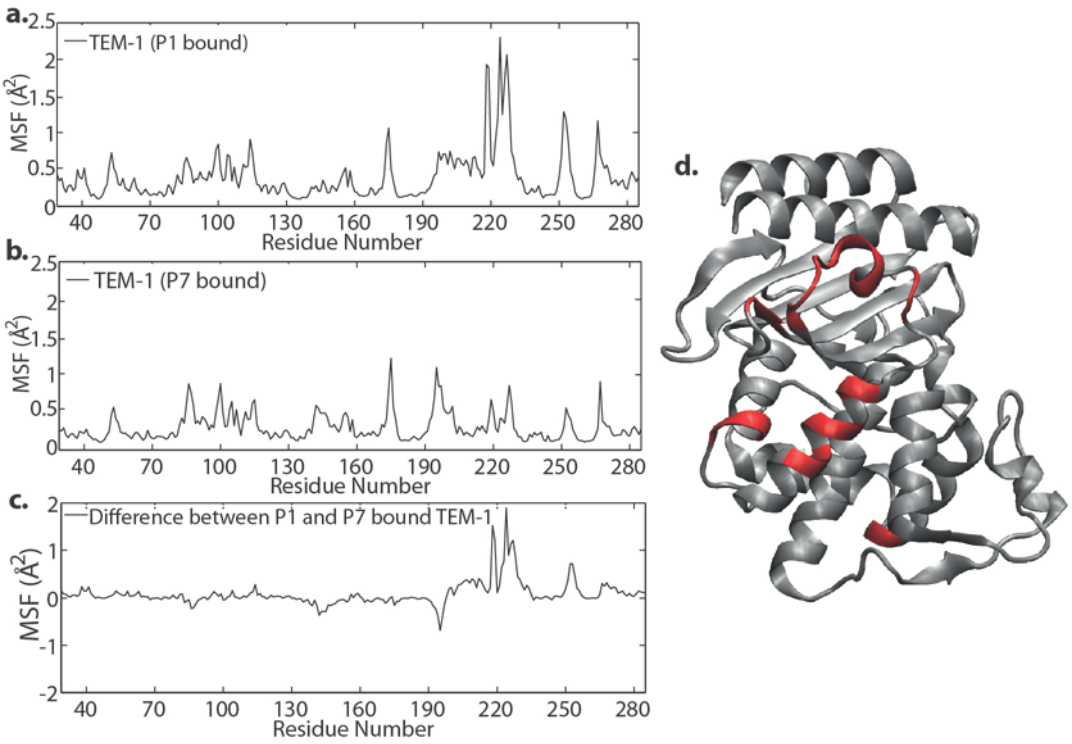

Figure 3.29. The MSF values for the C_α atoms of (a) P1 bound, (b) P7 bound TEM-1. (c) The difference in MSF values between P1 and P7 bound TEM-1 complexes. (d) TEM-1 structure in cartoon representation is shown with the red color indicating regions of MSF difference higher than 0.35 $Å^2$.

3.2.2.2. Change in Dynamics upon Binding of Peptides Designed Based on the 45-53 Region of BLIP. The simulations were carried out with the peptides which have an additional Tyr residue at the C-terminus. The wild type peptide designed based on the region comprised by residues 45 to 53 of BLIP is named as P8 (Table 3.11) and the comparison of motions of different simulation systems is going to be done with P8.

In order to see the effect of additional Tyr residue to the dynamic motions of simulations, MSF values of the 2 wild type peptides, P1 and P8, were analyzed and compared. As stated before, the regions with high motions in P1 bound simulation were localized to the loop connecting S1 and S2 beta sheets (especially Ser53), N and C-

terminus of the 99-112 loop, the flexible tip of the Ω loop (residues Pro174 and Asn175), the loop connecting H8 and H9 helices, H10 helix, the loop connecting S4 and S5 beta sheets and the C-terminus of the S5 beta sheet (Figure 3.30a). High fluctuations were observed at the C-terminus of the H2 helix, the middle part of the 99-112 loop spanning residues Glu104 and Tyr105, the flexible tip of the Ω loop, the loop connecting H8 and H9 helices, H10 helix and Lys254 which is located at the loop connecting S4 and S5 beta sheets, in the P8 bound simulation (Figure 3.30b). As it can be seen, similar regions show motions higher than threshold.

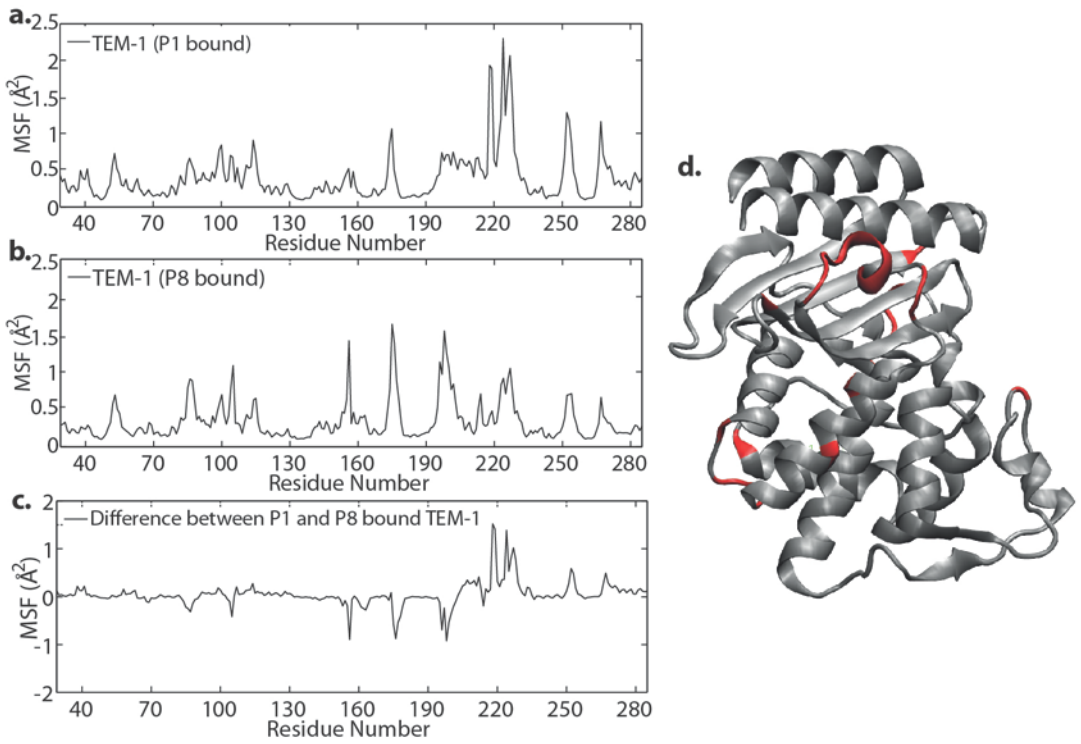

Figure 3.30. The MSF values for the C_α atoms of (a) P1 bound, (b) P8 bound TEM-1. (c) The difference in MSF values between P1 and P8 bound TEM-1 complexes. (d) TEM-1 structure in cartoon representation is shown with the red color indicating regions of MSF difference higher than 0.35 $Å^2$.

The ΔMSF values were examined in order to find out which region has higher fluctuations in which simulation, and it was observed that Tyr105 of the 99-112 loop, Gly156 at the C-terminus of H6 helix, the flexible tip of the Ω loop and the loop connecting H8 and H9 helices were more mobile in P8 bound simulation; H9-H10 helices, the C-terminus of the S4 and S5 beta sheets had higher motions in P1 bound simulation

(Figure 3.30c, d). It has to be noted that overall TEM-1 mobility was not significantly affected by P8 binding; the MSF values for TEM-1 in P1 and P8 bound simulation were 0.39 Å^2 and 0.34 Å^2, respectively (Table 3.12). Significant changes in motions of H10 helix and H9-H10 helices region were observed, their MSF values decreased to 0.62 and 0.50 Å^2 upon P8 binding, respectively. Ω loop mobility has decreased while active site residues are almost not affected (Table 3.13).

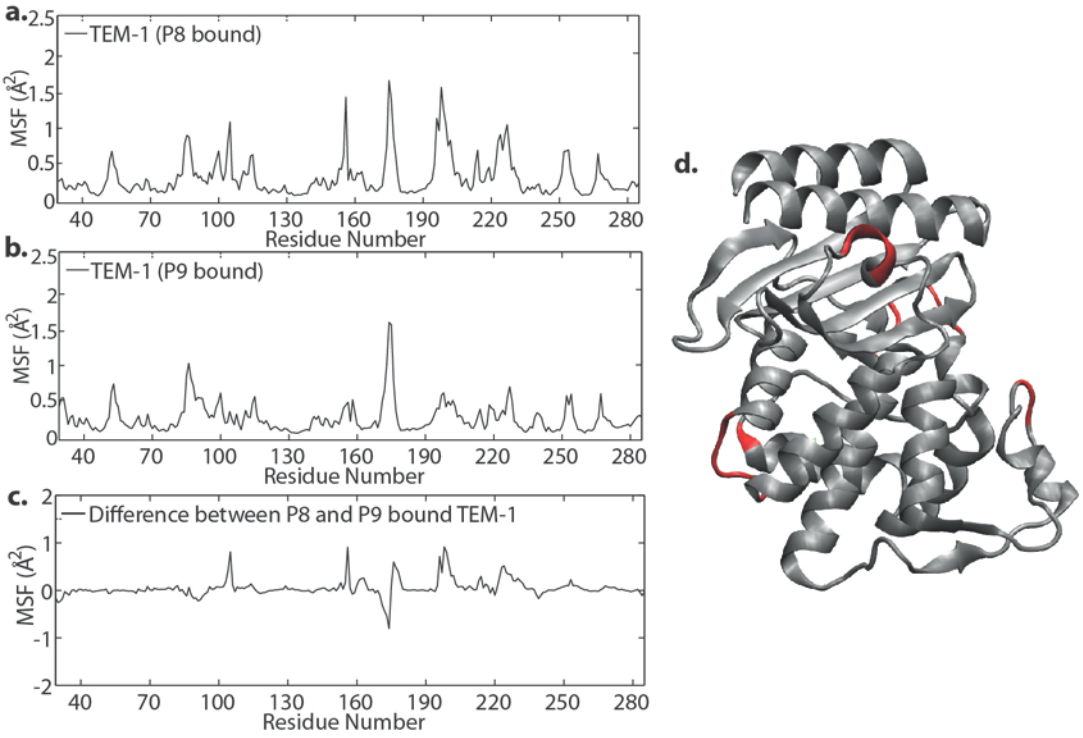

Figure 3.31. The MSF values for the C_α atoms of (a) P8 bound, (b) P9 bound TEM-1. (c) The difference in MSF values between P8 and P9 bound TEM-1 complexes. (d) TEM-1 structure in cartoon representation is shown with the red color indicating regions of MSF difference higher than 0.35 Å^2.

P9 binding to TEM-1 reduced the motions of TEM-1 compared to P8 bound simulations. The MSF values for enzyme, peptide and the complex in P9 bound simulation were 0.29, 0.47 and 0.32 Å^2, respectively (Table 3.12). G48F mutation reduced the fluctuations of the peptide significantly, from 1.22 Å^2 to 0.47 Å^2, and as a result of that effect the overall mobility of the complex has decreased. When the individual structural components were examined, the reducing effect of mutation in terms of mobility was apparent in H10, H9-H10, 99-112 region and the Ω loop MSF values. The flexible tip of

the Ω loop and the active site residues are almost not affected by the mutation (Table 3.13). The regions which have high fluctuations than the threshold of 0.7 Å^2 in P9 bound simulation were localized to Ser53 which is located at the loop connecting S1 and S2 beta sheets, the C-terminus of the H2 helix, the flexible tip of the Ω loop and Ala227 which is at the C-terminus of the H10 helix (Figure 3.31b). The difference between the P8 and P9 bound simulations show that all the regions with high motions are located at the wild type peptide bound simulation except the flexible tip of the Ω loop spanning residues 172 to 174 (Figure 3.31c, d).

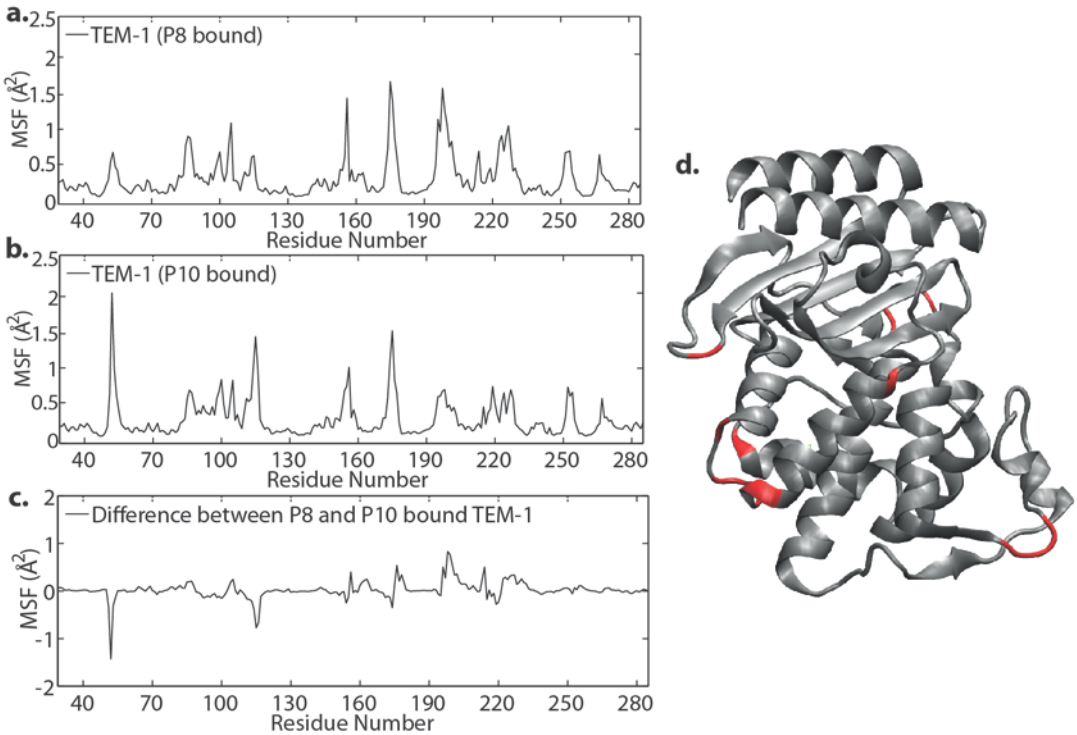

Figure 3.32. The MSF values for the C_α atoms of (a) P8 bound, (b) P10 bound TEM-1. (c) The difference in MSF values between P8 and P10 bound TEM-1 complexes. (d) TEM-1 structure in cartoon representation is shown with the red color indicating regions of MSF difference higher than 0.35 Å^2.

As mentioned before, P10 is the peptide with additional pVEC residues at the N-terminus of P8. The addition of these hydrophobic residues doesn't seem to affect the overall mobility of TEM-1, however possibly because of the long peptide size with respect to P8, the dynamic motions of peptide as well as the complex have increased (Table 3.12). The individual structural components of TEM-1 were not significantly affected except the

H10, H9-H10 helices and the flexible tip of the Ω loop. The MSF values of these mentioned regions were 0.62, 0.50 and 1.26 $Å^2$ in the P8 bound simulation and they became 0.49, 0.37 and 1.15 $Å^2$ upon P10 binding, respectively (Table 3.13). The residue based MSF calculation of the P10 bound simulation showed that the regions which have higher motions than the threshold were localized to the C-terminus of S1 beta sheet, Ala86 which is located at the C-terminus of H2 helix, 99-112 loop, C-terminus of the H6 helix, the flexible tip of the Ω loop, Leu198 which is in the loop connecting H8 and H9, Pro219 and Ala227 of the H10 helix, and one of the C-terminus residues of S4 beta sheet, Asp252 (Figure 3.32b). In these mentioned regions, Asn52 of the S1-S2 loop, 99-112 region residues, Thr114, Asp115 and Gly116, and Pro174 of the Ω loop had higher motions than the wild type peptide bound simulation. However fluctuations of Gly156 of the H6-H7 loop, the loop connecting H8 and H9 and the C-terminus of H9 were higher in P8 bound TEM-1 (Figure 3.32c, d).

3.2.3. Energy Calculations of the Simulation Systems

3.2.3.1. Intermolecular Interaction Energy Calculations. The intermolecular interaction energy between beta-lactamase and peptides was calculated and compared in order to analyze change in energetics upon binding of different peptides to enzyme. The energy terms were examined and average values were calculated for the production run period (4-10 ns), in all simulation systems (Table 3.14).

Nonbonded energy represents the overall nonbonded interactions between enzyme and ligand, comprising the electrostatic and van der Waals energy terms. The nonbonded energy between the wild type peptide designed based on the 45-52 region of BLIP and beta-lactamase was -228.88 kcal/mol (Table 3.14). TEM-1 – P1 complex (Figure 3.33a) has a stable energy profile with small fluctuations during the simulation timescale. The presence of a disulfide bond in the wild type peptide disfavored the nonbonded interactions observed in the peptide – enzyme interface, the energy value became -93.99 kcal/mol (Figure 3.33b). The disulfide bond in the peptide structure was previously determined to have an unfavorable effect on the inhibition of TEM-1 activity, with a K_i of 603 μM (Rudgers *et al.*, 2001). The decrease in the inhibitory effect was possibly caused by the reduced interactions between enzyme and peptide. Although the position scan done by

FoldX resulted in high preference of a Trp residue at position 46, substitution of the Trp residue instead of Ala resulted in weaker nonbonded interactions compared to wild type. The nonbonded energy between enzyme and peptide became -167.36 kcal/mol (Table 3.14); the energy profile during simulation timescale was similar to that of wild type (Figure 3.33c). With the mutation of D49A, a significant decrease was observed in the nonbonded interactions between enzyme and peptide. The energy value became -40.50 kcal/mol, while that of wild type peptide was -228.88 kcal/mol (Table 3.14). The loss of interactions between peptide and enzyme in the presence of the Ala residue at the position 49 was expected; Asp49 of BLIP was previously reported to be an important residue making crucial interactions with the active site residues of beta-lactamase, Ser130, Lys234, Ser235, Arg243. The energy profile of TEM-1 – P4 complex (Figure 3.33d) became unstable as a result of D49A mutation, sudden changes in the energy values were observed in the production run period. The nonbonded interaction between the peptide, with the mutation of Y50A, and beta-lactamase was weaker than that of observed in the presence of wild type peptide. The energy value became 195.16 kcal/mol (Table 3.14) as a result of the removal of phenolic ring of Tyr50. Removal of Tyr50 side chain was previously identified to increase the binding affinity toward TEM-1 (Zhang and Palzkill, 2003), however the energetic analysis of the TEM-1 – P5 complex resulted in weaker interactions opposed to previous outcomes. The nonbonded interactions between the peptide with the Y51A mutation, P6, and TEM-1 was weaker than that of wild type peptide; with the energy value of -160.18 kcal/mol (Table 3.14). It has to be noted that, Y51A mutation was shown to have no effect on binding affinity of BLIP to TEM-1 (Zhang and Palzkill, 2003). However the energetic analysis showed that, the Tyr residue at the position 51 is an important residue and the removal of its side chain disfavors the interactions at the peptide binding interface. The energy profiles of these two mutants (Figure 3.33e, f) were similar to the energy profile in the presence of the wild type peptide (Figure 3.33a). The peptide with the sequence of RRGHYY-NH_2, P7, was previously identified to inhibit TEM-1 beta-lactamase activity with a K_i of 136 μM, which was almost four times higher than the inhibitory effect of the peptide designed based on the 46-51 region of BLIP comprising a D49H mutation (Huang *et al.*, 2003). However with the energetic analysis of the simulation trajectories, a loss in the nonbonded interactions was observed in the presence of this peptide in complex with TEM-1, the energy value became -124.82 kcal/mol (Table 3.14). Nonbonded energy profile of TEM-1 – P7 complex (Figure 3.33g) showed a steep

descent at the beginning of simulation from the initial energy value at about 100 kcal/mol, but the system was equilibrated quickly with the minimization steps.

Table 3.14. The intermolecular interaction energy terms (kcal/mol) of the simulation systems. Standard deviations are in parenthesis

Simulation system	**Electrostatic energy**	**Van der Waals energy**	**Nonbonded energy**
TEM-1 – P1	-200.47 (19.90)	-28.41 (4.17)	-228.88 (17.40)
TEM-1 – P2	-68.55 (31.32)	-25.44 (3.74)	-93.99 (31.73)
TEM-1 – P3	-144.31 (12.23)	-23.05 (3.51)	-167.36 (11.65)
TEM-1 – P4	-24.22 (28.36)	-16.29 (5.96)	-40.50 (28.25)
TEM-1 – P5	-172.33 (19.39)	-22.84 (3.61)	-195.16 (18.71)
TEM-1 – P6	-141.76 (13.83)	-18.42 (3.62)	-160.18 (14.37)
TEM-1 – P7	-98.95 (26.55)	-25.88 (4.73)	-124.82 (25.02)
TEM-1 – P8	-136.94 (28.58)	-25.82 (4.06)	-162.77 (27.43)
TEM-1 – P9	-221.85 (15.85)	-41.77 (4.33)	-263.62 (14.33)
TEM-1 – P10	-136.24 (15.23)	-24.39 (6.04)	-160.63 (17.89)

Nonbonded energy between P8 and TEM-1 was -162.77 kcal/mol (Table 3.14). Addition of a Tyr residue to the C-terminus of P1 disfavors the nonbonded interaction between enzyme and peptide. The G48F mutation resulted in a significant favorable effect to the nonbonded interactions. Upon G48F mutation, the nonbonded energy became -263.62 from -162.77 kcal/mol (Table 3.14). The Gly at position 48 was proposed to fill the

region occupied by Phe142 of BLIP, which is a critical residue that makes important interactions with Glu104, Tyr105, Asn170, Gly238, Glu240 of TEM-1. The Phe residue substituted to Gly at position 48 possibly results in favorable interactions with beta-lactamase, like the ones observed in the presence of Phe142. P10 binding to TEM-1 has almost no effect on the nonbonded interactions between enzyme and peptide, suggesting that with the substitution of hydrophobic pVEC residues to the N-terminus of the peptide does not generate new interactions with beta-lactamase. The energy profiles of these three peptides designed based on the 45-53 region of BLIP were very similar to each other (Figure 3.33h, i, j).

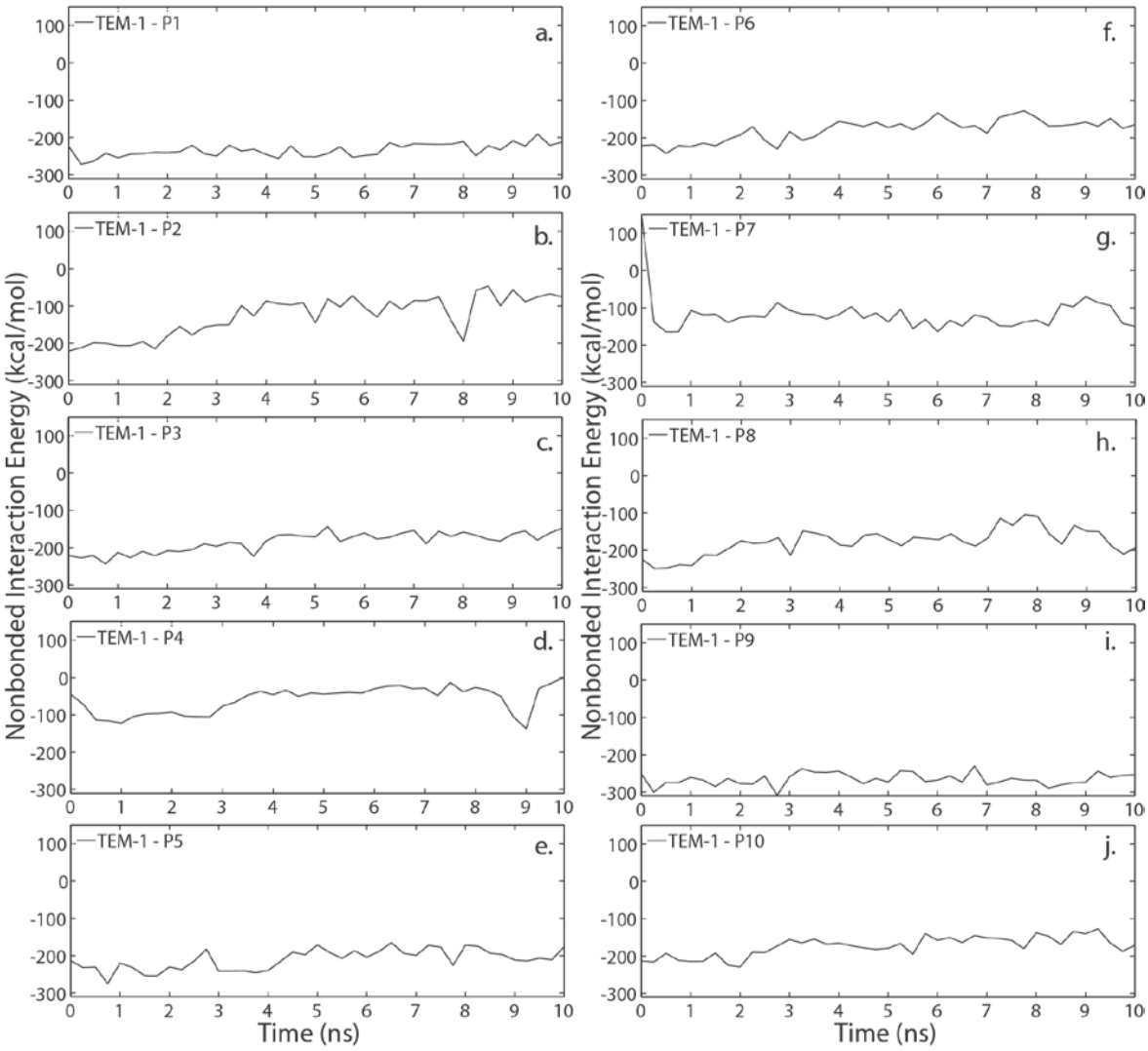

Figure 3.33. The nonbonded energy as a function of time TEM-1 bound (a) P1, (b) P2, (c) P3, (d) P4, (e) P5, (f) P6, (g) P7, (h) P8, (i) P9, (j) P10 complexes during 10 ns MD simulations.

The loss of nonbonded interactions between the peptides, P2, P3, P4, P5, P6, P7, and TEM-1 was mainly caused by the weak electrostatic interactions between enzyme and peptides compared to the electrostatic interactions present in the wild type peptide bound form of beta-lactamase.

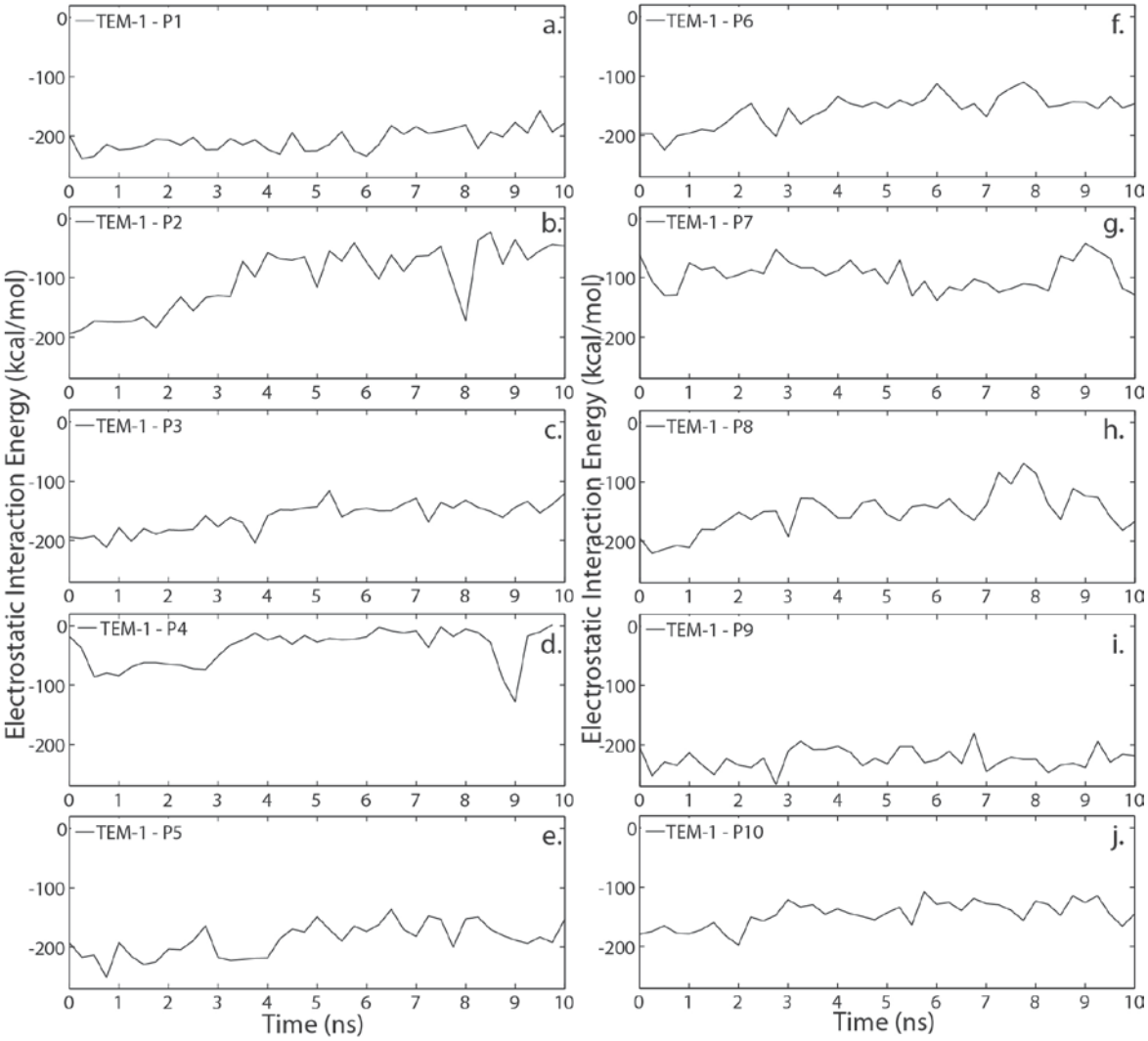

Figure 3.34. The electrostatic energy as a function of time of TEM-1 bound (a) P1, (b) P2, (c) P3, (d) P4, (e) P5, (f) P6, (g) P7, (h) P8, (i) P9, (j) P10 complexes during 10 ns MD simulations.

As stated before, the presence of a disulfide bond, A46W, D49A, Y50A, Y51A, and A46R, A47R, D49H mutations disfavored the nonbonded interactions, the same effect was observed in the coulombic interactions. Upon these mutations, the electrostic energy values became unfavorable (Table 3.14). The energy profiles of simulation systems (Figure 3.34)

also confirmed the unfavorable effect of these mutations with the sudden increase and decreases in the energy values, especially in the beta-lactamase complexes with cyclic peptide, P2, D49A mutant peptide, P4. The G48F mutation in the peptide designed based on the 45-53 region of BLIP, has favored the electrostatic interactions compared to the electrostatic interaction energy value of wild type peptide, P8, possibly by filling the region occupied by Phe142 of BLIP and mimicking the interactions observed in the presence of Phe142, as stated before. As mentioned before, addition of the hydrophobic pVEC residues to the N-terminus of the wild type peptide, P8, does not affect the electrostatic interactions. The relatively unstable energy profile of TEM-1 – P8 complex (Figure 3.34h) was stabilized upon G48F mutation (Figure 3.34i) and addition of the short sequence LLIIL residues to the N-terminus (Figure 3.34j).

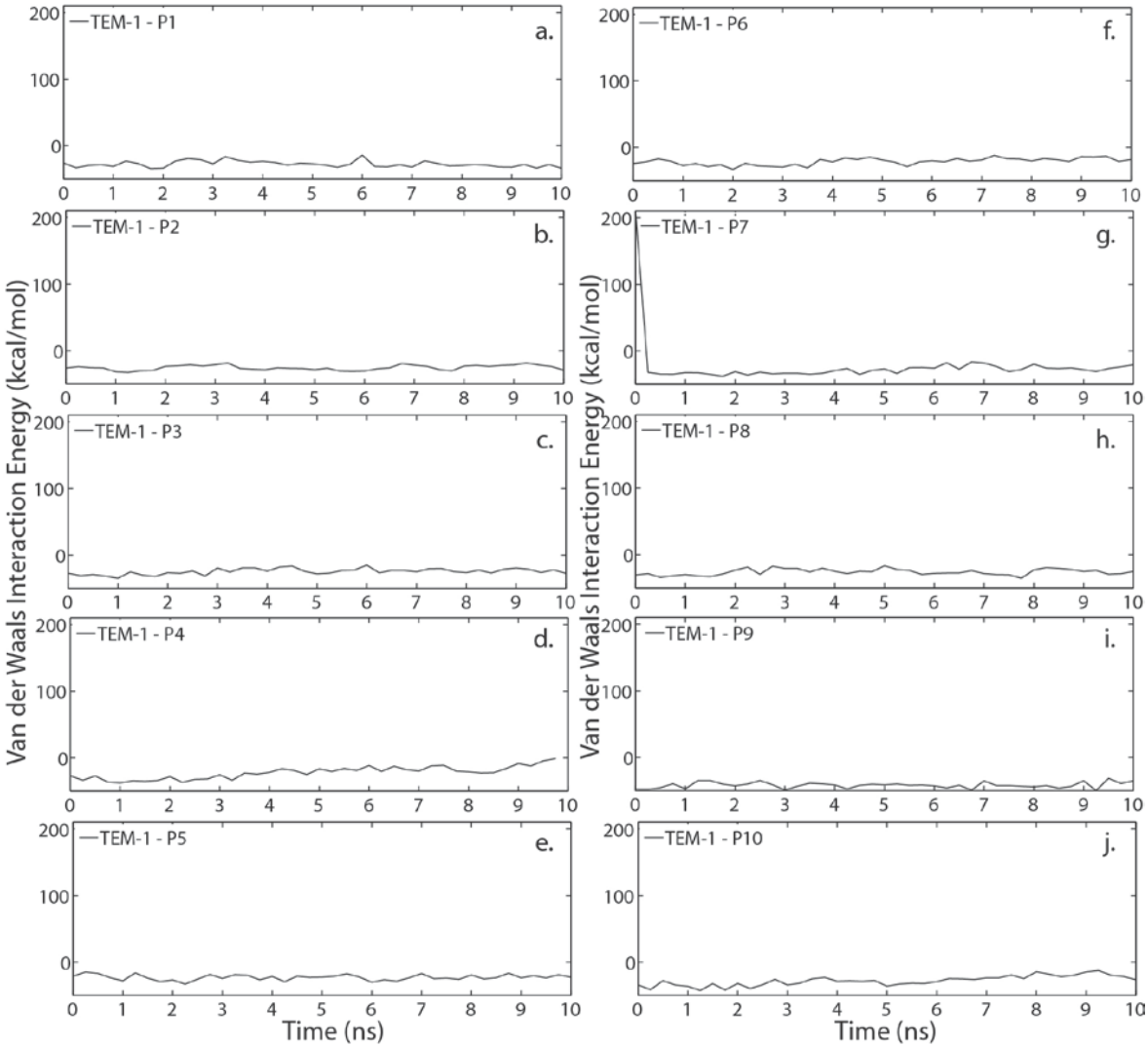

Figure 3.35. The van der Waals energy as a function of time of TEM-1 bound (a) P1, (b) P2, (c) P3, (d) P4, (e) P5, (f) P6, (g) P7, (h) P8, (i) P9, (j) P10 complexes during 10 ns MD simulations.

The change in the van der Waals interactions between enzyme and peptide was not as significant as that in the electrostatic interactions. Small decreases were observed upon mutations (Table 3.14), except the remarkably favorable effect of G48F mutation. It has to be noted that, almost no change in the van der Waals interactions was observed in TEM-1 – P10 complex. The van der Waals energy profiles of simulation systems were similar to each other (Figure 3.35), except the steep descent observed in the TEM-1 – P7 complex (Figure 3.35g) from the initial energy value of almost 200 kcal/mol. The unfavorable interactions observed at the beginning of the simulation were stabilized by the minimization steps.

3.2.3.2. Binding Free Energy Calculations. Binding free energy between enzyme and ligand was calculated and compared between the simulation systems in order to analyze the change in binding affinity as a result of different peptides binding to TEM-1. The effect of mutations and different peptide structures were examined. The binding free energy values and the contributing energy terms were calculated for the simulation snapshots by using FoldX algorithm and the energy values were averaged with respect to the six ns production run period (Table 3.15).

The binding free energy of TEM-1 – P1 complex is -7.32 kcal/mol. The contributing energy terms show that most of the favorable contribution was due to van der Waals (-6.39 kcal/mol) and hydrophobic solvation term (-8.14 kcal/mol). The cyclic peptide structure disfavors the binding of peptide to enzyme suggesting that the presence of the disulfide bond does not contribute the affinity toward beta-lactamase. The binding energy of the cyclic peptide was -3.57 kcal/mol; with corresponding decrease in electrostatic and van der Waals interactions as well as hydrophobic solvation. A46W mutation also disfavors the binding between enzyme and peptide with a value of -6.16 kcal/mol. The electrostatic and van der Waals interactions were weakened in A46W mutant, not a significant change was observed in entropic contributions. D49A mutation resulted in unfavorable interactions (Table 3.14) and binding free energy (Table 3.15) because of the importance of the Asp49 residue in the catalytic mechanism. The electrostatic and van der Waals interactions were lost, unfavorable changes were obtained in the hydrophobic solvation term; it has to be noted that the mutation also resulted in reduced entropic contributions.

Table 3.15. Binding free energy values and the contributing energy terms (kcal/mol) from FoldX. Standard deviations are in parenthesis.

Simulation System	Binding free energy	Elec.	VDW	Polar solvation	Hydrophobic solvation	Entropy sidechain	Entropy mainchain
TEM-1 – P1	-7.32 (1.96)	-2.67 (0.55)	-6.39 (0.74)	9.24 (0.94)	-8.14 (0.99)	2.83 (0.60)	2.49 (0.75)
TEM-1 – P2	-3.57 (1.07)	-0.58 (0.27)	-4.36 (0.80)	4.95 (1.18)	-6.21 (1.01)	2.17 (0.65)	2.16 (0.71)
TEM-1 – P3	-6.16 (1.51)	-1.85 (0.22)	-5.55 (0.53)	8.09 (0.69)	-6.82 (0.68)	1.88 (0.39)	2.07 (0.55)
TEM-1 – P4	-1.70 (1.09)	-0.18 (0.20)	-2.61 (1.15)	2.56 (1.23)	-3.88 (1.65)	1.58 (0.81)	1.78 (0.83)
TEM-1 – P5	-5.29 (1.54)	-1.84 (0.44)	-5.03 (0.70)	7.76 (0.93)	-6.54 (1.01)	2.03 (0.46)	2.32 (0.52)
TEM-1 – P6	-3.50 (1.25)	-1.71 (0.27)	-3.80 (0.66)	5.66 (0.96)	-4.62 (0.89)	1.79 (0.50)	2.02 (0.61)
TEM-1 – P7	-2.08 (0.87)	-0.55 (0.33)	-2.88 (0.55)	2.72 (0.79)	-4.09 (0.75)	3.06 (0.91)	1.54 (0.44)
TEM-1 – P8	-4.88 (1.34)	-1.64 (0.38)	-4.77 (0.58)	6.95 (0.96)	-6.30 (0.76)	1.89 (0.65)	2.41 (0.58)
TEM-1 – P9	-8.84 (1.41)	-2.86 (0.35)	-9.22 (0.65)	12.69 (0.94)	-11.26 (0.85)	3.52 (0.48)	3.76 (0.66)
TEM-1 – P10	-5.22 (1.57)	-1.41 (0.46)	-5.28 (1.04)	6.75 (1.18)	-6.88 (1.43)	2.46 (0.69)	2.32 (0.68)

The binding affinity of peptide towards enzyme was weakened as a result of Y50A (P5) and Y51A (P6) mutations. Compared to Y50A mutation, Y51A resulted in more unfavorable energy terms. The binding free energy values of TEM-1 – P5 and TEM-1 – P6 complexes were -5.29and -3.50 kcal/mol, respectively. In both mutations, the nonbonded interactions were lost, hydrophobic solvation term became unfavorable.

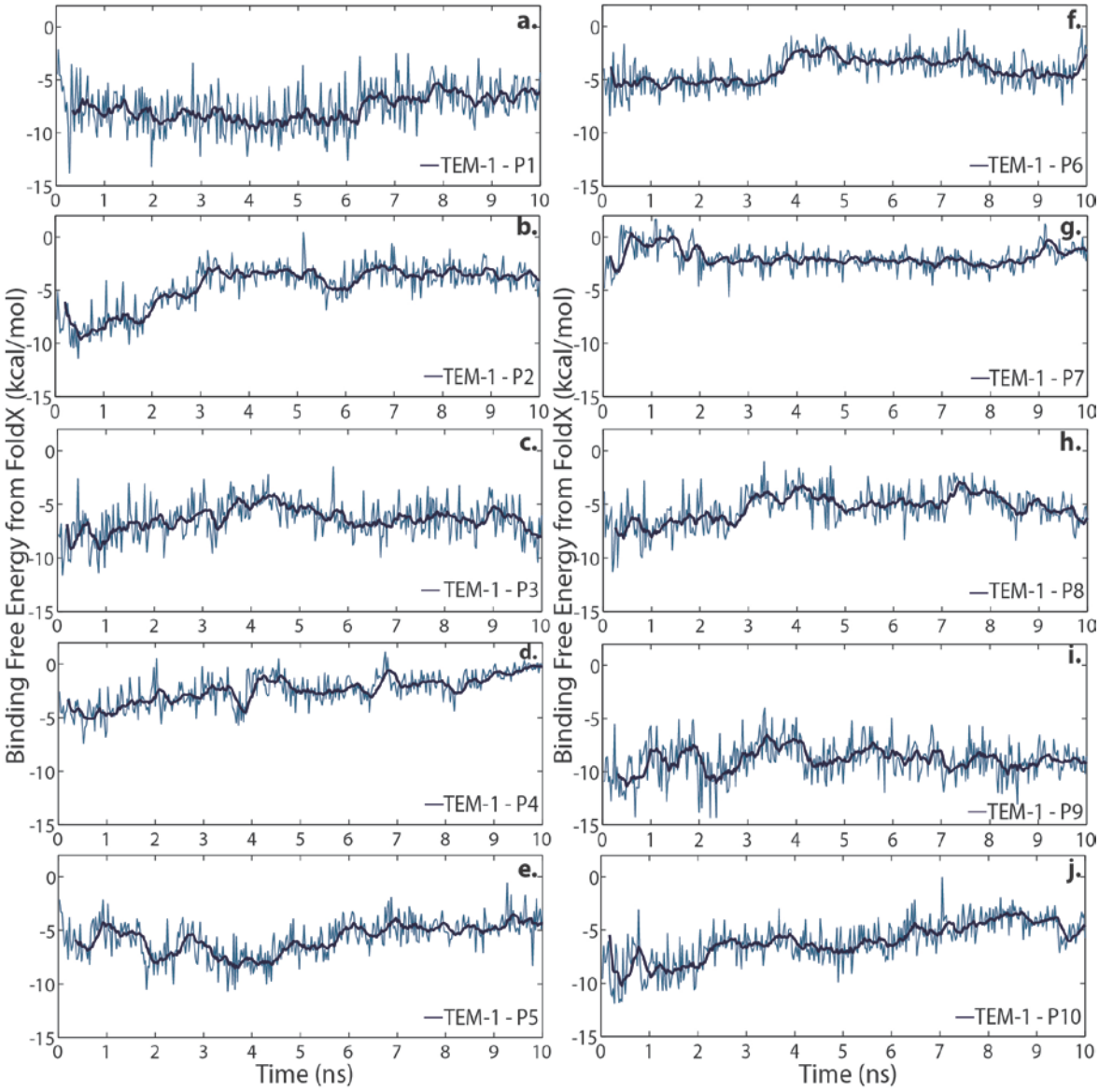

Figure 3.36. The binding free energy profiles of TEM-1 bound (a) P1, (b) P2, (c) P3, (d) P4, (e) P5, (f) P6, (g) P7, (h) P8, (i) P9, (j) P10 complexes during 10 ns MD simulations.

The peptide, P7, had weaker interactions and binding free energy. The binding free energy value became -2.08 kcal/mol compared to wild type peptide and a significant loss in the electrostatic and van der Waals interactions was observed. The inhibition effect of this peptide was previously determined to be important on TEM-1 beta-lactamase activity (Huang *et al.*, 2003), however the analysis of the simulation trajectories resulted in lower affinity of this peptide toward TEM-1. Addition of a Tyr to the C-terminus of the peptide also resulted in unfavorable energetic outcomes. The binding free energy value of the TEM-1 – P8 complex was -4.88kcal/mol while that of TEM-1 – P1 complex was -7.32 kcal/mol. The only mutation which resulted in favorable interactions was the G48F

mutation done on TEM-1 – P8 complex. G48F mutation favors the electrostatic and van der Waals interactions between the enzyme and peptide by mimicking the Phe142 of BLIP, the favorable outcomes were also observed in hydrophobic solvation and entropic contributions.

The addition of the hydrophobic pVEC residues to the N-terminus of the peptide increased the binding free energy value of the wild type peptide – enzyme complex, TEM-1 – P8, by affecting the van der Waals interactions and hydrophobic solvation in a favorable manner, also a more entropic contribution was obtained.

When the binding free energy profiles of the simulation systems were analyzed, the TEM-1 – P1 complex was found to have a stable profile during the simulation timescale (Figure 3.36a). The cyclic peptide structure (Figure 3.36b), mutations of A46W (Figure 3.36c), Y50A (Figure 3.36e) and Y51A (Figure 3.36f) had similar energy profiles compared to wild type peptide – enzyme complex. D49A mutation (Figure 3.36d) caused increasing fluctuations at the end of the simulation. The TEM-1 – P7 complex (Figure 3.36g) had more positive binding free energy values which tend to increase further at the beginning of the simulation. After two nanoseconds, the interactions reached a plateau value and thus more stable profile was maintained. The fluctuations observed in TEM-1 – P8 complex (Figure 3.36h) were similar to the ones in TEM-1 – P1 complex. The favorable effect of the G48F mutation was also observed in the energy profile with the fluctuations in more negative energy values (Figure 3.36i). Due to the addition of the hydrophobic pVEC residues, the binding free energy values of the simulation snapshots tend to increase in the production run period (Figure 3.36j).

3.2.4. Determination of the Interface Energy between Beta-lactamase and Peptides by Flexible Peptide Docking

Docking of the BLIP based peptides to TEM-1 beta-lactamase was carried out using Rosetta FlexPepDock, which is a flexible peptide – protein docking protocol that refines the initial structures in 200 independent simulations and rank them based on their Rosetta generic full atom energy score. 600 independent simulations were performed on 10 beta-

lactamase – peptide complexes and the results were ranked based on their interface energy scores (Table 3.16).

Table 3.16. The interface energy between beta-lactamase and peptides calculated by Flexpepdock.

Beta-lactamase – Peptide Complex	**Peptide based on BLIP region**	**Mutation**	**Interface Energy**
TEM-1 – P1	Residues 45 to 52	-	-15.72
TEM-1 – P2	Residues 45 to 52	-	-13.99
TEM-1 – P3	Residues 45 to 52	A46W	-12.07
TEM-1 – P4	Residues 45 to 52	D49A	-14.47
TEM-1 – P5	Residues 45 to 52	Y50A	-13.50
TEM-1 – P6	Residues 45 to 52	Y51A	-10.95
TEM-1 – P7	Residues 46 to 51	A46R, A47R, D49H	-15.54
TEM-1 – P8	Residues 45 to 53	-	-16.61
TEM-1 – P9	Residues 45 to 53	G48F	-20.77
TEM-1 – P10	Residues 45 to 53	-	-18.75

The interface energy of the TEM-1 – P1 complex was -15.72 kcal/mol. The unfavorable effect of the mutations were also observed with the interface energy calculations by Rosetta FlexPepDock; however the significant changes in the binding free energy values upon D49A and A46R, A47R, D49H mutations (Table 3.15) were not detected with the new energy calculations based on the Rosetta energy score. The interface energy between the peptide comprising BLIP residues 45 to 53, P8, and beta-lactamase was calculated to be -16.61 kcal/mol, which is almost the same as observed in TEM-1 – P1 complex; however previous examination of the nonbonded (Table 3.14) and binding free energy values (Table 3.15) indicated the presence of an additional Tyr residue at the C-terminus of the peptide disfavors binding. The favorable effect of G48F mutation was also observed in the interface energy calculations with Rosetta FlexPepDock. Addition of the hydrophobic pVEC residues to the N-terminus of the peptide was previously identified to have a minor favorable effect on the binding free energy calculations with FoldX. The Rosetta FlexPepDock interface energy calculations also confirmed the previous binding free energy results with the energy value of -18.75 kcal/mol (Table 3.16).

3.2.5. Detailed Examination of the Beta-lactamase – Peptide Binding Interface

The interactions in the peptide binding interface were examined in the simulation systems to analyze the change in the beta-lactamase – peptide interactions due to mutations and different peptide structures. The hydrogen bonding interactions were visually examined by displaying the hydrogen bonds between beta-lactamase and peptide residues in the simulation trajectories during the 10 ns timescale, with a distance cutoff of 3 Å (Table 3.17).

The interactions between all the residues of the wild type peptide designed based on the 45-52 region of BLIP, P1, and beta-lactamase were investigated. His45 of P1 was found to interact with Glu104, Tyr105, Lys215 and Asn274 of TEM-1. Ala46 of P1 made hydrogen bonds with Asp271 and Asn274 of beta-lactamase. No interactions between TEM-1 and Ala47 and Gly48 were observed. Asp49 of P1 forms hydrogen bonds with the active site residues, Ser70, Ser130, Lys234, Ser235 and Arg243 during the simulation timescale, consistent with the previous studies (Strynadka *et al.*, 1996). Tyr50 and Ala52 interact with Lys215, which is located at the H9-H10 loop of TEM-1. Tyr51 interacts with Asp214, Lys215, and Gly218, also located on the H9-H10 loop of TEM-1. Short term hydrogen bond was detected between Tyr51 and the catalytically important TEM-1 residue, Arg243.

Table 3.17. Number of hydrogen bonds between TEM-1 beta-lactamase and 10 different peptides, comprised of residues 45 to 53 of BLIP.

Position	P1	P2	P3	P4	P5	P6	P7	P8	P9	P10
45	+++ +	+	+	+++	+++ ++	++		++	-	+
46	++	-	++	+++	-	-	+++ +	-	+	-
47	-	+	-	++	+++	++	+++	+	+	++
48	-	+	-	+++	+	+	++	-	++	++
49	+++ ++	+++ +++ ++	+++ +++	+++ +	+++ +++ +	+++ +++	+++ ++	+++ ++	+++ ++	+++ ++
50	+	+	+	+++	-	++	+	++	+++ +	++
51	+++ +	++	++	++	+++ +	-	+	++	+++ +++	++
52	+	+	-	+	+++ +	+		+	-	-
53								+++ +	++	+++ +

With the binding of a cyclic peptide, P2, to TEM-1; some changes in the hydrogen bonding interactions were detected at the peptide binding interface. The interactions observed in P1 at the position 45 were lost; Cys45 interacted only with Tyr105 of TEM-1. Ala46 interactions with Asp271 and Asn274 of TEM-1 were lost in TEM-1 – P2 complex. Ala47 and Gly48 of P2 interacted with Tyr105 of TEM-1 while those of P1 has no interactions with beta-lactamase. The interactions of Asp49 with the active site residues, Ser70, Ser130, Lys234, Ser235, Gly236, Ala237, and Arg243 were maintained. A short term interaction was also detected between Asp49 of P2 and Asn132 of TEM-1. Tyr50 was found to interact with Lys215 of TEM-1. Tyr51 of P2 interacts with Lys215 and Val216 of TEM-1. The short term interaction between Tyr51 of P1 and Arg243 of TEM-1 was not detected in TEM-1 – P2 complex. Cys52 of P2 interacts with Lys111 instead of Lys215 compared to TEM-1 – P1 complex. The nonbonded interactions between P2 and TEM-1

was previously identified to be weakened as a result of the cyclic peptide structure (Table 3.14) and binding free energy of TEM-1 – P2 complex was also found to be unfavorable compared to TEM-1 – P1 complex (Table 3.15). The loss of the interactions because of the presence of a disulfide bond in the peptide structure were detected at positions 45, 46 and 51; suggesting that cyclic peptide structure is not optimal for binding to beta-lactamase. The results were consistent with the previous study in which the inhibitory effect of the cyclic peptide was found to be lower than that of the reduced peptide (Rudgers *et al.*, 2001).

Mutational analysis between TEM-1 and BLIP previously carried out in our laboratory by using FoldX. The results indicated a higher preference of a Trp residue at position 46 of the peptide. With this motivation, substitution of the Trp at position 46 instead of Ala was carried out. In the TEM-1 – P3 complex comprising A46W mutation, His45 was found to interact with Tyr105, as in the TEM-1 – P2 complex. However the interactions at position 45 with Glu104 and Asn274 of TEM-1, detected in the TEM-1 – P1 complex were not observed in TEM-1 – P3 complex. Substitution of a Trp residue at position 46 resulted in the interaction between the bulkier side chain of Trp46 with the Asn274 and catalytically important Arg243 of TEM-1. It has to be noted that the interaction with Arg243 of TEM-1 was not present in the TEM-1 – P1 complex. At positions 47 and 48, no interactions with TEM-1 were detected as in TEM-1 – P1 complex. The crucial interactions of Asp49 with the active site of TEM-1 were maintained in the presence of A46W mutation. Tyr50 was found to interact with Lys215 as in the wild type peptide complex; however the interactions of Tyr51 observed in the TEM-1 – P1 complex with H9-H10 loop residues and Arg243 of TEM-1 were lost in the A46W mutant; instead Tyr51 interacts with Asp271 and Asn274. No hydrogen bonds were detected at position 52. The binding free energy between P3 and TEM-1 was almost the same as that of P1 (Table 3.15). The minor difference between the binding free energy values was possibly caused by the loss of the interactions at positions 45, 51 and 52 of the peptide.

D49A mutation changes almost all the communication between beta-lactamase and peptide. The crucial interactions between Asp49 and active site residues of TEM-1 were lost as a result of the Ala substitution at this position. As a result, the peptide moves away from TEM-1 by ~8 Å (Table 3.12). Ala49 is found to be interacting with only two active

site residues, Ser130 and Ser235 of TEM-1, and also new interactions with Met129 and Lys215 of TEM-1 were detected. Similar interactions compared to wild type peptide, P1, complexed with TEM-1 were observed at position 45, with Glu104, Tyr105 and Glu110 of TEM-1. The D49A mutation caused Ala46 and Ala47 to interact with the catalytically important Arg243 of TEM-1, because of the loss of the interactions between this important TEM-1 residue with Ala49. Ala46 in TEM-1 – P4 complex also interacts with Tyr105 and Glu110 of TEM-1, and Ala47 interacts with Tyr105 of TEM-1 as well. The loss of the critical interactions with active site residues of TEM-1 at position 49 also caused Gly48 to interact with two active site residues, Ser130 and Arg243. The interactions with Lys215 of TEM-1 and Tyr50, Tyr51 and Ala52 of P4 were observed. Tyr50 also interacts with H9-H10 loop residues of TEM-1, Ala213 and Asp214. The loss of nonbonded interactions (Table 3.14) and lower binding affinity toward beta-lactamase (Table 3.15) observed in TEM-1 – P4 complex was caused by the loss of the crucial interactions of position 49 with active site residues of TEM-1; the effort of the surrounding residues to fulfill the missing interactions was not successful. Previously reported mutation of D49A resulted in ~40 fold decrease in the binding affinity of BLIP toward TEM-1 (Zhang and Palzkill, 2003).

With the Y50A mutation (P5), the interaction with Lys215 of TEM-1 at position 50 was lost. His45 of P5 had interactions with Lys215, Val216, Asp271 and Asn274 of TEM-1; and also a short term interaction with Arg243 was observed. No hydrogen bonds were detected at position 46. The interactions between Ala46 and Asp271 and Asn274 of TEM-1 were lost. Ala47 was found to interact with Tyr105, Arg243 and Asn274 of TEM-1, while in TEM-1 – P1 complex no interactions were present between Ala47 of P1 and beta-lactamase. A short term interaction between Gly48 and Arg243 was present in TEM-1 – P5 complex. The important interactions of Asp49 with the active site of TEM-1 were maintained in the presence of Y50A mutation. Tyr51 was interacting with Tyr105, Glu110, Lys215 and Met129 of TEM-1. Hydrogen bonds between the Ala52 of P5 and Tyr105, Glu110, Lys111 and Lys215 were observed. It has to be noted that in TEM-1 – P1 complex, Ala52 was only interacting with Lys215 of TEM-1. Y50A mutation was previously identified to increase the binding affinity of BLIP toward TEM-1 (Zhang and Palzkill, 2003), however this favorable effect was not in TEM-1 – peptide simulations; minor unfavorable changes were apparent in nonbonded interactions between enzyme and peptide (Table 3.14) and a little decrease was observed in the binding affinity (Table 3.15).

With the Y51A mutation (P6), the interactions observed at position 51 in TEM-1 – P1 complex were lost. His45 of P6 formed contacts with Tyr105 and Glu239 of TEM-1, while it was interacting with Asp214, Lys215, Gly218 and Arg243 of TEM-1 in TEM-1 – P1 complex. No interactions were detected at position 46 in P6; hence it could be said that the interactions at positions 45 and 46 of the peptide were lost as a result of Y51A mutation. Although no interactions were observed between Gly48 of P1 and beta-lactamase; Gly48 in P6 was interacting with Tyr105. The Asp49 interactions with active site of TEM-1 were maintained in the presence of Y51A mutation. Tyr50 was interacting with Tyr105 as in wild type peptide complex, additionally a new interaction with Thr128 of TEM-1 was detected in TEM-1 – P6 complex. Ala52 was interacting with Lys215 in wild type complex, in TEM-1 – P6 it was found to be interacting with Asp214. The loss of the nonbonded interactions (Table 3.14) and the lower affinity toward TEM-1 (Table 3.15) were possibly caused by the loss of interactions with TEM-1 beta-lactamase at positions 45, 46 and 51 as a result of Y51A mutation. Removal of the Tyr51 side chain previously reported to have no effect in binding affinity toward TEM-1 (Zhang and Palzkill, 2003), however the detailed analysis of the simulation trajectories show that removal of the phenolic ring of Tyr51 resulted in unfavorable outcomes suggesting the importance of this residue in the inhibition mechanism of TEM-1 beta-lactamase.

The peptide P7, with the sequence of RRGHYY, was previously identified to be a good TEM-1 inhibitor with a K_i value of 136 μM (Huang *et al.*, 2003). The analysis of the TEM-1 – P7 binding interface revealed the interactions of Arg46 with Tyr105, Val216, Asp271 and Asn274 of TEM-1 and Arg47 with Glu104, Tyr105 and Glu239 of TEM-1. Gly48 of P7 was interacting with Tyr105 and Glu239 of TEM-1. The critical interactions with the active site of TEM-1 at position 49 was maintained, however a short term hydrogen bond is present with catalytically important Arg243 while in wild type peptide – beta-lactamase complex the interaction between Asp49 of P1 and Arg243 of TEM-1 was continuous during the simulation timescale. The significant loss observed in nonbonded interactions between TEM-1 and P7 (Table 3.14) and also the lower affinity toward TEM-1 (Table 3.15) was possibly caused by the crucial interaction made with Arg243 of TEM-1. It has to be noted that Tyr50 was interacting with Met129 of TEM-1 and Tyr51 was interacting with Lys215 of TEM-1 in TEM-1 – P7 complex.

The interaction of the P8 residues with TEM-1 was similar to the ones observed in TEM-1 – P1 complex. The additional Tyr residue at the C-terminus of the peptide was found to be interacting with Tyr105, Ser106, Glu110 and Lys111, which are located at the protruding 99-112 loop of TEM-1. The nonbonded interactions between enzyme and peptide were lost with the addition of Tyr53 (Table 3.14) and lower binding affinity was observed (Table 3.15), possibly because of the short term interaction between the Asp49 of P8 and Arg243 of TEM-1 compared to TEM-1 – P1 complex.

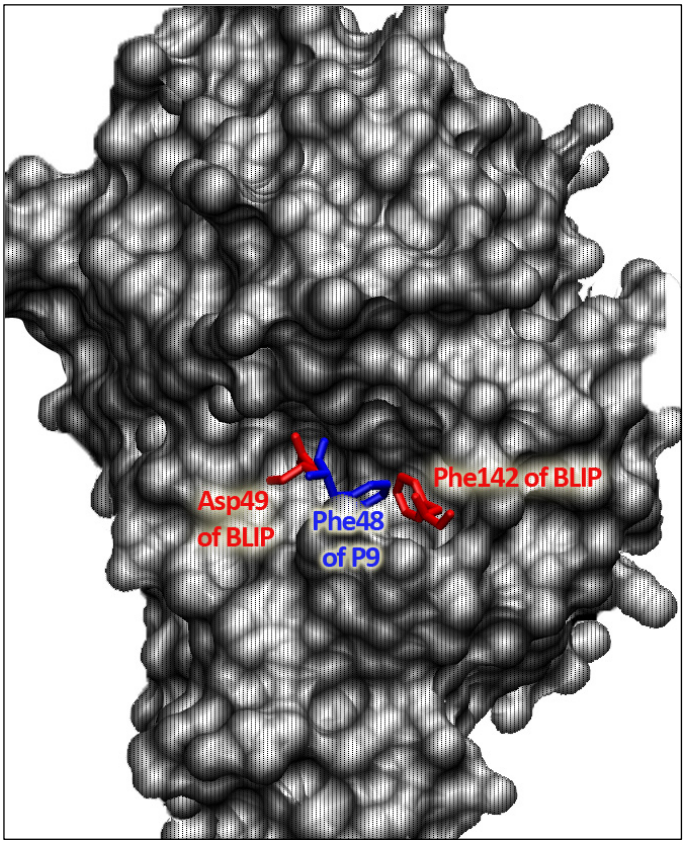

Figure 3.37. Binding cativities of TEM-1 (gray) occupied by Asp49 (red) and Phe142 (red) of BLIP. Phe48 of P9 (blue) filled the cavity occupied by Phe142 of BLIP.

With the G48F mutation, no interactions were detected between His45 of P9 and TEM-1. A short term interaction between Asn274 of TEM-1 and Ala46 of P9 was observed, and Ala47 was interacting with Tyr105 as in TEM-1 – P8 complex. Phe48 was identified to form short term interactions with Asn132 and Arg243 of TEM-1. The critical interactions between Asp49 of peptide and active site of TEM-1 were maintained; the interactions with Ser235 and Arg243 of TEM-1 were very strong and continuous compared

to those of TEM-1 – P8 complex. Additional interactions compared to TEM-1 – P8 complex were observed at position 50 with Thr128, Met129 and Val216 of TEM-1. Tyr51 of P9 was determined to be interacting with Lys215, Val216, Ala217, Ser235, Arg243 and Asn274 of TEM-1, the interactions with Val216 and Arg243 were relatively stronger than the others. Tyr53 was interacting with Ser106 and Glu110 of TEM-1, while no hydrogen bonds were detected at position 52. The favorable nonbonded interactions (Table 3.14) and higher affinity toward TEM-1 (Table 3.15) was due to the very strong interactions between Asp49 of P9 and two active site residues of TEM-1, Ser235 and Arg243; and the interactions with Arg243 of TEM-1 at positions 48 and 51. With G48F mutation, the binding cavity occupied by Phe142 of BLIP was successfully filled by the Phe48 of P9 (Figure 3.37).

The examination of the binding interface of P10 and TEM-1 showed that similar interactions were present compared to TEM-1 – P8 complex. The nonbonded interactions between enzyme and peptide were very similar in TEM-1 complexes with P8 and P10 (Table 3.14), suggesting that the additional pVEC residues at the N-terminus of the peptide does not making any interactions with TEM-1 beta-lactamase. The closer examination of the binding interface confirmed this hypothesis; no hydrogen bonds were detected between the hydrophobic pVEC residues and TEM-1. The relatively higher binding affinity observed in TEM-1 – P10 complex (Table 3.15) was possibly caused by the presence of very strong interactions with Arg243 of TEM-1 in TEM-1 – P10 complex compared to TEM-1 – P8 complex.

4. EXPERIMENTAL MATERIALS AND METHODS

4.1. Chemicals

All chemicals and solutions used in this study were purchased from MERCK (Germany) and SIGMA (USA).

4.2. Enzyme Activity Measurement Buffers and Solutions

Table 4.1. K^+PO_4 buffer (1 M, pH 7.0)

Chemical	Amount
1M K_2HPO_4	450 ml
1M KH_2PO_4	550 ml

4.2.1. CENTA Stock Solution

25 mg CENTA (Calbiochem) was dissolved in 10 ml 50 mM K^+PO_4 buffer and aliquoted and stored at -20 °C. The concentration of the stock solution was 4.7 mM.

4.3. Enzyme

In this study, purified TEM-1 beta-lactamase used in enzyme kinetic experiments was obtained from a previous study (Avcı, 2011).

4.4. Peptides

The peptide sequence corresponding to the BLIP residues 45 to 53 and its two variants were used in the experiments (Table 4.2). All peptides except kemptide acetate salt were purchased from Thermo Fisher Scientific (Germany). Kemptide acetate salt was purchased from SIGMA (USA).

Table 4.2. List of peptides used in experiments.

Peptide	**Sequence**	**Amount purchased**
Biotinylated-P8	Biotin-NH-HAAGDYYAY-$CONH_2$	5.6 mg
Fluoresceinated-P8	5/6-Fluorescein-NH-HAAGDYYAY-$CONH_2$	15 mg
Fluoresceinated-P10	5/6-Fluorescein-NH-LLIIL-HAAGDYYAY-$CONH_2$	10 mg
Kemptide acetate salt	LRRASLG-NH_2	5 mg

4.5. Laboratory Equipment

Table 4.3. List of laboratory equipment.

Absorbance measurement	Specord 200 (Analytikjena, UK)
Ice machine	FBOC Icematic
Incubation	FN500 Incubator (Nüve, Turkey)
Pipetting	1-10, 10-100, 100-1000 µl pipettes (Thermo Electron Corporation, Canada)
pH Measurement	pH Meter (SCHOTT, Germany)
Power supply	Power EC250-90 (Thermo Electron Corporation, Canada)
Refrigerating	Refrigerator (Samsung, RT59EBPN)
Sterile environment	Microbiologic Safety Cabinet MN 120 (Nüve, Turkey)
Sterilization	Steam Sterilizer OT40L (Nüve, Turkey)
Vortexing	Reax Top Vortex (Heidolph, Germany)
Water purification systems	MILLI-Q UF Plus (MILLIPORE, USA) MILLIPORE Elix® 5 UV (MILLIPORE, USA)
Weighing	Balance XB 220A (Precisa, Switzerland)

4.6. Peptide Aliquoting

Peptide aliquoting was carried out with sterilized equipment under laminar flow. All the equipment was sterilized at 1 atm and 121 °C for 15 min in an autoclave. The peptides were dissolved in 50 mM K^+PO_4 buffer and stock solutions were aliquoted and maintained at -20^{o}C. Dimethyl sulfoxide (DMSO) was used in dissolving the biotinylated P8, at a final concentration of 15%.

4.7. Enzyme Inhibition Assay

In this study, beta-lactamase inhibition by the proposed peptides was investigated by enzyme kinetic experiments under *in-vitro* conditions. To this end, a pre-determined amount of enzyme was mixed with various concentrations of peptides in 50 mM K^+PO_4 buffer in order to allow binding of the peptides to the enzyme. Same amounts of enzyme in 50 mM K^+PO_4 buffer were used as control. The mixtures, in a total volume of 400 µl, were incubated at 50 rpm and 37^{o}C, for 1 hour. After incubation, 50 mM K^+PO_4 buffer and 47 µM CENTA, the beta-lactamase substrate (Jones *et al.*, 1982), were added to the incubated mixture to a final volume of 1 ml. CENTA hydrolysis was monitored by the change in absorbance at 405 nm. The experiments were performed in triplicate and the beta-lactamase activities in the presence and absence of peptides were calculated.

Beta-lactamase activity was measured using the following equation;

$$U = \frac{V_t \, x \left(\frac{dA}{dt}\right) x \, 10^6}{\epsilon\lambda \, x \, V_s \, x \, d} \tag{4.1}$$

in which V_t is the total reaction volume (ml), dA/dt is the initial linear change in absorbance with time (min^{-1}), $\epsilon\lambda$ is the extinction coefficient of the substrate, CENTA, ($cm^2.mol^{-1}$) (6400 $M^{-1}cm^{-1}$ at 405 nm), V_s is the volume of enzyme (ml) and d is the light path (1 cm).

5. PEPTIDE BINDING ANALYZED BY *IN VITRO* EXPERIMENTS

In this part of the study, the inhibition potential of the selected peptides (Table 4.2), P8 and P10, and the control peptide, kemptide acetate salt without inhibitory activity on TEM-1 beta-lactamase (Huang *et al.*, 2003), was investigated by *in vitro* experiments. The motivation of the experiments was to analyze and confirm the inhibition potential of the peptides for which energetic and dynamic analysis were performed in Chapter 3, and also to compare the computational and experimental results. The inhibitory effect of the peptides was evaluated by comparing the activity of the enzyme in the presence and absence of the peptides. Total enzyme activity was calculated using the Equation 4.1. The experiments were carried out following the procedure described in Section 4.7. All experiments were performed in triplicate except the ones in which the peptide concentration was 200 μM and in which the fluorescinated-P8 peptide was used. In order to compare the results, the relative activities were calculated by fixing the activity of the control sets to 100 U. Total activities of the sample sets were re-calculated based on the new scale. This was done to normalize activities since enzyme activity decayed with time.

TEM-1 beta-lactamase used in this work was previously studied to analyze its inhibition by BLIP, and the results obtained showed that there was 80% inhibition in the presence of BLIP (Avcı, 2011).

5.1. Effect of Fluorescein on the Absorbance Values

As CENTA hydrolysis in the control and sample sets was measured, a major increase was observed in the samples with fluorescein labeled peptides. In order to find out if the increased absorbance values were due to fluorescein, K^+PO_4 buffers with different concentrations of fluorescein amine were prepared and their absorbances were measured at the wavelength at which the activity measurements were done.

Table 5.1. The effect of fluorescein to the absorbance values.

	OD at 405 nm
50 mM phosphate buffer (Reference)	0.00
100 μM fluorescein amine containing sample	0.4738
150 μM fluorescein amine containing sample	0.7046
200 μM fluorescein amine containing sample	0.9076

The measured absorbances (Table 5.1) explained the increase in absorbances observed in the experiments performed with fluorescein labeled peptides; increasing concentrations of fluorescein amine increased the absorbance measured at 405 nm.

5.2. Effect of Kemptide Acetate Salt on TEM-1 Beta-lactamase Activity

Kemptide acetate salt was previously reported without inhibitory effect on TEM-1 beta-lactamase activity (Huang *et al.*, 2003). Therefore, kemptide was used as a control to study inhibition of the enzyme. Three sets of experiments were carried out with 100 μM kemptide. The absorbance measured at 405 nm as a function of time is given in Table B.1.

The results obtained showed that the presence of 100 μM kemptide had no inhibitory effect on TEM-1 beta-lactamase activity (Figure 5.1, Table B.2).

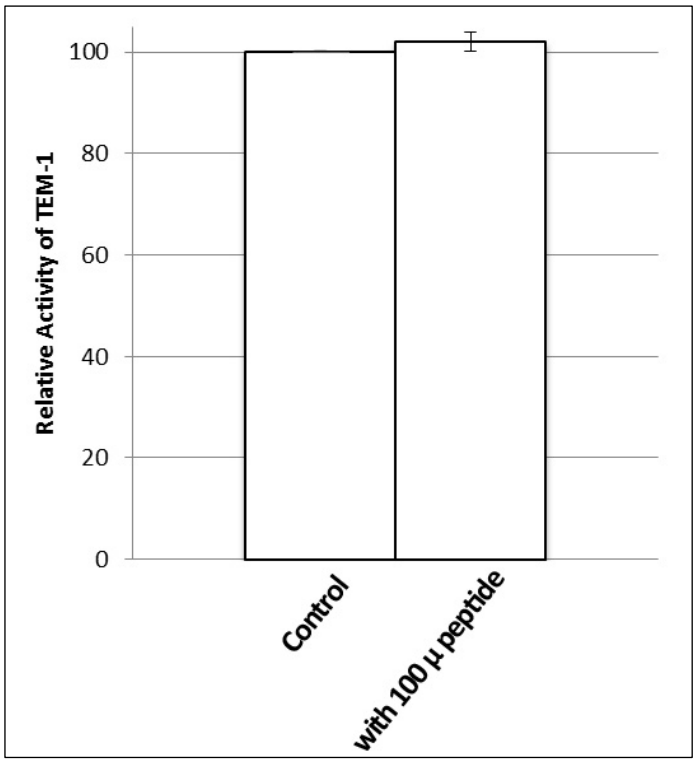

Figure 5.1. Relative activity values in the presence and absence of kemptide acetate salt. Error bars are represented with black lines.

5.3. Effect of Biotinylated-P8 on TEM-1 Beta-lactamase Activity

Experiments with the biotinylated-P8 peptide were performed in order to measure its inhibitory effect on the enzyme. The experiments in the presence of 100 μM peptide were performed in triplicate; the experiment with 200 μM peptide was performed once. Total enzyme activity in the presence and absence of the peptide were calculated. The absorbance measured at 405 nm as a function of time is given in Table B.3.

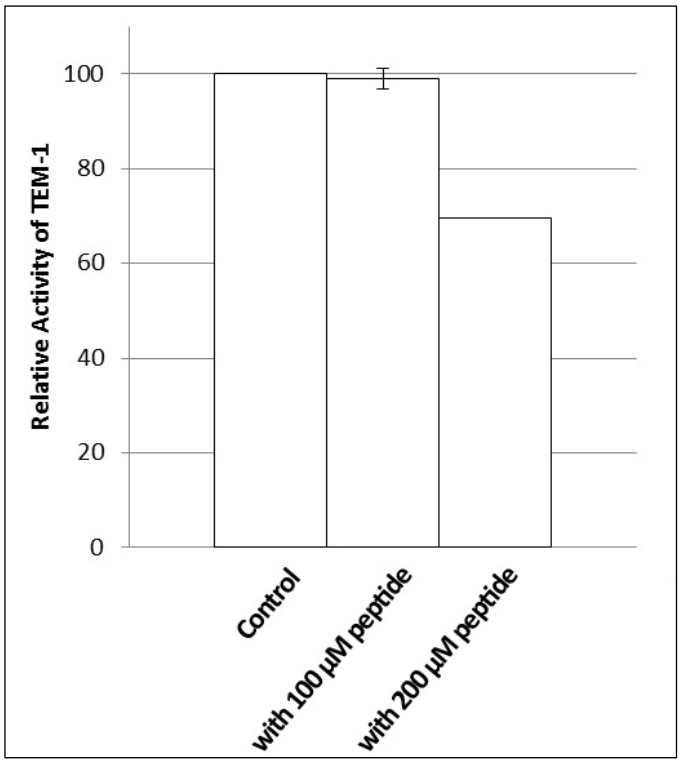

Figure 5.2. Relative activity values in the presence and absence of biotinylated-P8 peptide. Error bars are represented with black lines.

The presence of 100 μM biotinylated-P8 peptide has not significantly affected the activity of TEM-1 beta-lactamase (Figure 5.2, Table B.4). Increasing the concentration of the peptide to 200 μM in the final reaction mixture resulted in 30% decrease in the activity of TEM-1 (Figure 5.2, Table B.5).

5.4. Effect of Fluoresceinated-P8 on TEM-1 Beta-lactamase Activity

Duplicate experiments in the presence of 100 μM fluorescinated-P8 peptide were carried out in order to measure its inhibitory effect on TEM-1 beta-lactamase activity. Total enzyme activity in the presence and absence of the fluorescinated-P8 peptide was calculated; the absorbance measured at 405 nm as a function of time is given in Table B.6.

Addition of 100 μM peptide to the reaction mixture resulted in 21% decrease in TEM-1 activity (Figure 5.3, Table B.7). In order to find out if higher peptide concentrations might enhance inhibition on the enzyme, peptide concentration was raised to 200 μM. However the activity of enzyme was not affected by increased peptide

concentration, the decrease in the relative activity was 20% (Figure 5.3, Table B. 8), similar to the total enzyme activity observed in the presence of 100 μM peptide.

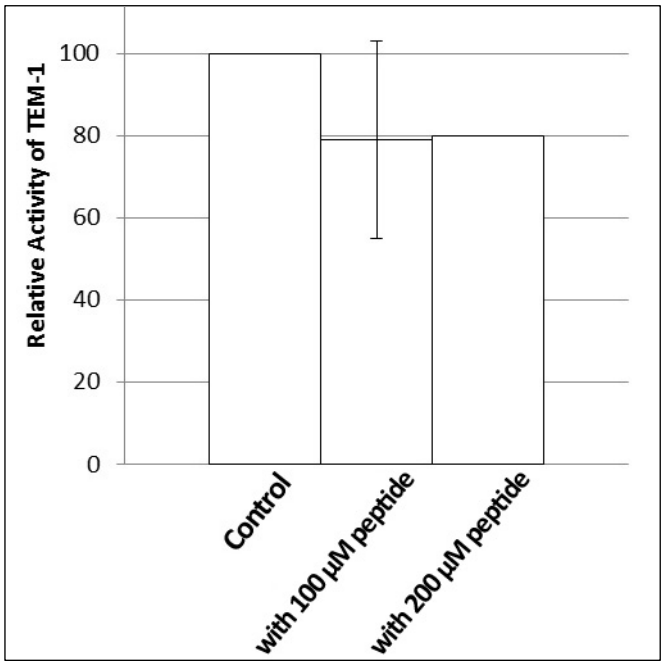

Figure 5.3. Relative activity values in the presence and absence of fluorescinated-P8 peptide. Error bars are represented with black lines.

5.5. Effect of Fluorescinated-P10 on TEM-1 Beta-lactamase Activity

As previously mentioned, P10 is the peptide that carries additional hydrophobic residues in its N-terminus, LLIIL, also found in the N-terminus of pVEC. These hydrophobic residues have been determined to play an important role in the penetration of the peptides through the cell membrane.

In order to determine the effect of different concentrations of fluoresceinated-P10 on the activity of TEM-1 beta-lactamase, experiments were carried out with four different concentrations of the peptide, 25, 50, 75 and 100 μM. Total enzyme activity calculations showed that (raw data for the experiments done with fluoresceinated-P10 are given in Table B.9 to Table B.18) fluoresceinated-P10 had a significant effect on the enzyme activity. The inhibitory effect of the peptide could even be seen in low concentrations; in

the presence of different concentrations of the fluoresceinated-P10 peptide 12-24% decrease in the enzyme activity was measured (Figure 5.4).

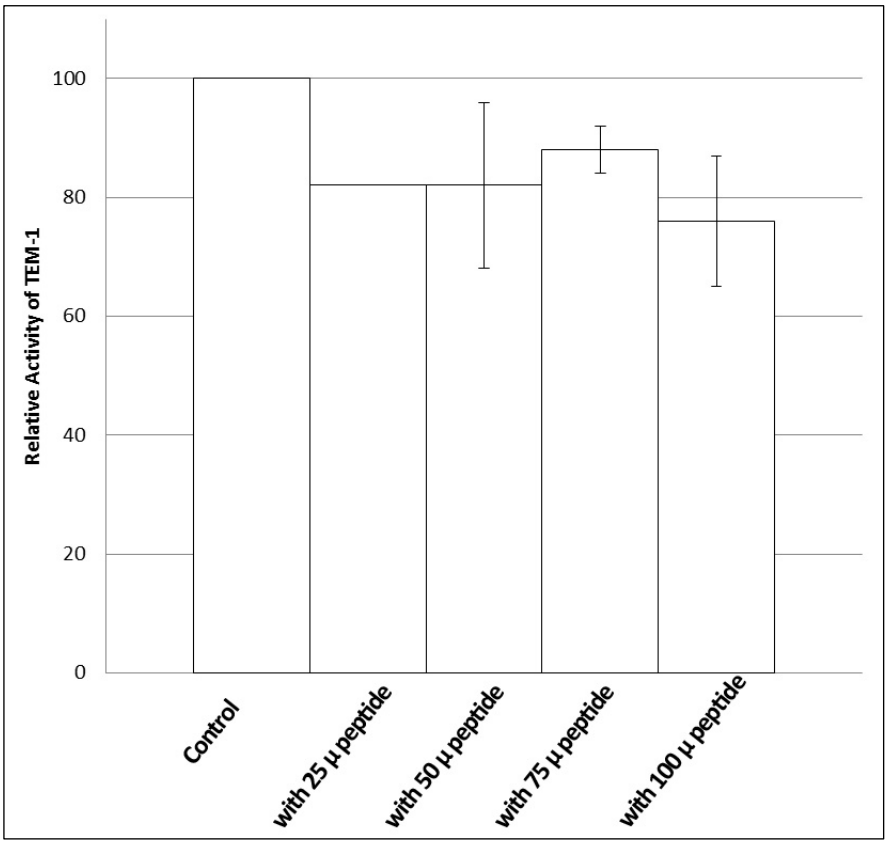

Figure 5.4. Relative activity values in the presence and absence of fluorescinated-P10 peptide with four different experiments done at different peptide concentrations. Error bars are represented with black lines.

5.6. Comparison of the Computational and Experimental Results

The binding free energy values of the P8 and P10 were very similar to each other, the energy values were -4.88 and -5.22 kcal/mol, respectively (Table 3.15), indicating that the affinity of these peptides towards beta-lactamase are almost the same. The *in vitro* experiments done with the fluorescein labeled versions of these peptides also confirmed this computational outcome with very similar inhibitory effects of these peptides. The decrease in TEM-1 beta-lactamase activity in the presence of 100 µM fluoresceinated-P8 and P10 is almost the same at around 20%.

6. CONCLUSIONS AND RECOMMENDATIONS

6.1. Conclusions

In this study, MD simulations were performed on apo and BLIP bound forms of wild type and W229A mutants of TEM-1 and SHV-1 beta-lactamases, and on 10 different TEM-1 – peptide complexes. The simulation trajectories were analyzed in order to identify the regions that contribute to affinity toward ligand. RMSD between the simulation snapshots and initial coordinates were calculated as a measure of the structural convergence. Change in the mobility of the beta-lactamase structures were examined by MSF calculations in order to identify the possible regions which might be important in catalytic activity. Individual residues, structural elements as well as individual energy components important for ligand recognition in the TEM-1 and SHV-1 beta-lactamases in both wild type and mutant forms were identified. 10 different peptides that comprise the type II beta turn of BLIP corresponding to residues 46 to 51 were designed. Different mutants of the peptides were simulated in order to identify a peptide with high binding affinity potential and to elucidate the mechanism by which these mutants interact with beta-lactamase.

Binding of BLIP to TEM-1 beta-lactamase resulted in decreased stability by increasing the RMSD of beta-lactamase with respect to its initial coordinates, and decreased mobility of beta-lactamase; however binding of BLIP to SHV-1 beta-lactamase increased stability by decreasing the RMSD of enzyme and increased mobility. BLIP was previously identified to bind TEM-1 with 1000 fold higher affinity than it binds to SHV-1 (Petrosino *et al.*, 1999). The energetic analysis performed in this study did not show a difference in binding free energy between TEM-1 – BLIP and SHV-1 – BLIP; however, the differential dynamic response of the two beta-lactamases to BLIP binding may cause the difference in their affinity toward BLIP. BLIP binding caused changes in the mobility of regions away from the binding site, such as H9 and H10 helices. H10 helix was previously identified to form a lid over an allosteric binding site in TEM-1 and SHV-1 beta-lactamases (Kuzin *et al.*, 1999; Horn and Shoichet, 2004). Examination of several class A beta-lactamases using sequence and structure homology revealed the presence of a

highly conserved residue, Trp229 near the allosteric inhibitor binding site (Meneksedag *et al.*, submitted) Trp229 forms a stacking interaction with two other conserved proline residues, Pro226 in the loop following H10 and Pro252 between S4 and S5 of main beta sheet. MD simulations were performed on W229A mutants of apo and BLIP bound beta-lactamase in order to elucidate the role of this highly conserved residue in the mechanism for allostery between the active site and allosteric binding site.

W229A mutation caused slightly decreased stability in the apo beta-lactamase simulations possibly due to the smaller size and loss of the stacking interaction as a result of the mutation, however, the simulations were stable based on RMSD and energy values. While mobility of apo TEM-1 was not affected by W229A mutation, that of apo SHV-1 increased with W229A mutation. H10 fluctuations were also found to be different in apo forms of the two beta-lactamases; H10 motions were dampened with the W229A mutation in TEM-1 while a significant increase in the H10 motions was observed in apo SHV-1.

Mobility of TEM-1 in the presence of BLIP increased as a result of W229A mutation, while the enzyme motions were almost the same in the BLIP bound structures of both wild type and mutant SHV-1. The mutant TEM-1 beta-lactamase had higher H10 fluctuations in the presence of BLIP, higher affinity to BLIP and higher cross-correlations with BLIP; mutant SHV-1 also had higher H10 motions in the presence of BLIP and higher cross correlations with BLIP were apparent. However the affinity of SHV-1 beta-lactamase toward BLIP in both wild type and mutant structures were almost the same. The results suggest that Trp229 modulates the hinge type motion, and higher mobility of H10 helix in the presence of W229A mutation in both beta-lactamases results in enhanced communication between the allosteric site and active site. The high correlation within the residues Pro226-Trp229-Pro252 also suggests the possible relevance of this hydrophobic interaction in modulating the mobility of H10 helix.

In an effort to identify peptide inhibitors against TEM-1 beta-lactamase, simulations were performed on 10 different TEM-1 – peptide complexes. Peptides were designed based on the 45-52 and 45-53 regions of BLIP as to comprise the type II beta turn. A46W, D49A, Y50A, Y51A mutants of the peptide comprising 45 to 52 of BLIP; and a cyclic form of this peptide were investigated. A46R, A47R and D49H mutations were done on

the peptide comprising BLIP residues 46 to 51. The peptide was extented to include the Tyr53 residue, and G48F mutation was performed on this relatively longer peptide. Finally addition of hydrophobic residues, which contribute to cellular uptake of the cell penetrating peptide pVEC, to the N-terminus of the peptide was investigated with dynamic and energetic analysis and structural examinations.

The mutations, A46W, D49A, Y50A, Y51A, performed on the peptide, with the sequence HAAGDYYA, resulted in weak interactions between beta-lactamase and peptide and decreased affinity toward beta-lactamase. The presence of a disulfide bond was determined to result in decreased affinity to beta-lactamase. The peptide previously identified to be a potent inhibitor of TEM-1 beta lactamase, with the sequence of RRGHYY, was also found to have low affinity toward TEM-1 beta-lactamase. Binding of the relatively longer peptide, with the sequence HAAGDYYAY, resulted in lower interactions between enzyme and peptide and lower affinity to TEM-1, compared to the peptide comprising 45-52 residues of BLIP due to the loss of the long range interactions with Arg243 of TEM-1. G48F mutation was carried out in order to test whether the Phe residue can interact with the pocket occupied by Phe142 of BLIP. Binding of the mutant peptide resulted in enhanced electrostatic and van der Waals interactions between enzyme and peptide, and also higher affinity toward TEM-1 due to the strong interactions between Asp49 of the peptide and the two active site residues of TEM-1, Ser235 and Arg243, and also the interactions with Arg243 of TEM-1 at positions 48 and 51 in the peptide. The cavity in TEM-1 occupied by Phe142 of BLIP was shown to be filled by the ring of Phe48 as proposed. The addition of the hydrophobic pVEC residues to the N-terminus of the peptide was determined to have almost no effect on the affinity to TEM-1; no interactions were detected between these hydrophobic residues and TEM-1 beta-lactamase.

The inhibitory effect of the peptides was further investigated with *in-vitro* kinetic experiments. The peptide corresponding to the 45-53 region of BLIP, with the sequence of HAAGDYYAY showed 21% inhibition. To enhance cellular uptake potential, this peptide was modified by adding LLIIL residues to its N-terminus. This peptide was identified to have similar inhibitory effect, with 18-25% inhibition on TEM-1 beta-lactamase activity. It has to be noted that the affinity of these peptides toward TEM-1 was also determined to be almost the same with MD simulations.

6.2. Recommendations for Future Studies

In this study, MD simulations resulted with a peptide that has the highest affinity toward beta-lactamase, carrying G48F mutation. Different mutations can be combined with G48F mutation in order to enhance the affinity toward beta-lactamase, and MD simulations can be performed on the new beta-lactamase – peptide complexes in order to analyze the change in interactions, dynamics and energetics upon binding of proposed peptides.

The simulations performed and analyzed revealed the interaction between the active site and allosteric site of beta-lactamases. Ligand binds to the active site of beta-lactamases in the simulations performed in this study. New inhibitors can be designed against the allosteric site; and computational and experimental analysis can be performed and compared to elucidate the difference in inhibitor binding to active site and allosteric site.

Affinity of BLIP toward TEM-1 is almost 1000 fold higher than that of SHV-1; however this significant difference could not be observed in this study with energetic analysis. Detailed entropic analysis can be carried out with the complexes of these two beta-lactamases in order to elucidate the difference in BLIP binding affinity.

The results obtained from the analysis of the simulation trajectories can be tested by experiments. Trp229 can be experimentally mutated to Ala, and mutant enzyme can be purified from *Escherichia coli* K12 strains expressing TEM-1 beta-lactamase from pUC18 plasmid. Kinetic experiments can be done in order to analyze the effect of W229A mutation on the ligand recognition mechanism of TEM-1.

In the experimental part of this study, *in vitro* experiments were carried out with different wild type peptides. *In vitro* kinetic experiments can be done with the peptide carrying G48F mutation, with the sequence of HAAFDYYAY. *In vivo* experiments can be performed in order to investigate the effect of peptide addition on the growth properties of resistant bacteria expressing beta-lactamase. Kinetic parameters and inhibition constants of the proposed peptide inhibitors can be determined in order to compare their effects with the previously identified peptides.

APPENDIX A: INPUT FILES USED IN COMPUTATIONAL STUDIES

Table A.1. The list of 28 class A beta-lactamases used in the sequence and structure homology analysis of beta-lactamases in Section 1.2.1.

PDB code	Beta-lactamase Name	Ligand
1bsg	Beta-Lactamase From Streptomyces Albus G	Acetate Ion
1bue	Imipenem-Hydrolysing Beta-Lactamase	-
1dy6	Imipenem-Hydrolysing Beta-Lactamase SME-1	-
1e25	Extended-Spectrum Beta-Lactamase PER-1	Sulfate Ion
1n4o	Class A beta-lactamase L2	Sulfate Ion
1n9b	SHV-2 Beta-Lactamase	4-(2-Hydroxyethyl)-1-Piperazine Ethanesulfonic Acid, Cyclohexyl-Hexyl-Beta-D-Maltoside, (4S)-2-Methyl-2,4-Pentanediol
1yt4	TEM-76 Beta-lactamase	-
2cc1	Mycobacterium fortuitum class A beta-lactamase	-
2p74	CTX-M-9a Beta-lactamase	Potassium Ion, Phosphate Ion
2qpn	GES-1 Beta-lactamase	Sulfate Ion
2wk0	BS3 Beta-lactamase	6-Beta-Iodopenicillanate
3i7j	Mb2281c Beta-lactamase	-
3lez	Halotolerant bacterial beta-lactamase	Calcium Ion, Chloride Ion, 4-(2-Hydroxyethyl)-1-Piperazine Ethanesulfonic Acid
3m6b	TB B-lactamase	Ertapenem Pre-isomerized Covalent Adduct
1m40	TEM-1 Beta-lactamase	Pinacol Methaneboronate, Potassium Ion, Phosphate Ion
1lhy	TEM-30 Beta-Lactamase	Phosphate Ion
1g68	PSE-4 Carbenicillinase	Sulfate Ion
1n4o	L2 Beta-Lactamase	Sulfate Ion
1i2s	Bacillus licheniformis BS3 class A beta-lactamase	Citric Acid, Sodium Ion
3cg5	TB B-lactamase	Clavulanate
2ov5	KPC-2 carbapenemase	Bicine
1ylt	CTX-M-14 beta-lactamase	Sulfate Ion, Sucrose
1iys	Toho-1 beta-lactamase	Sulfate Ion
1hzo	Class A Cephalosporinase	2-(N-Morpholino)-Ethanesulfonic Acid
3bfe	Class A beta-lactamase Sed1	Thiocyanate Ion
3p09	Beta-Lactamase from Francisella tularensis	Glycerol, Sulfate Ion
3m6b	TB B-lactamase	Carbapenems Ertapenem and Doripenem

NAMD Configuration File

This configuration file is used in running MD simulations.

```
#############################################################
## JOB DESCRIPTION ##
#############################################################

# Minimization and Equilibration of
# TEM-1 – BLIP Complex

#############################################################
## ADJUSTABLE PARAMETERS ##
#############################################################


structure          ionized.psf
coordinates        ionized.pdb
set temperature    300
set outputname     TEMBLIP
set init_temp      50
firsttimestep      0

#############################################################
## SIMULATION PARAMETERS ##
#############################################################

# Input
paraTypeCharmm     on
parameters         … /toppar/par_all27_prot_lipid.prm
temperature        $init_temp

# Force-Field Parameters
```

```
exclude                 scaled1-4
1-4scaling              1.0
cutoff                  12.
switching               on
switchdist              10.
pairlistdist            13.5

# Integrator Parameters
timestep                1.0  ;# 1fs/step
rigidBonds              all  ;# needed for 2fs steps
nonbondedFreq           1
fullElectFrequency      2
stepspercycle           10

# Constant Temperature Control
langevin                on    ;# do langevin dynamics
langevinDamping         5     ;# damping coefficient (gamma) of 5/ps
langevinTemp            $init_temp
langevinHydrogen        off    ;# don't couple langevin bath to hydrogens

# Periodic Boundary Conditions
cellBasisVector1        85.96100330352783   0.   0.
cellBasisVector2        0. 100.81399631500244  0.
cellBasisVector3        0.   0.  82.19200134277344
cellOrigin              -32.22344970703125 36.47468566894531 19.699106216430664
margin                  3
wrapAll                 on

# PME (for full-system periodic electrostatics)
PME                     yes
PMEGridSizeX            90
PMEGridSizeY            108
PMEGridSizeZ            90
```

```
# Constant Pressure Control (variable volume)
useGroupPressure      yes ;# needed for rigidBonds
useFlexibleCell       no
useConstantArea       no

langevinPiston        on
langevinPistonTarget  1.01325 ;#  in bar -> 1 atm
langevinPistonPeriod  100.
langevinPistonDecay   50.
langevinPistonTemp    $init_temp

# Output
outputName        $outputname

restartfreq           500     ;# 500steps = every 1ps
dcdfreq               250
xstFreq               250
outputEnergies        100
outputPressure        100

#############################################################
## EXTRA PARAMETERS ##
#############################################################

constraints on
consexp 2
consref               ionized.pdb
conskfile             cons.pdb
conskcol B
constraintScaling 5
#############################################################
## EXECUTION SCRIPT   ##
#############################################################
```

```
# turn off until later

#langevinPiston       off

# Minimization

minimize             1000
output mini.cons5

constraintScaling 3

minimize             1000

output mini.cons3

constraintScaling 0

minimize             1000

output mini.all

reinitvels     $init_temp
run                  4000

for { set TEMP [expr ($init_temp + 10) } { $TEMP < $temperature } { incr TEMP 10
} {
   langevinTemp      $TEMP
   LangevinPistonTemp $TEMP
   run               4000
}

langevinTemp         $temperature
#LangevinPistonTemp $TEMP
```

```
run                     10000000
```

PGN File for Generating PSF Files

The initial psf and pdb files used in MD simulations were created by using the following commands.

```
package require psfgen
topology … /toppar/top_all27_prot_lipid.inp
pdbalias residue HIS HSE
pdbalias atom ILE CD1 CD
segment A {pdb betalactamase.pdb}
patch DISU A:77 A:123
coordpdb betalactamase.pdb A
segment B {pdb blip.pdb}
patch DISU B:30 B:42
patch DISU B:109 B:131
coordpdb blip.pdb B
guesscoord
writepdb TEMBLIP.pdb
writepsf TEMBLIP.psf
```

Generating Average Simulation Structures in VMD

The average simulation coordinates used in the trajectory analysis were created by the following VMD commands.

```
mol load pdb filename.pdb dcd filename.dcd
mol load pdb filename.pdb
set protein [atomselect 0 “chain A”]
set avg [atomselect 1 “chain A”]
$avg set {x y z} [measure avpos $protein first 16000 last 40000]
```

MSF Calculation in MATLAB

The MSF calculation of the simulation trajectories with respect to their initial coordinates were done with the following MATLAB script.

```
X=readdcd ('CA_TEM-BLIP_10ns_chainA.dcd', 4:260);
x=bestfit(X);
r=findrmsd(x);
figure; plot(r);
size(x)
y=x(16000:40000,:);
y=bestfit(y);
figure;msf=findmsf(y,29:285);
mean(msf)

% Individual structural components: H10, H9-H10, 99-112, omega, omega_flexible
mean(msf(190:202))
mean(msf(173:202))
mean(msf(71:84))
mean(msf(133:151))
mean(msf(146:148))

% Active side residues [70 73 130 166 170 234]
mean(msf([42 45 102 138 142 206]))

% TEM clusters
mean(msf([102 206 207 215]))
mean(msf([76 77 142]))
mean(msf([71 72]))
mean(msf([75 139 140]))
mean(msf([101 188]))
mean(msf([82]))
```

```
%chain B
X=readdcd ('CA_TEM-BLIP_10ns_chainB.dcd', 4:162);
x=bestfit(X);
r=findrmsd(x);
size(x)
y=x(16000:40000,:);
y=bestfit(y);
msf=findmsf(y);
mean(msf)

%protein
X=readdcd ('CA_TEM-BLIP_10ns_protein.dcd', [4:260 264:422]);
x=bestfit(X);
r=findrmsd(x);
size(x)
y=x(16000:40000,:);
y=bestfit(y);
msf=findmsf(y);
mean(msf)
```

Residue Based MSF Calculation in MATLAB

In order to calculate the individual MSF values of the residues, the following MATLAB script was used.

```
clc;
clear all;
close all
X1=readdcd ('CA_TEMunbound_10ns_chainA.dcd', 4:260);
x1=bestfit(X1);
r1=findrmsd(x1);
figure; plot(r1);
size(x1)
```

```
y1=x1(16000:40000,:);
y1=bestfit(y1);
figure;msf1=findmsf(y1,29:285);

X2=readdcd ('CA_TEM-BLIP_10ns_chainA.dcd', 4:260);
x2=bestfit(X2);
r2=findrmsd(x2);
figure; plot(r2);
size(x2)
y2=x2(16000:40000,:);
y2=bestfit(y2);
figure;msf2=findmsf(y2,29:285);

resno=29:285;
msf_apoTEM_TEMBLIP=msf1-msf2;
figure;
subplot(3,1,1); plot(29:285, msf1);
xlabel('Residue Number');
ylabel(['MSF (', char(197), '^2) ']);
[r1 c1 v1]=find(abs(msf1)>0.7);
for i=1:length(c1);
   text(resno(c1(i)),msf1(c1(i)),num2str(resno(c1(i))))
end

subplot(3,1,2);plot(29:285, msf2);
xlabel('Residue Number');
ylabel(['MSF (', char(197), '^2) ']);
[r1 c1 v1]=find(abs(msf2)>0.7);
for i=1:length(c1);
   text(resno(c1(i)),msf2(c1(i)),num2str(resno(c1(i))))
end

subplot(3,1,3);plot(29:285, msf_apoTEM_TEMBLIP);
```

```
xlabel('Residue Number');
ylabel(['MSF (', char(197), '^2) ']);
[r1 c1 v1]=find(abs(msf_apoTEM_TEMBLIP)>0.35);
for i=1:length(c1);
   text(resno(c1(i)),msf_apoTEM_TEMBLIP(c1(i)),num2str(resno(c1(i))))
end
```

Generating Cross Correlation Maps in MATLAB

To generate the cross-correlation maps between beta-lactamase and BLIP, the following MATLAB script was used.

```
X=readdcd ('CA_TEM-BLIP_10ns_protein.dcd', 1:428);
x=bestfit(X);
y=x(16000:40000,:);
y=bestfit(y);
a=corres_20jan(y);
mean(mean(a([1:263] , [264:428])))

correlation_complex(a, 0.5, 'outputfilename')
```

corres_20jan script

```
function rr = corres(X, rlim, res, z)

% Finds the correlation between the residues taking only the r, distance from the average, into consideration.
% Blue -> Anticorrelated
% Red -> Correlated
%
% I/O format: r = corres(X, rlim, res)
%
% where X is the matrix of dimensions, samples x (3 x res no.)
```

```
%       rlim (default = 0.2) is the lower threshold value for
%       correlation
%       res (default = 1 : n) is the residue numbers
%

if nargin < 3 | isempty(res)
   res = 1 : size(X, 2)/3;
else
   res = res(:)';
end

nofres = length(res);

if nargin < 2 | isempty(rlim)
   rlim = .05;
end

[m, n] = size(X);
X = mncn(X);
C    = zeros(n/3, n/3);
Cnew = zeros(n/3, n/3);

X = reshape(X', [3 n/3 m]);

for i = 1 : m
   x = squeeze(X(:, :, i));
   Cnew = x'*x;
   C = C + Cnew;
end

C = C / (m-1);

D = diag(C);
```

```
r = C ./ sqrt(D*D');
rr=r;

% ind1 = find(r < -0.30);%yellow
% ind2 = find(r < -0.15);%light grey
% ind3 = find(r < -0.05);%white
% ind4 = find(r < 0.05);%dark grey
% ind5 = find(r < 0.15);%red
% ind6 = find(r < 0.25);%dark red
% ind7 = find(r < 0.45);%blue
% ind8 = find(r <= 1);%black
% r(ind1)= -.2;
% r(setdiff(ind2, ind1)) = -.15;
% r(setdiff(ind3, ind2)) = -0.05;
% r(setdiff(ind4, ind3)) = 0.05;
% r(setdiff(ind5, ind4)) = 0.15;
% r(setdiff(ind6, ind5)) = 0.25;
% r(setdiff(ind7, ind6)) = 0.45;
% r(setdiff(ind8, ind7)) = 1;
%
indresX = ones(nofres, 1) * res;
indresY = indresX';
%
colormap(    [0 0 0;0 0 1;0 0 1;0 0 1;0 0 1;0 0 1;0 0 1;0 0 1;0 0 1;0 0 1;0 0 1;0 0 1;0 0 1;0 1
1;0 1 1;0 1 1;0 1 1;0 1 1;0 1 1;0 1 1;0 1 0.1098;0 1 0.0915;0 1 0.0732;0 1 0.0549;0 1 0.0366;0 1
0.0183;0 1 0;1 1 1;1 1 1;1 1 1;1 1 1;1 1 1;1 1 1;1 1 1;1 1 1;1 1 1;1 1 1;1 1 1;1 1 1;1 1 1;1 1 1;1 1
1;1 0 1;1 0 1;1 0 1;1 0 1;1 0 1;1 0 1;1 0 1;1 0 0;1 0 0;1 0 0;1 0 0;1 0 0;1 0 0;0.8471 0.1608
0;0.8471 0.1608 0;0.8471 0.1608 0;0.8471 0.1608 0;0.8471 0.1608 0;0.8471 0.1608
0;0.8471 0.1608 0;0.8471 0.1608 0;0.8471 0.1608 0;0.8471 0.1608 0;0.8471 0.1608 0;0 0
0]);
pcolor(indresX, indresY, r),
 caxis([-1 1])
shading('interp')
```

```
% function createfigure(ZData1, CData1)
% %CREATEFIGURE(ZDATA1,CDATA1)
% %  ZDATA1:  surface zdata
% %  CDATA1:  surface cdata
%
% %  Auto-generated by MATLAB on 20-Jan-2010 17:03:05
%
% % Create figure
% figure1 = figure('Colormap',...
%     [0 0 0;0 0 1;0 0 1;0 0 1;0 0 1;0 0 1;0 0 1;0 0 1;0 0 1;0 0 1;0 0 1;0 0 1;0 0 1;0 0 1;0 1 1;0 1 1;0 1 1;0 1 1;0 1 1;0 1 1;0 1 1;0 1 1;0 1 1;0 1 1;0 1 0.1098;0 1 0.0915;0 1 0.0732;0 1 0.0549;0 1 0.0366;0 1 0.0183;0 1 0;1 1 1;1 1 1;1 1 1;1 1 1;1 1 1;1 1 1;1 1 1;1 1 1;1 1 1;1 1 1;1 1 1;1 1 1;1 1 1;1 1 1;1 1 1;1 1 1;1 1 1;1 0 1;1 0 1;1 0 1;1 0 1;1 0 1;1 0 1;1 0 1;1 0 0;1 0 0;1 0 0;1 0 0;1 0 0;1 0 0;1 0 0;0.8471 0.1608 0;0.8471 0.1608 0;0.8471 0.1608 0;0.8471 0.1608 0;0.8471 0.1608 0;0.8471 0.1608 0;0.8471 0.1608 0;0.8471 0.1608 0;0.8471 0.1608 0;0.8471 0.1608 0;0.8471 0.1608 0;0.8471 0.1608 0;0 0 0]);
%
% % Create axes
% axes1 = axes('Parent',figure1,'CLim',[-1 1]);
% % Uncomment the following line to preserve the X-limits of the axes
% % xlim([1 263]);
% % Uncomment the following line to preserve the Y-limits of the axes
% % ylim([1 263]);
% box('on');
% hold('all');
%
% % Create surface
% surface(ZData1,'Parent',axes1,'FaceColor','interp','EdgeColor','none',...
%     'CData',CData1);

colorbar

%xlabel('Residue no.')
```

```
%ylabel('Residue no.')

%set(gcf, 'Color', 'w')
```

correlation_complex script

```
% this finds those residues from chain A and chain B whose cross correlation is higher than the cutoff
function correlation_complex(a,cutoff,outputfile)
[m,n]=find ( a > cutoff);
x=[m,n];
[r1 c1]=find(x(:,1)<264 & x(:,2)>263);
fid = fopen (outputfile, 'w');
for i=1:length(r1)
      fprintf (fid,'%d\n', x(r1(i),1));
      fprintf (fid,'%d\n', x(r1(i),2));
end
fclose (fid);
```

PDB Extracting by Wordom

The simulation snapshots used in binding free energy analysis by FoldX were created by using this Ruby script.

```
#!/usr/bin/env ruby

system("clear")

File.open('framelist.ods', 'r+') do |f1|

while line5 = f1.gets
frameno2=line5.split(//)
```

```
i=0
frameno=""
  while number = frameno2[i]
    if number=="\n"
      number=""
    end
    frameno<<number
    i=i+1
  end

@pdbname = @name= ARGV[0]
# @pathway= ARGV[1]
 @pathway= "…/Applications/"

system("…/Applications/wordom/wordom_0.21-rc6.x86-64 -f "+frameno+" -itrj
"+@name+".dcd -imol "+@name+".pdb -omol "+@name+"_"+frameno+".pdb")
@name=@name.to_s+"_"+frameno
end
end
```

Repairing PDB by FoldX

The simulation files were repaired with the following commands before the energetic analysis by FoldX.

```
<TITLE>FOLDX_runscript;
<JOBSTART>#;
<PDBS>#;
<BATCH>list.txt;
<COMMANDS>FOLDX_commandfile;
<RepairPDB>#;
<END>#;
<OPTIONS>FOLDX_optionfile;
<Temperature>300;
```

<R>#;
<pH>7;
<IonStrength>0.050;
<water>-CRYSTAL;
<metal>-CRYSTAL;
<VdWDesign>2;
<OutPDB>true;
<pdb_hydrogens>false;
<END>#;
<JOBEND>#;
<ENDFILE>#;

Binding Free Energy Analysis by FoldX

After repairing the simulation snapshots, the following FoldX commands were used to calculate the binding free energy between enzyme and ligand.

<TITLE>FOLDX_runscript;
<JOBSTART>#;
<PDBS>#;
<BATCH>list.txt;
<COMMANDS>FOLDX_commandfile;
<AnalyseComplex>#,A;
<END>#;
<OPTIONS>FOLDX_optionfile;
<Temperature>300;
<R>#;
<pH>7;
<IonStrength>0.050;
<water>-CRYSTAL;
<metal>-CRYSTAL;
<VdWDesign>2;
<OutPDB>false;

<pdb_hydrogens>false;
<END>#;
<JOBEND>#;
<ENDFILE>#;

Extracting Energy Terms from FoldX Outputs by Ruby

The energy terms calculated by FoldX were extracted from the outputs by using following Ruby script.

```
#!/usr/bin/env ruby

system("clear")
File.open('framelist.rb', 'r+') do |f1|
#######
while line5 = f1.gets
frameno2=line5.split(//)

 i=0
frameno=""
  while number = frameno2[i]
    if number=="\n"
      number=""
    end
    frameno<<number
    i=i+1
  end
#################
@name="outputname"
@name=@name.to_s+"_"+frameno
File.open("Interaction_AnalyseComplex_RepairPDB_"+@name+".fxout", 'r') do |f2|
while line = f2.gets
mynumber=""
```

```
  if line =~ /Interaction Energy/
  line= f2.gets
  words = line.split
  mynumber << words[5]
i=0
while i<=words.length do
  if words[i] =~ /[0123456789.+E]/ then
  mynumber << words[i]
  end
 i=i+1
end
mynumber2=mynumber.split(//)
mynumber2.delete_at(0)
i=0

while number = mynumber2[i]
words<<number
i=i+1
end
File.open("InteractionEnergies.ods", 'a+') {|f| f.write(mynumber)}
File.open("InteractionEnergies.ods", 'a+') {|f| f.write("\n")}
 end
 end
end
end
end
```

APPENDIX B: EXPERIMENTAL DATA

Table B.1. OD versus time values in the presence of 100 μM kemptide acetate salt.

Time (min)	**Control**			**Sample**		
	Set -1	Set-2	Set-3	Set-1	Set-2	Set-3
0.12	0.0548	0.0713	0.0511	0.0745	0.0619	0.0681
0.20	0.0878	0.1003	0.0792	0.1054	0.0860	0.1017
0.28	0.1199	0.1317	0.1082	0.1369	0.1109	0.1320
0.37	0.1474	0.1618	0.1356	0.1674	0.1362	0.1628
0.45	0.1760	0.1922	0.1627	0.1999	0.1611	0.1900
0.53	0.2023	0.3195	0.1888	0.2290	0.1853	0.3196
0.62	0.2273	0.2445	0.2133	0.2551	0.2080	0.2467
0.70	0.2504	0.2677	0.2358	0.2813	0.2279	0.2685
0.78	0.2723	0.2899	0.2581	0.3021	0.2463	0.2898
0.87	0.2917	0.3108	0.2782	0.3223	0.2658	0.3098
0.95	0.3095	0.3299	0.2978	0.3400	0.2857	0.3284
1.03	0.3263	0.3464	0.3146	0.3551	0.3038	0.3460
1.12	0.3399	0.3610	0.3285	0.3672	0.3228	0.3619
1.20	0.3517	0.3726	0.3419	0.3770	0.3340	0.3759
1.28	0.3612	0.3832	0.3537	0.3858	0.3463	0.3878
1.37	0.3698	0.3927	0.3652	0.3930	0.3573	0.3973
1.45	0.3774	0.4008	0.3750	0.3987	0.3674	0.4038
1.53	0.3830	0.4059	0.3830	0.4041	0.3771	0.4096
1.62	0.3885	0.4089	0.3896	0.4082	0.3849	0.4130
1.70	0.3933	0.4116	0.3948	0.4119	0.3915	0.4157
1.78	0.3969	0.4144	0.3999	0.4150	0.3981	0.4188
1.87	0.3999	0.4168	0.4033	0.4167	0.4038	0.4222
1.95	0.4031	0.4189	0.4067	0.4172	0.4088	0.4253
2.03	0.4046	0.4206	0.4087	0.4170	0.4131	0.4269

Table B.2. Activity and relative activity values in the presence of 100 μM kemptide acetate salt. The values that were used for averaging data are in bold.

	Control			**Sample**		
	Set-1	Set-2	Set-3	Set-1	Set-2	Set-3
Slope	0.3530	0.3508	0.3258	0.3651	0.2945	0.3555
Activity (U)	**1379**	**1370**	1273	**1426**	1150	**1389**
Average values (U)	1375			1407		
Relative activity	100			102		

Table B.3. OD versus time values in the presence of 100 and 200 μM biotinylated-P8 peptide.

Time (min)	**Control**				**Sample**			
					100 μM peptide			**200 μM peptide**
	Set-1	Set-2	Set-3	Set-4	Set- 1	Set-2	Set- 3	Set-1
0.12	0.071	0.0556	0.0587	0.0566	0.086	0.0727	0.0711	0.0799
0.20	0.1054	0.0825	0.0893	0.0821	0.1199	0.1097	0.1032	0.0969
0.28	0.1382	0.1082	0.1165	0.1091	0.1536	0.1404	0.1343	0.1176
0.37	0.1697	0.1352	0.1445	0.1353	0.1827	0.1671	0.1667	0.1374
0.45	0.2012	0.1593	0.1723	0.1607	0.2096	0.1973	0.1946	0.1523
0.53	0.2276	0.1837	0.1979	0.1854	0.2356	0.2200	0.2227	0.1687
0.62	0.2526	0.206	0.2215	0.2097	0.2615	0.2436	0.2476	0.1869
0.70	0.2759	0.2275	0.2442	0.2329	0.2852	0.2656	0.271	0.2046
0.78	0.2976	0.2494	0.2653	0.2554	0.3052	0.2859	0.2917	0.2221
0.87	0.3149	0.2677	0.2848	0.2755	0.3241	0.3091	0.3120	0.2394
0.95	0.3306	0.286	0.3026	0.2952	0.3402	0.3279	0.3299	0.2553
1.03	0.3456	0.3033	0.3186	0.3146	0.3543	0.3440	0.3435	0.2703
1.12	0.2570	0.3194	0.3333	0.3316	0.3667	0.3588	0.3549	0.2847
1.20	0.3663	0.3337	0.3464	0.345	0.3766	0.3715	0.3656	0.2993
1.28	0.3745	0.3457	0.3577	0.3586	0.3853	0.3823	0.3754	0.3111
1.37	0.3808	0.3565	0.3672	0.3710	0.392	0.3914	0.3838	0.3236
1.45	0.3853	0.366	0.3751	0.3830	0.3978	0.4000	0.3905	0.3343
1.53	0.3893	0.3744	0.3819	0.3922	0.4028	0.4068	0.3957	0.3441
1.62	0.3927	0.3815	0.3874	0.3996	0.4069	0.4134	0.3997	0.3541
1.70	0.3948	0.3872	0.3925	0.4069	0.4106	0.4181	0.4034	0.3631
1.78	0.3965	0.3922	0.3966	0.4127	0.4133	0.4219	0.4064	0.3714
1.87	0.3978	0.3961	0.3996	0.4178	0.4162	0.4252	0.4084	0.3793
1.95	0.3988	0.3993	0.4016	0.4224	0.4191	0.4279	0.4089	0.3867
2.03	0.4000	0.4015	0.4031	0.4262	0.4212	0.4295	0.4096	0.3909

Table B.4. Activity and relative activity values in the presence of 100 μM biotinylated-P8 peptide. The values that were used for averaging data are in bold.

	Control			**Sample**		
	Set-1	Set-2	Set-3	Set-1	Set-2	Set-3
Slope	0.3652	0.3020	0.3263	0.3488	0.3387	0.3552
Activity (U)	**1426**	1180	**1275**	**1362**	**1323**	1387
Average values (U)	1350			1343		
Relative activity	100			99		

Table B.5. Activity and relative activity values in the presence of 200 μM biotinylated-P8 peptide.

	Control	**Sample**
	Set-1	Set-1
Slope	0.3075	0.2140
Activity (U)	4805	3344
Relative activity	100	69.6

Table B.6. OD versus time values in the presence of 100 and 200 μM fluoresceinated-P8 peptide.

Time (min)	**Control**			**Sample**		
				100 μM peptide		**200 μM peptide**
	Set-1	Set-2	Set-3	Set-1	Set-2	Set-1
0.12	0.0765	0.0531	0.0733	0.2211	0.2549	0.4580
0.20	0.1148	0.0763	0.1019	0.2445	0.2687	0.4942
0.28	0.1494	0.0966	0.1335	0.2704	0.2834	0.5227
0.37	0.1785	0.1167	0.1624	0.2936	0.2997	0.5479
0.45	0.2046	0.1373	0.1902	0.3151	0.3172	0.5709
0.53	0.2292	0.1580	0.2144	0.3373	0.3335	0.5946
0.62	0.2538	0.1741	0.2423	0.3570	0.3512	0.6161
0.70	0.2767	0.1962	0.2651	0.3754	0.3669	0.6378
0.78	0.2967	0.2144	0.2873	0.3914	0.3833	0.6583
0.87	0.3165	0.2324	0.3084	0.4078	0.3971	0.6773
0.95	0.3341	0.2501	0.3274	0.4241	0.4121	0.6956
1.03	0.3487	0.2658	0.3435	0.4384	0.4256	0.7114
1.12	0.3627	0.2812	0.3575	0.4486	0.4381	0.7260
1.20	0.3749	0.2954	0.3706	0.4572	0.4498	0.7400
1.28	0.3859	0.3082	0.3816	0.4641	0.4618	0.7514
1.37	0.3955	0.3203	0.3916	0.4715	0.4734	0.7619
1.45	0.4037	0.3318	0.3992	0.4779	0.4842	0.7715
1.53	0.4106	0.3423	0.4062	0.4836	0.4945	0.7794
1.62	0.4157	0.3524	0.4116	0.4884	0.5045	0.7870
1.70	0.4195	0.3612	0.4153	0.4923	0.5131	0.7935
1.78	0.4228	0.3694	0.4183	0.4961	0.5216	0.7991
1.87	0.4255	0.3759	0.4209	0.4981	0.5289	0.8033
1.95	0.4282	0.3822	0.4231	0.4997	0.5361	0.8063
2.03	0.4306	0.3880	0.4247	0.5012	0.5426	0.8090

Table B.7. Activity and relative activity values in the presence of 100 μM fluoresceinated-P8 peptide.

	Control		**Sample**	
	Set-1	Set-2	Set-1	Set-2
Slope	0.3497	0.2430	0.2734	0.1938
Activity (U)	**5464**	**3797**	**4272**	**3028**
Average values (U)	4630		3650	
Relative activity	100		79	

Table B. 8. Activity and relative activity values in the presence of 200 μM fluoresceinated-P8 peptide.

	Control	**Sample**
	Set-1	Set-1
Slope	0.3380	0.2709
Activity (U)	5281	4232
Relative activity	100	80

Table B.9. OD versus time values in the presence of 25 μM fluoresceinated-P10.

Time (min)	**Control**			**Sample**		
	Set-1	Set-2	Set-3	Set-1	Set-2	Set-3
0.12	0.0100	0.0043	0.0043	0.1082	0.1035	0.0934
0.20	0.0157	0.0091	0.0097	0.1104	0.1069	0.0964
0.28	0.0199	0.0133	0.0142	0.1126	0.1103	0.1000
0.37	0.0240	0.0177	0.0184	0.1154	0.1135	0.1025
0.45	0.0277	0.0251	0.0229	0.1169	0.1167	0.1036
0.53	0.0319	0.0256	0.0278	0.1184	0.1203	0.1044
0.62	0.0352	0.0292	0.0336	0.1205	0.1235	0.1056
0.70	0.0391	0.0331	0.0371	0.1222	0.1281	0.1077
0.78	0.0435	0.0372	0.0402	0.1240	0.1306	0.1101
0.87	0.0480	0.0414	0.0438	0.1260	0.1315	0.1122
0.95	0.0520	0.0454	0.0479	0.1276	0.1323	0.1147
1.03	0.0557	0.0493	0.0520	0.1295	0.1345	0.1162
1.12	0.0592	0.0531	0.0563	0.1322	0.1372	0.1183
1.20	0.0628	0.0570	0.0605	0.1349	0.1402	0.1200
1.28	0.0669	0.0608	0.0645	0.1375	0.1431	0.1219
1.37	0.0708	0.0647	0.0689	0.1399	0.1459	0.1236
1.45	0.0747	0.0689	0.0730	0.1418	0.1485	0.1255
1.53	0.0786	0.0721	0.0773	0.1436	0.1512	0.1274
1.62	0.0824	0.0759	0.0810	0.1455	0.1542	0.1295
1.70	0.0860	0.0793	0.0848	0.1477	0.1570	0.1315
1.78	0.0897	0.0831	0.0890	0.1499	0.1605	0.1337
1.87	0.0936	0.0868	0.0931	0.1514	0.1638	0.1352
1.95	0.0975	0.0904	0.0969	0.1537	0.1670	0.1367
2.03	0.1009	0.0940	0.1008	0.1552	0.1702	0.1387

Table B.10. Activity and relative activity values in the presence of 25 μM fluoresceinated-P10. The values that were used for averaging data are in bold.

	Control			**Sample**		
	Set-1	Set-2	Set-3	Set-1	Set-2	Set-3
Slope	0.0488	0.0481	0.0517	0.0233	0.0399	0.0245
Activity (U)	**762**	**751**	808	364	**623**	383
Average values (U)	757			623		
Relative activity	100			82		

Table B.11. OD versus time values in the presence of 50 μM fluoresceinated-P10.

Time (min)	**Control**			**Sample**		
	Set-1	Set-2	Set-3	Set-1	Set-2	Set-3
0.12	0.0062	0.009	0.0106	0.2193	0.2214	0.2148
0.20	0.0111	0.0141	0.0146	0.2227	0.2238	0.2185
0.28	0.0144	0.0179	0.0189	0.2262	0.2274	0.2224
0.37	0.0178	0.0226	0.0228	0.2291	0.2299	0.2250
0.45	0.0215	0.0275	0.0271	0.2303	0.2325	0.2275
0.53	0.0250	0.0298	0.0320	0.2321	0.2356	0.2314
0.62	0.0280	0.033	0.0360	0.2333	0.2384	0.2360
0.70	0.0310	0.0368	0.0402	0.2354	0.241	0.2404
0.78	0.0346	0.0418	0.0444	0.2373	0.2436	0.2457
0.87	0.0382	0.0465	0.0489	0.2396	0.2461	0.2488
0.95	0.0414	0.0507	0.0533	0.2428	0.249	0.2524
1.03	0.0444	0.0545	0.0575	0.2454	0.2521	0.2560
1.12	0.0477	0.0582	0.0616	0.2471	0.255	0.2586
1.20	0.0510	0.062	0.0659	0.2483	0.257	0.2612
1.28	0.0545	0.0661	0.0701	0.2514	0.2584	0.2638
1.37	0.0578	0.0699	0.0743	0.2533	0.2606	0.2664
1.45	0.0614	0.0742	0.0785	0.2556	0.2639	0.2698
1.53	0.0649	0.0784	0.0833	0.2583	0.2669	0.2736
1.62	0.0683	0.0823	0.0881	0.2614	0.27	0.2775
1.70	0.0717	0.0861	0.0924	0.2628	0.2733	0.2806
1.78	0.0751	0.0881	0.0969	0.2646	0.2768	0.2837
1.87	0.0783	0.0938	0.1014	0.2663	0.28	0.2866
1.95	0.0812	0.0982	0.1055	0.2688	0.2837	0.2893
2.03	0.0840	0.1018	0.1090	0.2701	0.2875	0.2920

Table B.12. Activity and relative activity values in the presence of 50 μM fluoresceinated-P10. The values that were used for averaging data are in bold.

	Control			**Sample**		
	Set-1	Set-2	Set-3	Set-1	Set-2	Set-3
Slope	0.0414	0.048	0.0514	0.0265	0.0333	0.0405
Activity (U)	**647**	**750**	803	414	**520**	**633**
Average values (U)	698			576		
Relative activity	100			82		

Table B.13. OD versus time values in the presence of 75 μM fluoresceinated-P10.

Time (min)	**Control**			**Sample**		
	Set-1	Set-2	Set-3	Set-1	Set-2	Set-3
0.12	0.0064	0.0017	-	0.2731	0.3311	0.3161
0.20	0.0092	0.0046	0.0044	0.2774	0.3353	0.3194
0.28	0.0114	0.0071	0.0087	0.2789	0.3397	0.3210
0.37	0.0145	0.0097	0.0137	0.2838	0.3439	0.3235
0.45	0.0175	0.0122	0.0168	0.2884	0.3487	0.3272
0.53	0.0217	0.0152	0.0208	0.2893	0.3507	0.3305
0.62	0.0249	0.0177	0.0253	0.2921	0.3533	0.3335
0.70	0.0272	0.0204	0.0295	0.2954	0.3556	0.3378
0.78	0.0295	0.0232	0.0332	0.2999	0.3583	0.3410
0.87	0.0324	0.0255	0.0369	0.3035	0.3617	0.3435
0.95	0.0351	0.0279	0.0417	0.3055	0.364	0.3458
1.03	0.0379	0.0302	0.0458	0.3072	0.3645	0.3491
1.12	0.0408	0.0326	0.0493	0.3101	0.3659	0.3519
1.20	0.0437	0.0352	0.0530	0.3141	0.3665	0.3555
1.28	0.0467	0.0376	0.0568	0.3185	0.3691	0.3583
1.37	0.0495	0.0402	0.0615	0.3219	0.3707	0.3604
1.45	0.0523	0.0428	0.0658	0.3239	0.3737	0.3628
1.53	0.0553	0.0452	0.0699	0.3260	0.3768	0.3658
1.62	0.0580	0.0478	0.0738	0.3273	0.3814	0.3686
1.70	0.0609	0.0502	0.0778	0.3286	0.3847	0.3724
1.78	0.0636	0.0528	0.0815	0.3306	0.3882	0.3762
1.87	0.0664	0.0558	0.0855	0.3336	0.3915	0.3788
1.95	0.0692	0.0582	0.0895	0.3366	0.3948	0.3824
2.03	0.0718	0.0607	0.0935	0.3410	0.3962	0.3851

Table B.14. Activity and relative activity values in the presence of 75 μM fluoresceinated-P10. The values that were used for averaging data are in bold.

	Control			**Sample**		
	Set-1	Set-2	Set-3	Set-1	Set-2	Set-3
Slope	0.0369	0.0318	0.0491	0.0392	0.0389	0.0369
Activity (U)	**576**	497	**767**	612	**608**	**576**
Average values (U)	671			592		
Relative activity	100			88		

Table B.15. OD versus time values in the presence of 100 μM fluoresceinated-P10.

Time (min)	**Control**			**Sample**		
	Set-1	Set-2	Set-3	Set-1	Set-2	Set-3
0.12	0.0032	0.0064	0.0002	0.4315	0.4234	0.4298
0.20	0.0075	0.0103	0.0018	0.4327	0.4267	0.4340
0.28	0.0109	0.0144	0.0046	0.4343	0.4283	0.4377
0.37	0.0142	0.0184	0.0056	0.4368	0.4306	0.4427
0.45	0.0176	0.0223	0.0064	0.4394	0.432	0.4431
0.53	0.0207	0.0261	0.0094	0.4420	0.4359	0.4457
0.62	0.0265	0.0301	0.0112	0.4434	0.4412	0.4487
0.70	0.0288	0.0343	0.0124	0.4462	0.4463	0.4517
0.78	0.0308	0.0383	0.0143	0.4491	0.448	0.4553
0.87	0.0339	0.0423	0.0156	0.4519	0.4472	0.4577
0.95	0.0372	0.0468	0.0171	0.4536	0.4485	0.4605
1.03	0.0405	0.0511	0.0187	0.4556	0.4515	0.4624
1.12	0.0438	0.0551	0.0201	0.4573	0.4557	0.4624
1.20	0.0474	0.0584	0.0214	0.4597	0.4595	0.4652
1.28	0.0510	0.0617	0.0228	0.4619	0.4628	0.4681
1.37	0.0549	0.0653	0.0242	0.4645	0.4669	0.4710
1.45	0.0583	0.0692	0.0258	0.4666	0.4715	0.4741
1.53	0.0613	0.0733	0.0273	0.4686	0.4762	0.4778
1.62	0.0644	0.0774	0.0292	0.4707	0.4775	0.4816
1.70	0.0673	0.0809	0.0304	0.4724	0.4798	0.4836
1.78	0.0702	0.0848	0.0318	0.4737	0.482	0.4861
1.87	0.0731	0.0886	0.0332	0.4742	0.4831	0.4884
1.95	0.0763	0.0926	0.0348	0.4753	0.4844	0.4907
2.03	0.0794	0.0964	0.0364	0.4773	0.4856	0.4936

Table B.16. Activity and relative activity values in the presence of 100 μM fluoresceinated-P10. The values that were used for averaging data are in bold.

	Control			**Sample**		
	Set-1	Set-2	Set-3	Set-1	Set-2	Set-3
Slope	0.0407	0.0481	0.021	0.0269	0.0312	0.0366
Activity (U)	**636**	**751**	328	420	**487**	**572**
Average values (U)	693			529		
Relative activity	100			76		

Table B.17. OD versus time values in the presence of 100 μM fluoresceinated-P10 determined by repeated experiments.

Time (min)	**Control**			**Sample**		
	Set-1	Set-2	Set-3	Set-1	Set-2	Set-3
0.12	0.0601	0.057	0.0464	0.4478	0.4778	0.4399
0.20	0.0901	0.0882	0.0737	0.4682	0.5017	0.4676
0.28	0.118	0.1197	0.1007	0.4935	0.529	0.4971
0.37	0.145	0.1491	0.127	0.5221	0.5513	0.5188
0.45	0.1709	0.1768	0.1543	0.5385	0.5755	0.5442
0.53	0.1961	0.2018	0.1782	0.5582	0.5977	0.5688
0.62	0.2201	0.2243	0.2025	0.5785	0.6197	0.5901
0.70	0.2415	0.2476	0.224	0.5977	0.6412	0.6125
0.78	0.2639	0.2701	0.2438	0.6151	0.6638	0.6334
0.87	0.2832	0.2905	0.2625	0.6326	0.6849	0.6517
0.95	0.2993	0.3115	0.28	0.6508	0.7024	0.6684
1.03	0.315	0.3288	0.2956	0.6672	0.7182	0.6838
1.12	0.3286	0.3427	0.31	0.6832	0.7338	0.6975
1.20	0.3412	0.3536	0.3226	0.6976	0.748	0.7118
1.28	0.3514	0.3642	0.3339	0.712	0.7613	0.7238
1.37	0.3569	0.3711	0.344	0.724	0.7744	0.7365
1.45	0.3669	0.3788	0.3536	0.7335	0.7864	0.7479
1.53	0.3728	0.3852	0.3625	0.7425	0.7965	0.7596
1.62	0.3781	0.3912	0.3696	0.7513	0.804	0.7667
1.70	0.3821	0.3958	0.3765	0.7594	0.8109	0.7704
1.78	0.3849	0.4	0.3815	0.7645	0.8163	0.7747
1.87	0.3869	0.4045	0.3853	0.7692	0.8206	0.7788
1.95	0.3886	0.4072	0.3882	0.7732	0.8244	0.7821
2.03	0.3899	0.4099	0.3904	0.778	0.8278	0.7845

Table B.18. Activity and relative activity values in the presence of 100 μM fluoresceinated-P10 of repeated experiments.

The values that were used for averaging data are in bold.

	Control			**Sample**		
	Set-1	Set-2	Set-3	Set-1	Set-2	Set-3
Slope	0.3255	0.3494	0.3179	0.2645	0.2847	0.3072
Activity (U)	**1271**	**1365**	**1242**	**1033**	**1112**	**1200**
Average values (U)	1293			1115		
Relative activity	100			86		

REFERENCES

Allen, P. B., 2004, "Introduction to Molecular Dynamics Simulations", *Computational Soft Matter: From Synthetic Polymers to Proteins,Lecture Notes, NIC Series,* Vol. 23, pp. 1-28.

Altschul, S. F., W. Gish, W. Miller, E. W. Myers, and D. J. Lipman, 1990, "Basic local alignment search tool", *J Mol Biol,* Vol. 215, pp. 403-10.

Ambler, R. P., 1980, "The structure of beta-lactamases", *Philos Trans R Soc Lond B Biol Sci,* Vol. 289, pp. 321-31.

Ambler, R. P., A. F. Coulson, J. M. Frere, J. M. Ghuysen, B. Joris, M. Forsman, R. C. Levesque, G. Tiraby, and S. G. Waley, 1991, "A standard numbering scheme for the class A beta-lactamases", *Biochem J,* Vol. 276 (Pt 1), pp. 269-70.

Avcı, N. G., 2011, "Production and Purification of RTEM-1 Beta-lactamase and Its Inhibition by Peptides", M. S. Thesis, Marmara University.

Babic, M., A. M. Hujer, and R. A. Bonomo, 2006, "What's new in antibiotic resistance? Focus on beta-lactamases", *Drug Resist Updat,* Vol. 9, pp. 142-56.

Berman, H. M., J. Westbrook, Z. Feng, G. Gilliland, T. N. Bhat, H. Weissig, I. N. Shindyalov, and P. E. Bourne, 2000, "The Protein Data Bank", *Nucleic Acids Res,* Vol. 28, pp. 235-42.

Buynak, J. D., 2006, "Understanding the longevity of the beta-lactam antibiotics and of antibiotic/beta-lactamase inhibitor combinations", *Biochem Pharmacol,* Vol. 71, pp. 930-40.

Crooks, G. E., G. Hon, J. M. Chandonia, and S. E. Brenner, 2004, "WebLogo: a sequence logo generator", *Genome Res,* Vol. 14, pp. 1188-90.

Darden, T., D. York, and L. Pedersen, 1993, "Particle mesh Ewald: An N log(N) method for Ewald sums in large systems", *J. Chem. Phys.* , Vol. 98, pp. 10089-10092.

Das, R. and D. Baker, 2008, "Macromolecular Modeling with Rosetta", *Annu. Rev. Biochem.* , Vol. 77, pp. 363-82.

Doğan, A., 2011, "Investigation of TEM-1 and SHV-1 Beta-lactamases Binding to BLIP and TEM-1 Binding to BLIP Based Peptides", M. S. Thesis, Boğaziçi University.

Doran, J. L., B. K. Leskiw, S. Aippersbach, and S. E. Jensen, 1990, "Isolation and characterization of a beta-lactamase-inhibitory protein from Streptomyces clavuligerus and cloning and analysis of the corresponding gene", *J Bacteriol,* Vol. 172, pp. 4909-18.

Doucet, N., P. Y. Savard, J. N. Pelletier, and S. M. Gagne, 2007, "NMR investigation of Tyr105 mutants in TEM-1 beta-lactamase: dynamics are correlated with function", *J Biol Chem,* Vol. 282, pp. 21448-59.

Elmquist, A., M. Hansen, and U. Langel, 2006, "Structure-activity relationship study of the cell-penetrating peptide pVEC", *Biochim Biophys Acta,* Vol. 1758, pp. 721-9.

Essack, S. Y., 2001, "The development of beta-lactam antibiotics in response to the evolution of beta-lactamases", *Pharm Res,* Vol. 18, pp. 1391-9.

Fisette, O., S. Morin, P. Y. Savard, P. Lague, and S. M. Gagne, 2010, "TEM-1 backbone dynamics-insights from combined molecular dynamics and nuclear magnetic resonance", *Biophys J,* Vol. 98, pp. 637-45.

Fisher, J. F., S. O. Meroueh, and S. Mobashery, 2005, "Bacterial resistance to beta-lactam antibiotics: compelling opportunism, compelling opportunity", *Chem Rev,* Vol. 105, pp. 395-424.

Hanes, M. S., K. A. Reynolds, C. McNamara, P. Ghosh, R. A. Bonomo, J. F. Kirsch, and T. M. Handel, 2011, "Specificity and cooperativity at beta-lactamase position 104 in TEM-1/BLIP and SHV-1/BLIP interactions", *Proteins,* Vol. 79, pp. 1267-76.

Horn, J. R. and B. K. Shoichet, 2004, "Allosteric inhibition through core disruption", *J Mol Biol,* Vol. 336, pp. 1283-91.

Huang, W., Z. Beharry, Z. Zhang, and T. Palzkill, 2003, "A broad-spectrum peptide inhibitor of beta-lactamase identified using phage display and peptide arrays", *Protein Eng,* Vol. 16, pp. 853-60.

Huang, W., Z. Zhang, and T. Palzkill, 2000, "Design of potent beta-lactamase inhibitors by phage display of beta-lactamase inhibitory protein", *J Biol Chem,* Vol. 275, pp. 14964-8.

Humphrey, W., A. Dalke, and K. Schulten, 1996, "VMD: visual molecular dynamics", *J Mol Graph,* Vol. 14, pp. 33-8, 27-8.

Ichiye, T. and M. Karplus, 1991, "Collective motions in proteins: a covariance analysis of atomic fluctuations in molecular dynamics and normal mode simulations", *Proteins,* Vol. 11, pp. 205-17.

Jelsch, C., L. Mourey, J. M. Masson, and J. P. Samama, 1993, "Crystal structure of Escherichia coli TEM1 beta-lactamase at 1.8 A resolution", *Proteins,* Vol. 16, pp. 364-83.

Jones, R. N., H. W. Wilson, W. J. Novick, Jr., A. L. Barry, and C. Thornsberry, 1982, "In vitro evaluation of CENTA, a new beta-lactamase-susceptible chromogenic cephalosporin reagent", *J Clin Microbiol,* Vol. 15, pp. 954-8.

Kanlıkılıçer, P., 2008, "Investigation of Beta-lactamase Ligand Binding In Vivo and In Silico", M.S. Thesis, Boğaziçi University.

Karplus, M. and J. A. McCammon, 2002, "Molecular dynamics simulations of biomolecules", *Nat Struct Biol,* Vol. 9, pp. 646-52.

Kuzin, A. P., M. Nukaga, Y. Nukaga, A. M. Hujer, R. A. Bonomo, and J. R. Knox, 1999, "Structure of the SHV-1 beta-lactamase", *Biochemistry,* Vol. 38, pp. 5720-7.

Lim, D., H. U. Park, L. De Castro, S. G. Kang, H. S. Lee, S. Jensen, K. J. Lee, and N. C. Strynadka, 2001, "Crystal structure and kinetic analysis of beta-lactamase inhibitor protein-II in complex with TEM-1 beta-lactamase", *Nat Struct Biol,* Vol. 8, pp. 848-52.

London, N., B. Raveh, E. Cohen, G. Fathi, and O. Schueler-Furman, 2011, "Rosetta FlexPepDock web server--high resolution modeling of peptide-protein interactions", *Nucleic Acids Res,* Vol. 39, pp. W249-53.

Mackerell, A. D., D. Bashford, M. Bellott, R. L. Dunbrack, J. D. Evanseck, M. J. Field, S. Fischer, J. Gao, H. Guo, S. Ha, D. Joseph-McCarthy, L. Kuchnir, K. Kuczera, F. T. K. Lau, C. Mattos, S. Michnick, T. Ngo, D. T. Nguyen, B. Prodhom, W. E. Reiher, B. Roux, M. Schlenkrich, J. C. Smith, R. Stote, J. Straub, M. Watanabe, J. Wiorkiewicz-Kuczera, D. Yin, and M. Karplus, 1998, "All-Atom Empirical Potential for Molecular Modeling and Dynamics Studies of Proteins", *J. Phys. Chem. B.,* Vol. 102, pp. 3586-3616.

Mackerell, A. D., M. Feig, and C. L. Brooks, 2004, "Extending the Treatment of Backbone Energetics in Protein Force Fields: Limitations of Gas-Phase Quantum Mechanics in Reproducing Protein Conformational Distributions in Molecular Dynamics Simulations", *J Comput Chem,* Vol. 25, pp. 1400-1415.

Majiduddin, F. K., I. C. Materon, and T. G. Palzkill, 2002, "Molecular analysis of beta-lactamase structure and function", *Int J Med Microbiol,* Vol. 292, pp. 127-37.

McCammon, J. A., B. R. Gelin, and M. Karplus, 1977, "Dynamics of folded proteins", *Nature,* Vol. 267, pp. 585-90.

Meneksedag, D., A. Dogan, P. Kanlikilicer, and E. Ozkirimli, submitted, "Communication between the active site and the allosteric site in class A beta-lactamases".

Minasov, G., X. Wang, and B. K. Shoichet, 2002, "An ultrahigh resolution structure of TEM-1 beta-lactamase suggests a role for Glu166 as the general base in acylation", *J Am Chem Soc,* Vol. 124, pp. 5333-40.

Papadopoulos, J. S. and R. Agarwala, 2007, "COBALT: constraint-based alignment tool for multiple protein sequences", *Bioinformatics,* Vol. 23, pp. 1073-9.

Petrosino, J., G. Rudgers, H. Gilbert, and T. Palzkill, 1999, "Contributions of aspartate 49 and phenylalanine 142 residues of a tight binding inhibitory protein of beta-lactamases", *J Biol Chem,* Vol. 274, pp. 2394-400.

Phichith, D., S. Bun, S. Padiolleau-Lefevre, A. Guellier, S. Banh, M. Galleni, J. M. Frere, D. Thomas, A. Friboulet, and B. Avalle, 2010, "Novel peptide inhibiting both TEM-1 beta-lactamase and penicillin-binding proteins", *FEBS J,* Vol. 277, pp. 4965-72.

Phillips, J. C., R. Braun, W. Wang, J. Gumbart, E. Tajkhorshid, E. Villa, C. Chipot, R. D. Skeel, L. Kale, and K. Schulten, 2005, "Scalable molecular dynamics with NAMD", *J Comput Chem,* Vol. 26, pp. 1781-802.

Reichmann, D., M. Cohen, R. Abramovich, O. Dym, D. Lim, N. C. Strynadka, and G. Schreiber, 2007, "Binding hot spots in the TEM1-BLIP interface in light of its modular architecture", *J Mol Biol,* Vol. 365, pp. 663-79.

Reichmann, D., O. Rahat, M. Cohen, H. Neuvirth, and G. Schreiber, 2007, "The molecular architecture of protein-protein binding sites", *Curr Opin Struct Biol,* Vol. 17, pp. 67-76.

Reynolds, K. A., J. M. Thomson, K. D. Corbett, C. R. Bethel, J. M. Berger, J. F. Kirsch, R. A. Bonomo, and T. M. Handel, 2006, "Structural and computational

characterization of the SHV-1 beta-lactamase-beta-lactamase inhibitor protein interface", *J Biol Chem,* Vol. 281, pp. 26745-53.

Roberts, E., J. Eargle, D. Wright, and Z. Luthey-Schulten, 2006, "MultiSeq: unifying sequence and structure data for evolutionary analysis", *BMC Bioinformatics,* Vol. 7, p. 382.

Roccatano, D., G. Sbardella, M. Aschi, G. Amicosante, C. Bossa, A. Di Nola, and F. Mazza, 2005, "Dynamical aspects of TEM-1 beta-lactamase probed by molecular dynamics", *J Comput Aided Mol Des,* Vol. 19, pp. 329-40.

Rudgers, G. W., W. Huang, and T. Palzkill, 2001, "Binding properties of a peptide derived from beta-lactamase inhibitory protein", *Antimicrob Agents Chemother,* Vol. 45, pp. 3279-86.

Ryckaert, J. P., G. Ciccotti, and H. J. C. Berendsen, 1977, "Numerical Integration of the Cartesian Equations of Motion of a System with Constraints: Molecular Dynamics of n-Alkanes", *Journal of Computational Physics,* Vol. 23, pp. 327-341.

Savard, P. Y. and S. M. Gagne, 2006, "Backbone dynamics of TEM-1 determined by NMR: evidence for a highly ordered protein", *Biochemistry,* Vol. 45, pp. 11414-24.

Schymkowitz, J., J. Borg, F. Stricher, R. Nys, F. Rousseau, and L. Serrano, 2005, "The FoldX web server: an online force field", *Nucleic Acids Res,* Vol. 33, pp. W382-8.

Seeber, M., M. Cecchini, F. Rao, G. Settanni, and A. Caflisch, 2007, "Wordom: a program for efficient analysis of molecular dynamics simulations", *Bioinformatics,* Vol. 23, pp. 2625-7.

Stec, B., K. M. Holtz, C. L. Wojciechowski, and E. R. Kantrowitz, 2005, "Structure of the wild-type TEM-1 beta-lactamase at 1.55 A and the mutant enzyme Ser70Ala at 2.1 A suggest the mode of noncovalent catalysis for the mutant enzyme", *Acta Crystallogr D Biol Crystallogr,* Vol. 61, pp. 1072-9.

Strynadka, N. C., H. Adachi, S. E. Jensen, K. Johns, A. Sielecki, C. Betzel, K. Sutoh, and M. N. James, 1992, "Molecular structure of the acyl-enzyme intermediate in beta-lactam hydrolysis at 1.7 A resolution", *Nature,* Vol. 359, pp. 700-5.

Strynadka, N. C., S. E. Jensen, P. M. Alzari, and M. N. James, 1996, "A potent new mode of beta-lactamase inhibition revealed by the 1.7 A X-ray crystallographic structure of the TEM-1-BLIP complex", *Nat Struct Biol,* Vol. 3, pp. 290-7.

Strynadka, N. C., S. E. Jensen, K. Johns, H. Blanchard, M. Page, A. Matagne, J. M. Frere, and M. N. James, 1994, "Structural and kinetic characterization of a beta-lactamase-inhibitor protein", *Nature,* Vol. 368, pp. 657-60.

Sun, W., Y. Hu, J. Gong, C. Zhu, and B. Zhu, 2005, "Identification of beta-lactamase inhibitory peptide using yeast two-hybrid system", *Biochemistry (Mosc),* Vol. 70, pp. 753-60.

Weiner, P. K. and P. A. Kollman, 1981, "Amber: Assisted Model Building with Energy Refinement. A General Program for Modeling Molecules and Their Interactions", *Journal of Computational Chemistry,* Vol. 2, pp. 287-303.

Wiedemann, B., C. Kliebe, and M. Kresken, 1989, "The epidemiology of beta-lactamases", *J Antimicrob Chemother,* Vol. 24 Suppl B, pp. 1-22.

Wilke, M. S., A. L. Lovering, and N. C. Strynadka, 2005, "Beta-lactam antibiotic resistance: a current structural perspective", *Curr Opin Microbiol,* Vol. 8, pp. 525-33.

Williams, J. D., 1999, "Beta-lactamases and beta-lactamase inhibitors", *Int J Antimicrob Agents,* Vol. 12 Suppl 1, pp. S3-7; discussion S26-7.

Xie, L., M. Xu, T. Yang, C. Zhu, B. Zhu, and Y. Hu, 2010, "Studies on amino acid replacement and inhibitory activity of a beta-lactamase inhibitory peptide", *Biochemistry (Mosc),* Vol. 75, pp. 336-41.

Yribarren, A. S., D. Thomas, A. Friboulet, and B. Avalle, 2003, "Selection of peptides inhibiting a beta-lactamase-like activity", *Eur J Biochem*, Vol. 270, pp. 2789-95.

Zafaralla, G., E. K. Manavathu, S. A. Lerner, and S. Mobashery, 1992, "Elucidation of the role of arginine-244 in the turnover processes of class A beta-lactamases", *Biochemistry*, Vol. 31, pp. 3847-52.

Zhang, Z. and T. Palzkill, 2004, "Dissecting the protein-protein interface between beta-lactamase inhibitory protein and class A beta-lactamases", *J Biol Chem*, Vol. 279, pp. 42860-6.

Zhang, Z. and T. Palzkill, 2003, "Determinants of binding affinity and specificity for the interaction of TEM-1 and SME-1 beta-lactamase with beta-lactamase inhibitory protein", *J Biol Chem*, Vol. 278, pp. 45706-12.